

JSC-11552

CONTROL SYSTEMS DEVELOPMENT DIVISION
INTERNAL NOTE 76-EG-18

(NASA-TM-80445) ANALYTICAL MODELING OF THE
DYNAMICS OF BRUSHLESS dc MOTORS FOR
AEROSPACE APPLICATIONS: A CONCEPTUAL
FRAMEWORK (NASA) 102 p HC A06/MF A01

N79-25310

CSCL 09A G3/33

Unclassified
22273

ANALYTICAL MODELING OF THE
DYNAMICS OF BRUSHLESS DC MOTORS
FOR AEROSPACE APPLICATIONS:
A CONCEPTUAL FRAMEWORK



National Aeronautics and Space Administration
LYNDON B. JOHNSON SPACE CENTER

Houston, Texas

AUGUST 18, 1976

REPRODUCED BY
NATIONAL TECHNICAL
INFORMATION SERVICE
U.S. DEPARTMENT OF COMMERCE
SPRINGFIELD, VA 22161

NOTICE.

THIS DOCUMENT HAS BEEN REPRODUCED
FROM THE BEST COPY FURNISHED US BY
THE SPONSORING AGENCY. ALTHOUGH IT
IS RECOGNIZED THAT CERTAIN PORTIONS
ARE ILLEGIBLE, IT IS BEING RELEASED
IN THE INTEREST OF MAKING AVAILABLE
AS MUCH INFORMATION AS POSSIBLE.

CONTROL SYSTEMS DEVELOPMENT DIVISION
INTERNAL NOTE 76-EG-18

ANALYTICAL MODELING OF THE
DYNAMICS OF BRUSHLESS DC MOTORS
FOR AEROSPACE APPLICATIONS:
A CONCEPTUAL FRAMEWORK

Prepared by

Nabeel A. O. Demerdash

Nabeel A. O. Demerdash
Visiting Scientist
NASA-ASEE Summer Faculty Institute

Approved by

Forrest E. Eastman
Forrest E. Eastman, Chief
Power Distribution and Control Branch

R G Chilton
Robert G. Chilton, Chief
Control Systems Development Division

NATIONAL AERONAUTICS AND SPACE ADMINISTRATION
LYNDON B. JOHNSON SPACE CENTER
HOUSTON, TEXAS

August 18, 1976

ABSTRACT

This report describes an investigation which lays the conceptual framework within which the NASA/VPI (Virginia Polytechnic Institute) analysis of the dynamics of permanent magnet-brushless d.c. machines, for aerospace applications and particularly for electromechanical actuator systems, will take place. This analytical effort will be carried out in two stages. The first stage will entail a preliminary numerical model with a simplified (elementary) representation of the brushless d.c. machine for its instantaneous operation. The present report lays in detail the foundation and basic assumptions and principles on which the preliminary numerical model will be based. The brushless d.c. machine, when functioning as part of an electromechanical actuator, operates as a motor, generator, and brake. This report describes how these modes of operation are accomplished and the corresponding machine characteristics (current flows, torque-position characteristics, etc.) during these modes of operation. This report lays the groundwork of the detailed numerical model which will be developed in the second stage of the NASA/VPI analytical effort. In this stage, a more detailed brushless d.c. machine representation will be used, with rigorous accounts of the interaction between the machine windings and other important system components on an instantaneous basis.

CONTENTS

<u>Section</u>	<u>Page</u>
ABSTRACT	ii
1.0 INTRODUCTION	1
2.0 MACHINE MODELING AS A MOTOR-MODE 1	2
3.0 MACHINE FUNCTION AS PART OF A SYSTEM-MOTOR, GENERATOR AND BRAKE	9
4.0 MACHINE MODELING AS A BRAKE - MODE 3	11
5.0 MACHINE MODELING AS A GENERATOR - MODE 2 . . .	12
6.0 OVERALL MACHINE MODELING - IMMEDIATE AND LONG RANGE ANALYSIS EFFORT	15
7.0 RECOMMENDED TESTING IN SUPPORT OF PLANNED ANALYTICAL EFFORT	17
8.0 CONCLUSIONS	20
9.0 BIBLIOGRAPHY	21
APPENDIX A - ELECTROMECHANICAL ACTUATOR SYSTEM	A-1
APPENDIX B - EXAMPLE MOTOR - SOME DESIGN FEATURES . .	B-1
APPENDIX C - MOTOR TORQUE - POSITION CALCULATION . . .	C-1

FIGURES

<u>Number</u>		<u>Page</u>
2-1	STATE #1-A, MODE #1	23
2-2	STATE #1-B, MODE #1	24
2-3	STATE #2-A, MODE #1	25
2-4	STATE #2-B, MODE #1	26
2-5	STATE #3-A, MODE #1	27
2-6	STATE #3-B, MODE #1	28
2-7	STATE #4-A, MODE #1	29
2-8	STATE #4-B, MODE #1	30
2-9	STATE #5-A, MODE #1	31
2-10	STATE #5-B, MODE #1	32
2-11	STATE #6-A, MODE #1	33
2-12	STATE #6-B, MODE #1	34
2-13	TRANSISTOR SWITCHING SEQUENCE MODE 1 - MOTOR	35
2-14	LOOPS - STATE #1-A, MODE #1	36
2-15	LOOPS - STATE #1-B, MODE #1	37
2-16	LOOPS - STATE #2-A, MODE #1	38
2-17	LOOPS - STATE #2-B, MODE #1	39
2-18	LOOPS - STATE #3-A, MODE #1	40
2-19	LOOPS - STATE #3-B, MODE #1	41
2-20	LOOPS - STATE #4-A, MODE #1	42
2-21	LOOPS - STATE #4-B, MODE #1	43

<u>Number</u>		<u>Page</u>
2-22	LOOPS - STATE #5-A, MODE #1	44
2-23	LOOPS - STATE #5-B, MODE #1	45
2-24	LOOPS - STATE #6-A, MODE #1	46
2-25	LOOPS - STATE #6-B, MODE #1	47
2-26	ROTOR POSITION AND WINDINGS SCHEMATIC DIAGRAM	48
2-27	MACHINE AS MOTOR WITH POSITIVE SPEED - MODE #1 - STATE #1	49
2-28	MACHINE AS MOTOR WITH POSITIVE SPEED - MODE #1 - STATE #2	50
2-29	MACHINE AS MOTOR WITH POSITIVE SPEED - MODE #1 - STATE #3	51
2-30	MACHINE AS MOTOR WITH POSITIVE SPEED - MODE #1 - STATE #4	52
2-31	MACHINE AS MOTOR WITH POSITIVE SPEED - MODE #1 - STATE #5	53
2-32	MACHINE AS MOTOR WITH POSITIVE SPEED - MODE #1 - STATE #6	54
2-33	TORQUE-ROTOR POSITION CHARACTERISTIC OF BRUSHLESS DC MOTOR - MODE #1	55
3-1	SCHEMATIC DIAGRAM SHOWING THE SIX POSSIBLE MODES OF OPERATION, MODES #1 THROUGH #6 . .	56
3-2	MODE #1 - MOTOR WITH POSITIVE SPEED . . .	57
3-3	MODE #2 - GENERATOR (REGENERATIVE BRAKE) WITH POSITIVE SPEED	58
3-4	MODE #3 - BRAKE WITH POSITIVE SPEED . . .	59

<u>Number</u>		<u>Page</u>
3-5	MODE #4 - MOTOR WITH NEGATIVE SPEED	60
3-6	MODE #5 - GENERATOR (REGENERATIVE BRAKE) WITH NEGATIVE SPEED	61
3-7	MODE #6 - BRAKE WITH NEGATIVE SPEED	62
3-8	MODE 1 CURRENTS MOTOR - POSITIVE SPEED - Q_m ON	63
3-9	MODE 1 CURRENTS MOTOR - POSITIVE SPEED - Q_m OFF	64
3-10	MODE 2 CURRENTS - GENERATOR POSITIVE SPEED - Q_b ON	65
3-11	MODE 2 CURRENTS - GENERATOR POSITIVE SPEED - Q_b OFF	66
3-12	MODE 3 CURRENTS - BRAKE POSITIVE SPEED - Q_m ON	67
3-13	MODE 3 CURRENTS - BRAKE POSITIVE SPEED - Q_m OFF	68
4-1	MACHINE AS BRAKE WITH POSITIVE SPEED - MODE #3 - STATE #1	69
4-2	TORQUE - ROTOR POSITION CHARACTERISTIC OF BRUSHLESS DC MACHINE OPERATING AS BRAKE MODE #3	70
5-1	MACHINE AS GENERATOR WITH POSITIVE SPEED - MODE #2 - STATE #1	71
5-2	TORQUE - ROTOR POSITION CHARACTERISTIC OF BRUSHLESS DC MACHINE OPERATING AS GENERATOR MODE #2	72

<u>Number</u>		<u>Page</u>
7-1	OPEN CIRCUIT VOLTAGE AND FLUX DENSITY DISTRIBUTION WAVEFORMS AT NO-LOAD	73
7-2	TEST #2, MOTOR TORQUE-POSITION CHARACTERISTICS	74
7-3	TEST #2, MOTOR TORQUE-POSITION CHARACTERISTICS (CONTINUED)	75
7-4	TEST #2, MOTOR TORQUE-POSITION CHARACTERISTICS (CONTINUED)	76
7-5	TEST #3, SELF AND MUTUAL INDUCTANCES OF WINDINGS	77
7-6	TEST #4, STEP LOAD RESPONSE OF MOTOR	78
7-7	TEST #5, GENERATOR LOADING	79
7-8	TEST #6, CURRENT PATH DETERMINATION	80

1.0 INTRODUCTION

This report examines the basic physical principles on which the operation of permanent magnet brushless d.c. motors are based. These motors are a prime candidate for use as prime-movers in future electromechanical actuators suited for applications in the aerospace industry. Among the most important of these applications are electromechanical actuators for flight control of spacecraft and aircraft. Such a system would, if adopted, replace the present hydraulic system planned for the Space Shuttle Orbiter in particular and can be used on various types of aircraft in lieu of that system. The electromechanical actuator system can, if properly designed and optimized, lead to considerable weight and volume reductions which are very critical considerations in these applications. Weight and volume reductions can be achieved by resorting to higher fluid pressures in the hydraulic actuator systems. Higher fluid pressures have their own technical disadvantages in design and operation of such systems. It is also believed that the electromechanical system will be more trouble-free and more durable with less maintenance problems than the present hydraulic systems. A preliminary system components concept of the electromechanical actuator was given in one of the reports prepared by the Delco Electronics Company (Report No. S76-1). A copy of the basic diagrams describing these concepts to be implemented for the electromechanical actuator is given in Appendix A for completeness and convenience of the reader.

The brushless d.c. motor consists of a permanent magnet rotor and a three-phase winding on the stator. The stator winding is supplied by a d.c. source through an inverter consisting of transistors and diodes. The transistors are fired by

signals which are derived from a rotor position sensing device. The nature of the constructional features of an example motor developed by the Delco Electronics Company is included in Appendix B, for completeness and convenience.

In the functioning of the electromechanical actuator, the motor will have to operate in a motor, generator (regenerative-brake), and brake modes. Modeling of the machine under these modes of operation and the determination of the various characteristics of the machine under these conditions is the subject of the following sections of this report.

2.0 MACHINE MODELING AS A MOTOR-MODE 1

Throughout the development which will follow in this report, the load (consumer) system of notation will be adopted. That is, current is taken positive when it is into the terminal with the higher potential for a two-terminal device. On that basis the A, B, and C currents can be idealized as shown in figure 2-1 by the solid rectangles. The entire 360° electrical degrees cycle is divided into six states—STATE #1 through STATE #6, as shown in figure 2-1. The ripple shown in the current waveforms is expected to be caused by the action of the chopper transistor, Q_m , which in turn is turned on and off by a current sensing device shown in the network in order to control the motor current and hence motor torque. Switching from one state to the next is done by turning on and off the various inverter transistors Q_1 through Q_6 . In turn, Q_1 through Q_6 receive their on-off signals from a rotor position sensing device.

For State #1, Q_1 and Q_5 are on as shown in figure 2-1. Also shown in figure 2-1 are the various possible current paths when the chopper transistor Q_m is on. On the other hand, when the chopper transistor Q_m is off, the possible current paths are altered and are shown in figure 2-2. It can be seen that the function D_6 is to help in the commutation process in carrying the decaying current, I_C . It can also be seen from figure 2-2 that the diode D_m helps provide a path for the chopper-inductor current when Q_m is off. As it will be seen in the other five states, the function of the various diodes D_1 through D_6 is helping the commutation process by providing a path for the decaying current.

Figures 2-3 and 2-4 show State #2 with its possible current paths when Q_m is on and off respectively. In this state, transistors Q_1 and Q_6 are on, while the diode D_2 helps commutation of I_B .

Figures 2-5 and 2-6 show State #3 with its possible current paths when Q_m is on and off respectively. In this state, transistors Q_2 and Q_6 are on, while the diode D_4 helps commutation of I_A .

Figures 2-7 and 2-8 show State #4 with its possible current paths when Q_m is on and off respectively. In this state, transistors Q_1 and Q_6 are on, while the diode D_3 helps commutation of I_C .

Figures 2-9 and 2-10 show State #5 with its possible current paths when Q_m is on and off respectively. In this state, transistors Q_3 and Q_4 are on, while the diode D_5 helps commutation of I_B .

Figures 2-11 and 2-12 show State #6 with its possible current paths when Q_m is on and off respectively. In this state, transistors Q_3 and Q_5 are on, while the diode D_1 helps commutation of I_A .

Figure 2-13 summarizes the various transistors switching sequence for Q_1 through Q_6 , as well as the durations (sequence) of conduction of the diodes D_1 through D_6 are also shown.

Corresponding to the current paths shown in figures 2-1 through 2-12, there are current loop topologies which are shown in: Figures 2-41 and 2-15 for State #1; figures 2-16 and 2-17 for State #2; figures 2-18 and 2-19 for State #3; figures 2-20 and 2-21 for State #4; figures 2-22 and 2-23 for State #5; also figures 2-24 and 2-25 for State #6. These loop topologies will be used in developing the appropriate formulation coupling the motor to the supply and power electronics part of the setup. This formulation will be instrumental in the preliminary numerical model to be developed under the NASA/VPI effort. In these loops, the motor phase windings are represented by their leakage inductances in series with the back emf, calculated from knowledge of the resultant air-gap flux density and instantaneous rotor speed. The phase emf's will be calculated based on the simple rule, $e = Blv$, where B is the resultant air-gap flux density at a given angular position. The resultant air-gap flux density is calculated including the demagnetizing (or magnetizing effect of the armature reaction (mmf)).

In order to obtain the torque-rotor position characteristic of the motor, one makes use of the fundamental formulation

of a force, \bar{F} , on a current carrying conductor. That is:

$$\bar{F} = (\bar{I} \times \bar{B}) \cdot l$$

Where; \bar{I} is the current in the conductor represented as a space vector,

\bar{B} is the flux density vector to which the conductor is subject,

and l is the length of the conductor.

Therefore, one must obtain the distribution in space (throughout motor cross-section) of the currents and flux densities.

One must obtain such distributions throughout the durations of the various States #1 through #6. As a first step to obtain these distributions, consider figure 2-26. Figure 2-26 depicts an elementary three-phase winding consisting of three individual coils (or turns) and a permanent magnet rotor. The magnetic axes of these windings and the rotor direction of rotation (counter clockwise) are drawn such that a sequence (A B C) is produced, as the direct axis "d" of the rotor cuts the three magnetic axes of the three windings. A rotor positioning angle "g" will always be taken in this report as the angle between the A and d axes. Now, if one redraws figure 2-26 in a developed (straight line) fashion, starting from the magnetic axis of phase A, the coil sides would be lined in the following order: -B, A, -C, B, -A, and C. Here the "-" sign indicates the return side of the phase. For the example Delco motor, there are six slots per pole pair. Therefore, for a pole pair there would be six slots labeled in the order -B, A, -C, B, -A, and C as shown in figure 2-27. Now, for the motor under consideration, there are 24 stator slots and eight poles; therefore, one gets the pattern shown in figure 2-27 in its entirety as labeled. For

each of the various States #1 through #6, one must determine the direction of the phase currents in the various slots.

For State #1, figure 2-1 reveals for the idealized currents that phase A carries a positive current "I" (that is into the winding according to the adopted notation). Phase B carries a negative current "-I" while phase C carries no current. Positive currents will be represented by a dot current, that is out of the plane of the page in the developed diagrams; while negative currents will be represented by a cross current, that is into the plane of the page. With this notation in mind, one gets the current distribution depicted in figure 2-27 in the various stator slots.

Assuming that the currents in the various stator slots are current filaments instead of being uniformly distributed over the cross-sections of the conductors, one obtains a stator mmf pattern (reference 3) for State #1 as shown in figure 2-27. The angular positions, in mechanical degrees, of the various positive and negative half-waves of the stator mmf are based on the fact that the stator slot angular pitch is equal to $\frac{360}{24} = 15^\circ$ mechanical. If the rotor position sensing device is adjusted to fire the appropriate transistors to initiate State #1, such that the initial angle between the stator mmf position axis and the corresponding north pole axis is 90° electrical (in this case 22.5° mechanical), the resulting rotor position would be as shown in the top diagram in figure 2-27. (The 90° electrical is according to reference 5, section 1.2.2, page 5.) This corresponds to zero advance angle of commutation. In this case, $\delta = -30^\circ$ mech. (always measured from the axis of winding A). The stator mmf is frozen in the same position in space throughout the duration of State #1. That

is the case because the idealized phase currents are frozen throughout the duration of the state. The rotor is in continuous motion and its relative position with respect to the stator mmf throughout the duration of State #1 is continuously changing.

At the start of State #1, one obtains the mechanical forces affecting the stator conductors by applying the well known formula given earlier, equation 2-1. This results in a force pattern as shown in figure 2-27. There are 16 conductors experiencing a force, F , in the direction opposite to rotation shown in the figure 2-27. This results in a torque which the stator frame experiences. This torque, T , is given as

$$T = 16 F.R = 10.66325 I.R \quad (2-2)$$

where R is the arm of the force measured radially from the middle of the slot to the center line of the shaft. For details of the calculations, reference should be made to Appendix C. As the rotor continues to move with respect to the stator, there comes a time during State #1 at which the conductors of phase B cease to be under the influence of the rotor flux, at which time the torque, T , is reduced in half and it becomes

$$T = 8 F.R = 5.33162 I.R \quad (2-3)$$

The reader should consult Appendix C for more details. One should point out that this pattern of torque pulsation between the values given in equations 2-2 and 2-3 takes place in the shape of rectangular pulses subject to the assumption that the rotor flux density waveforms (permanent magnet waveforms) are rectangular in shape and are not altered by the stator mmf presence. This assumption will be abandoned in the later analytical NASA/VPI effort.

Figure 2-28 depicts the start of State #2 where the phase currents, figure 2-3, are such that phase A carries a positive current, I , and phase C carries a negative current, $-I$. Again, at the start of State #2 the north-pole axis on the rotor should lag behind the stator mmf axis by 90° electrical (22.5° mechanical), if the advance commutation angle is equal to zero. It is noticed that the mechanical forces in this state are equal to those in State #1, except that they are shifted to the left by one slot pitch. The same torque pulsation between the two values given in equations 2-2 and 2-3 takes place as the stator mmf remains frozen in place (in space) while the rotor is moving continuously.

Figure 2-29 depicts the start of State #3 where the phase currents, figure 2-5, are such that phase B carries positive current, I , and phase C carries negative current, $-I$. The force pattern is shown in figure 2-29 and is identical to the force pattern in the previous two states except that it is shifted one more slot pitch. Again, throughout the duration of the state, the torque alternates between the two magnitudes given by equations 2-2 and 2-3. —

Similarly, figures 2-30, 2-31, and 2-32 show the States #4 through #6. These figures correspond to the current polarity shown in figures 2-7, 2-9, and 2-11 on a one-to-one basis.

Using the six figures 2-27 through 2-32, the torque-rotor angle-characteristic is obtained as shown in Appendix C and as depicted in figure 2-33. The rectangular pulsating shape results when the stator currents are treated as current filaments concentrated at the stator slot centers. When the stator current is distributed throughout the stator slot

width, as it is physically, the torque-position characteristic takes the sawtooth shape in figure 2-33. The average developed torque, T_{av} , remains the same where it is given as:

$$T_{av} = 7.997 I \cdot R \quad (2-4)$$

Again for details of the calculation, reference should be made to Appendix C. These calculations were conducted for the example Delco motor shown in Appendix A. The pulsating nature of the torque given in figure 2-33 is certainly in agreement with the general nature of the same type of characteristic obtained by test and given in reference 2, chapter 5.

3.0 MACHINE FUNCTION AS PART OF A SYSTEM-MOTOR, GENERATOR AND BRAKE

The brushless d.c. motor must function as a part of an overall control system, a preliminary conception of which is given in Appendix A. This means that the motor must operate as a motor, generator (regenerative brake) and brake in both the positive and negative speeds (counterclockwise and clockwise) respectively. This means that the motor must have the capability to operate in the six modes shown in figure 3-1. These various modes of operation shown in figure 3-1 are categorized as modes #1 through #6.

The various modes #1 through #6 are demonstrated by an elementary one-conductor machine with the basic variables: Velocity, current, flux density, force, induced emf and external voltage vectors in relative direction (sense). These are in figures 3-2 through 3-7. The basic rules that apply here are:

$$\bar{F} = \bar{I} \times \bar{B} \quad (3-1)$$

$$\bar{e} = \bar{v} \times \bar{B} \quad (3-2)$$

In the motor modes #1 and #4, the force and velocity vectors, \bar{F} and \bar{v} , are in the same direction. For the two motor modes the current flows in the conductors into the positive end as shown in figures 3-2 and 3-5. The external voltage (source) and the induced emf are subtractive to each other around the loops.

In the generator modes #2 and #5, the force and velocity vectors, \bar{F} and \bar{v} , are in opposite directions. For the two generator modes, the current flows in the conductors at the positive end as shown in figures 3-3 and 3-6. The external voltage (source) and the induced emf are subtractive to each other around the loops.

In the brake modes #3 and #6, the force and velocity vectors, \bar{F} and \bar{v} , are in opposition. For the two modes, the current flows out of the positive end of the conductors as shown in figures 3-4 and 3-7. The external voltage (source) and the induced emf are additive around the loops.

Figures 3-8 and 3-9 show the possible current paths for State #1 of mode #1, with the chopper transistor, Q_m , on and off respectively. The dotted current path represents that path which carries the decaying currents during commutation. Figures 3-10 and 3-11 show the possible current paths for State #1 of mode #2, with the transistor Q_b on and off respectively. Here the diodes D_1 through D_6 are the elements carrying the generator currents while the transistors Q_1 through Q_6 play no role. The dotted current paths show the decaying currents during the process of commutation. Figures 3-12 and 3-13 show the possible current paths for State #1 of mode #3, with the chopper transistor, Q_m , in the on and

off states respectively. Again, here the dotted current path represents the decaying current path. Similar current path diagrams can be obtained in the same fashion, for the various other States #2 through #6 as well as for the other modes #4 through #6.

These current path diagrams will be used to develop loop topologies for the various modes and states, as a first step in obtaining the desired dynamic model of the machine. There are 12 loop topologies for each mode, that is a total of 72 possible loop topologies for the entire six modes of operation of the brushless d.c. machine.

4.0 MACHINE MODELING AS A BRAKE - MODE 3

Modeling of the machine as a brake consists of two steps which are similar in nature to what has already been described for the motor. The first step is the determination of the current paths and hence loop topologies during the various states. This has been partly examined by depicting State #1 for mode #3 in figures 3-12 and 3-13. Ten more similar figures are needed for the States #2 through #6 for mode #3 and 12 more figures are needed for States #1 through #6 for mode #6 in order to develop all the loop topologies in the brake case, as well as the loop formulation. Also, torque-rotor position characteristics are needed.

There are two theoretically feasible ways to achieve a brake. The first that comes to mind is that of reversing the current sequence in the stator winding through the switching sequence of the transistors Q₁ through Q₆ to produce an ACB current sequence. However, this requires a much more complex position sensing device, in addition to

possible dead bands in the motor operation as a component of an overall control system. Therefore, the manufacturer of the present rotor resorted to the obvious alternative of simply altering the switching sequence of the transistors Q_1 through Q_6 to produce the effect of reversing the polarity of the external d.c. source (battery) as shown in the elementary brake in figure 3-4 in comparison to the motor in figure 3-2. Thus, instead of firing transistors Q_1 and Q_5 for the motor as shown in figures 3-9 and 3-10, the transistors Q_4 and Q_2 are fired which has the effect of reversing the polarity of the external source to achieve a brake as shown in figures 3-12 and 3-13.

If this scheme is followed, a developed space diagram for the stator currents and rotor position at the start of State #1 can be drawn, in a similar fashion as was done for the motor case, as shown here in figure 4-1. Similar diagrams for the other five states #2 through #5 can be drawn. The resulting torque-rotor position characteristic is identical to that deduced earlier for the motor case, except that the torque is opposing the direction of rotation, and hence can be considered to be negative. This torque-position characteristic is shown, with the various States #1 through #6 and their sequence of occurrence in figure 4-2.

5.0 MACHINE MODELING AS A GENERATOR - MODE 2

Modeling of the brushless d.c. machine as a generator consists of two steps which are similar in nature to the procedures described earlier in sections 3.0 and 4.0 for the motor and brake modes. The first step is the determination of the current paths and hence loop topologies during the various

states. This has been partly examined by depicting State #1 for mode #2 in figures 3-10 and 3-11. However, the phase conduction here does not depend on rotor position sensing devices as was the case in the motor and brake cases. The phase conduction rather depends in this case on two aspects of the motor design and the power electronics circuitry. One aspect is the polarity of the induced emf in a given phase (which is a major factor in determining the polarity of the voltages across the various diodes). The second aspect is the characteristics of the various diodes and the level of forward bias at which conduction begins, as well as the inherent impedances in the diode circuitry. If one assumes an idealized diode characteristic, that is conduction starts instantly as soon as any forward bias appears across a given diode, conduction angles for the various phases will fundamentally depend on the polarity of the induced voltage in a conductor (or a phase). In turn this is related to the rotor relative position with respect to the various phases on the stator. A conductor will carry current in this case as long as it is under the influence of the flux of one of the permanent magnets on the rotor. With a pole face width (68% of a pole pitch) of 30.6° mechanical, a corresponding possible phase conduction angle of $30.6^\circ \times 4 = 122.4^\circ$ electrical can take place. When the various idealizing assumptions regarding the diode and power electronics characteristics are abandoned, it may very well turn out that the conduction angle per phase is about 120° electrical as the Delco designers contended during technical discussions with this author (see reference 6). Taking a conduction angle per phase of 120° electrical, one gets the current conduction pattern shown in figures 3-10 and 3-11 for the States #1 through #6. The corresponding current paths for State #1 with Q_b in the on and off states are shown in figures 3-10 and 3-11 respectively. The

corresponding current distribution, in space, for State #1 is shown in figure 5-1, with the rotor shown in its position at the beginning of State #1, then in the middle of the state and finally at its end. The beginning of State #1 is when the leading tips of the magnets (poles) begin to cover the centers of slots that belong to phase A to give that phase the negative current it has to carry during that state.

If one follows the mechanical force pattern produced in the generator case, there are always 16 conductors experiencing a force, F , as shown in figure 5-1, to give a torque, T , that is given as

$$T = 10.66325 I.R \quad (5-1)$$

(see Appendix C for detailed torque calculations) for the given motor under consideration. However, because the permanent magnet width is 122.4° electrical which is greater by 2.4° electrical than the angular distance between the phase carrying the decaying current and the other phase which carries the increasing current during the commutation process, if one assumes the idealized currents given earlier, one obtains a repetitive pattern of angular positions of the rotor at which there are 24 conductors experiencing a force, F . This gives rise to a torque, T , given by

$$T = 15.99486 I.R \quad (5-2)$$

The angular positions at which such torque is developed is shown in the generator torque-rotor position angle characteristic given in figure 5-2, subject to all the idealizing assumptions mentioned earlier. These include treating the stator conductors as filaments, neglecting the distortion effect that the stator mmf has on the air-gap flux waveforms, assuming idealized stator currents and idealized rectangular flux density waveforms for the permanent magnets.

The next phase of this report will include an overall view of the modeling approach which will be taken for the desired preliminary model as well as what should be done to accomplish it.

6.0 OVERALL MACHINE MODELING -
IMMEDIATE AND LONG RANGE
ANALYSIS EFFORT

Previous investigators have analyzed the brushless d.c. motors using phasor (steady-state) and frequency domain concepts (reference 1 and 2). However, in this particular motor at hand, even if the motor is running at a steady-state speed, the motor is constantly in a dynamic (transient) mode because of the continuous switching-on and off of the various transistors in the inverter and chopper circuitry. Therefore, only dynamic circuit modeling along with dynamic modeling of the motor with its associated mechanical system would be useful in this case.

The development of a dynamic model for this machine will be done under the NASA/VPI effort in two stages. The first stage is immediate and will follow this work. This stage includes the development of the loop state equations for the six modes #1 through #6 with their various states (#1 through #6), possibly yielding a set of 72 loop state equations. In these loop equations, the motor phase windings will be represented by a simplified resistance, leakage inductance and induced back emf calculated from Blv type formulation where B is the actual air-gap flux density waveform, taking into account the magnetizing and/or demagnetizing effects of the armature (stator winding) mmf. In the power electronics, the diodes will be represented by voltage drops which can be varied as one desires in the input data of the numerical model and

the transistors will be represented by resistive elements to account for the power dissipation in them during the various modes and states. The motor torque will be calculated using the various instantaneous phase currents as determined by the solution of the loop equations. The dynamics of the load and motor as rotating masses will be included. These features have been discussed and agreed upon between NASA/VPI and Delco (reference 6).

The second stage includes more detailed modeling of the motor as outlined in detail in reference 7 and in the work statement of NASA/VPI contract. Experience with the motor model which will be developed under the first stage effort will help shape and/or modify some of the modeling concepts and methods used for the second stage. This includes possible improvements in the power electronics representation, if the need arises.

Future investigations beyond the present NASA/VPI contract certainly can include refinement of the method by which motor winding parameters were obtained. This includes making use of the method of finite elements (reference 8) in order to obtain much more accurately the various motor winding mutual and self-inductances which are critical for the detailed motor model. This method enables one to obtain a very accurate picture of the magnetic field in the motor, which enables one to determine more precise estimates of losses in the core, pole face of the magnet, leakage flux of the permanent magnet and stator leakage, etc. All of these factors impinge on the dynamic performance of the motor. Also, the scope of such future investigations should include the development of a more general model to handle various phase configurations for the brushless d.c. motor such as two-phase or six-phase configurations with varying stator and rotor geometries. In

addition, the finite element modeling mentioned above should be developed in a generalized fashion to allow the analysis of these various phase configurations with a complete capability of handling various stator and rotor geometric configurations and various magnetic material characteristics. Another phase of such a future effort should include a consistent and rigorous application of model order reduction techniques to these detailed nonlinear dynamic models. This would yield simplified, yet relatively accurate, models of such motors for use in comprehensive and large closed loop control system studies of the type which has to be conducted for an overall evaluation of the performance of multichannel actuator systems operating in parallel. The combined result of such an analytical effort would be a capability to optimize performance, weight, volume, and most likely cost of implementation of these systems to many aerospace applications.

7.0 RECOMMENDED TESTING IN SUPPORT OF PLANNED ANALYTICAL EFFORT

This section of the report includes a set of suggested tests to be applied to the brushless d.c. motor developed by Delco, with the objective of being able to use the test results to verify and check some of the results of the analytical models which will be developed in the course of the NASA/VPI effort. These tests can best be summarized as follows:

Test #1 (See figure 7-1): The purpose of this test is to determine the open-circuit voltage waveform, and hence determine also the no-load mid-gap flux density waveform. This is done by taking Polaroid type photographs of the voltage waveform of one of the motor phases, such as phase A, as

shown in figure 7-1, at various speeds of 900, 4500, and 9000 rpm, for example. There should be no armature current throughout this test.

Test #2 (See figures 7-2, 7-3, and 7-4): The purpose of this test is the determination of the torque-rotor position characteristic of the motor using idealized d.c. currents in the armature windings. There are six states to be represented which are detailed in the figures. The purpose of this test is to check the validity of some of the concepts which will be used in the preliminary NASA/VPI analytical model (the first stage of the NASA/VPI effort). The test should preferably be conducted at rated armature current levels. No chopper or power electronics should be connected in this case, only a simple d.c. source (battery) and a current limiting rheostat in series with the motor, or a potential divider if desired with the variable voltage taken as input to the energized motor windings. The rotor must be rotated very slowly during such a torque measurement with δ varying from 0° to 360° for each state.

Test #3 (See figure 7-5): The purpose of this test is the determination of the self and mutual inductances between the motor windings as functions of the rotor angular position, under various armature current magnitudes and frequencies. The reason for checking the inductances at various current magnitudes is to check the effect of saturation on the parameters. The reason for the various frequencies is to check the effect of the eddy currents in the pole face of the permanent magnets on the inductances: The rotor should be turned very slowly in this experiment, while pure variable sinusoidal voltage is applied to one of the windings during which measurement is made of that voltage and the corresponding

current in the winding as well as the terminal voltages across the terminals of the other open windings. Each reading should be taken for a fixed and known rotor position. The desired currents, frequencies, and range of δ is given in figure 7-5. Knowledge of these inductances is very important in verifying some of the motor parameter calculations which will be used in the detailed model of the motor.

Test #4 (Figure 7-6): The purpose of this test is to obtain the dynamic response of the motor to a sudden (step) load without any external controls except those of the current sensing device and the chopper only. The test results consisting of a record of phase currents, phase voltages to neutral, torque, speed, d.c. voltage, and d.c. current versus time will be compared with corresponding numerical results obtained from the analytical model. This comparison will be instrumental in verifying the detailed analytical model of the motor and power electronics package. The test should be carried into the steady-state region of operation after the transients have subsided. The goal should be for two or three tests with steady-state outputs of perhaps 2.5, 5.0, and 7.5 HP.

Test #5 (Figure 7-7): The purpose of this test is to obtain the dynamic generator response to a sudden (step) load without any external controls except the current sensors and chopper. Immediately after such a sudden load, photos must be taken of the phase A, B, and C current transients as well as the phase voltages to neutral. Steady-state should be allowed to develop, and steady-state readings should be taken of these currents and voltages, as well as photos for steady-state voltage and current waveforms. The speed of the generator

should also be monitored and recorded during the transient and steady-state operations. This test will be simulated using the detailed analytical model in order to verify and check the accuracy of the numerical results of the model for the generator mode of operation.

Test #6 (Figure 7-8): The purpose of this test is to verify and check the various possible current paths in the power electronics package during the motoring, generating, and breaking modes, under normal conditions.

8.0 CONCLUSIONS

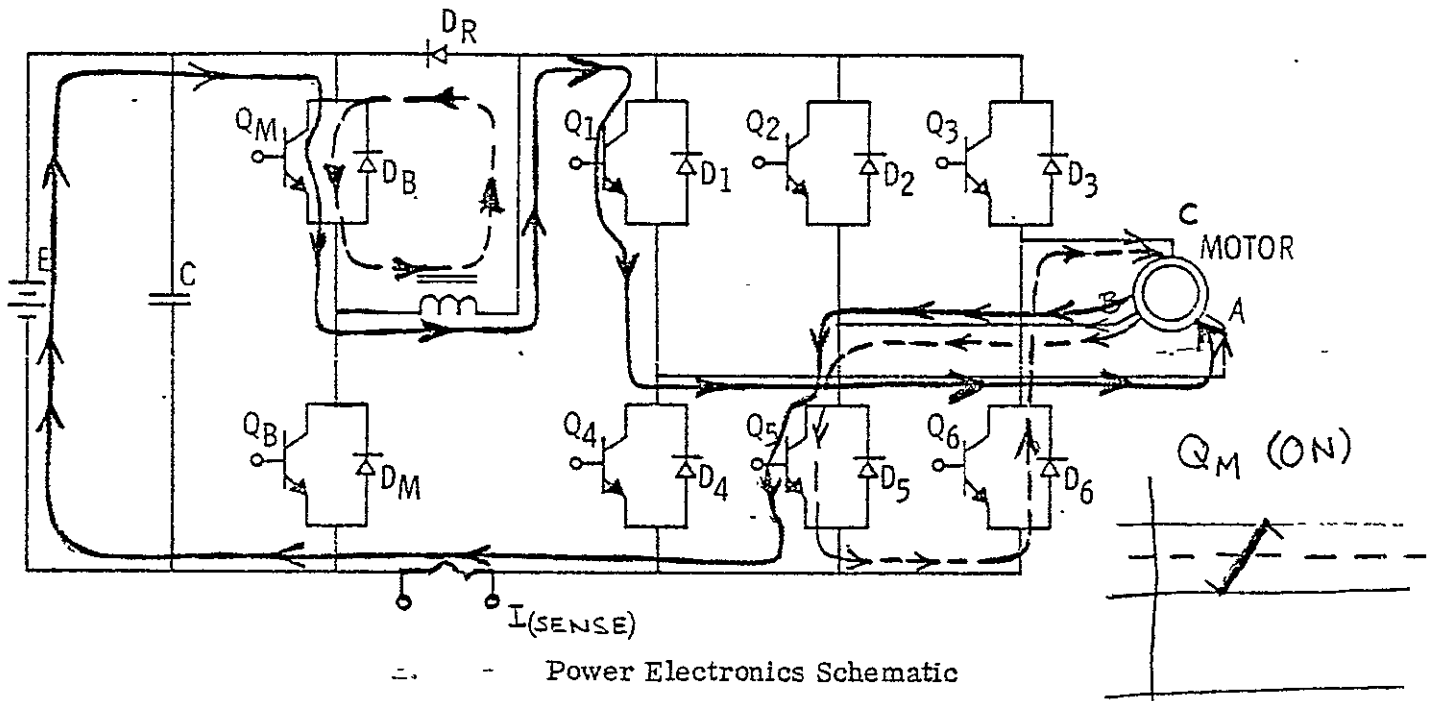
This report lays the foundation for the NASA/VPI analytical effort to model the dynamics of the brushless d.c. motor. The NASA/VPI effort consists of two stages. The first stage is a preliminary model which is based largely on the development described in this report. In this stage, a full account will be made of the various modes of operation including the torque-rotor angle position characteristics for the motor, generator, and brake. The second stage of the NASA/VPI effort will be directed towards detailed motor modeling. The work described earlier in this report will be instrumental in affecting the conceptual framework within which this detailed model will be developed. This report lays the outline of various tests to be conducted on the brushless d.c. motor to verify the analytical models. Also, this report outlines possible future investigative endeavors beyond the scope of the presently planned NASA/VPI effort.

9.0 BIBLIOGRAPHY

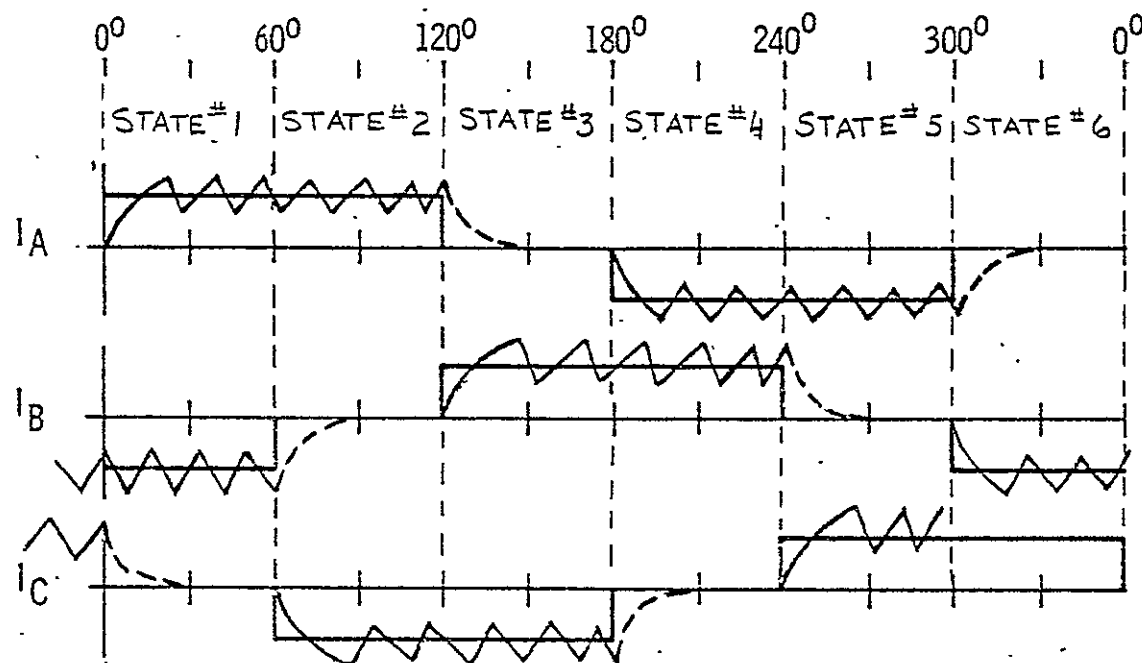
- (1) Sato, N., "A Brushless DC Motor with Armature Induced Voltage Commutation," IEEE Transactions on Industry and General Applications, 1972, pp 1485-1492.
- (2) Ramshaw, R. S., Power Electronics-Thyristor Controlled Power for Electric Motors, Chapman and Hall, London, 1973. (CH 5: Figure 5.4)
- (3) Fitzgerald, A. E., and Kingsley, C., Jr., Electric Machinery, 2nd Edition, McGraw-Hill, New York, 1961. (CH 3)
- (4) Electromechanical Flight Control Surface Actuation, Report No. S76-1, January 1976, Delco Electronics, Santa Barbara, California.
- (5) Motor and Power Electronics for an Electromechanical Actuator, Report No. R76-32, February 1976, Delco Electronics, Santa Barbara, California.
- (6) Edge, J. T., and Demerdash, N. A., "Trip Report on a Visit to Delco Electronics at Santa Barbara, California," Submitted to the NASA-JSC Control Systems Development Division Chief, August 12, 1976.
- (7) Dynamic Modeling of Brushless DC Motors for Aerospace Applications, An Unsolicited Proposal Submitted to NASA by Nabeel A. O. Demerdash, Virginia Polytechnic Institute and State University, December 1975.

(8) Demerdash, N. A., and Nehl, T. W., "Flexibility and Economics of Implementation of the Finite Element and Difference Techniques in Nonlinear Magnetic Fields of Power Devices," Paper No. 7D-2, Presented at the Joint MMM-International Magnetics Conference, Pittsburgh, June 15-18, 1976, To be published in the September 1976 Issue of IEEE Transactions on Magnetics.

(1)



ELECTRICAL ANGLE

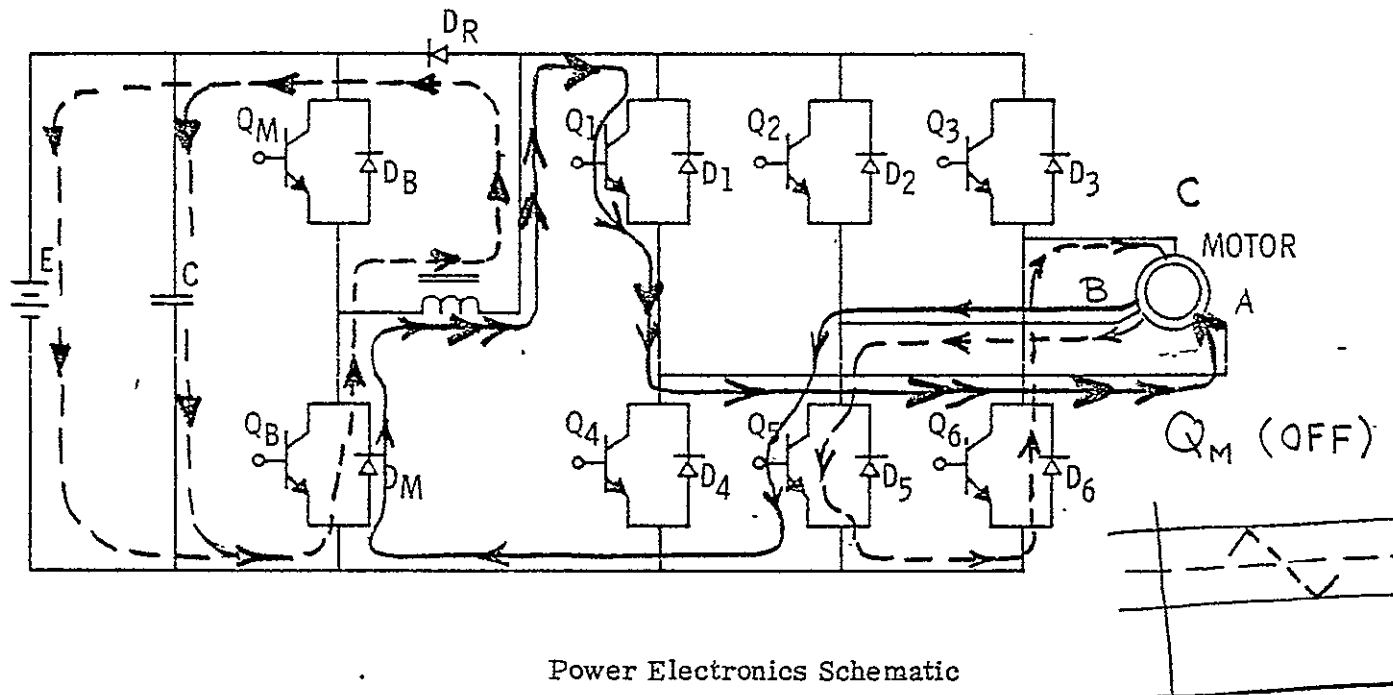


* STATE 1-(a) MODE #1

C. W. Demarest
July 1, 1976

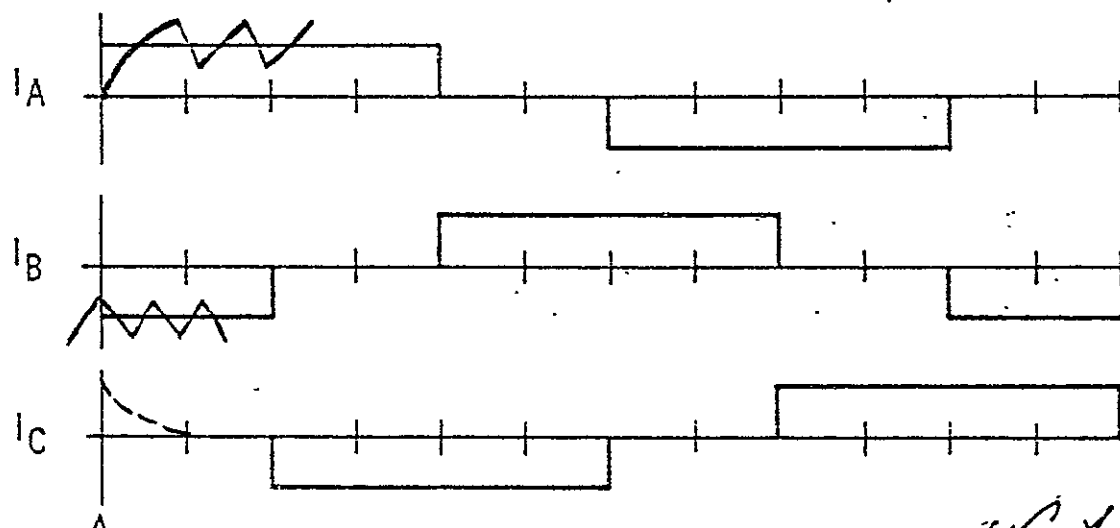
FIGURE(2-1) Mode (1) - St[#] 1-a

(2)



ELECTRICAL ANGLE

0° 60° 120° 180° 240° 300° 0°



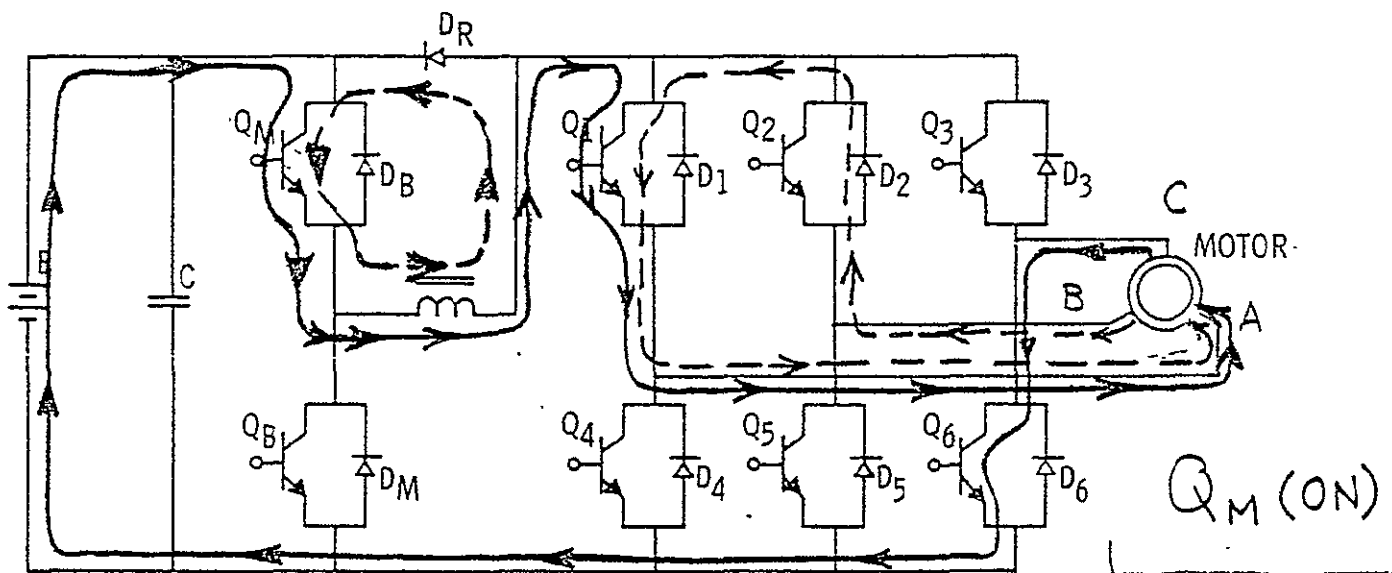
Idealized Motor Phase Currents

* STATE 1-(b) - MODE #1

R. A. Denclash
July 1, 1976
2

FIG.(2-2) Mode(1)-St[#]1-b

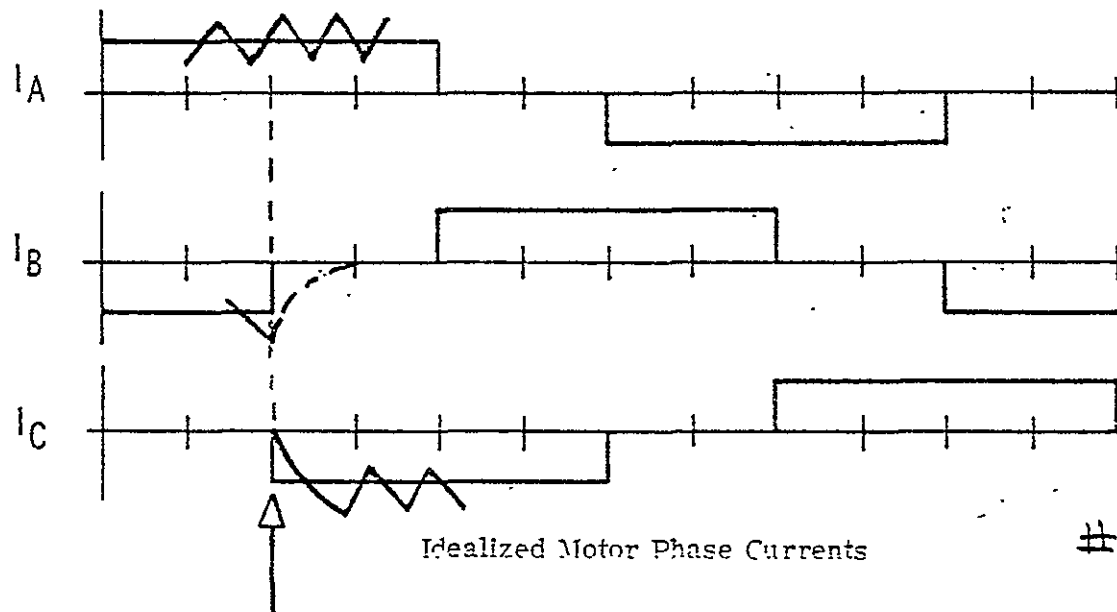
(3)



Power Electronics Schematic

ELECTRICAL ANGLE

0° 60° 120° 180° 240° 300° 0°



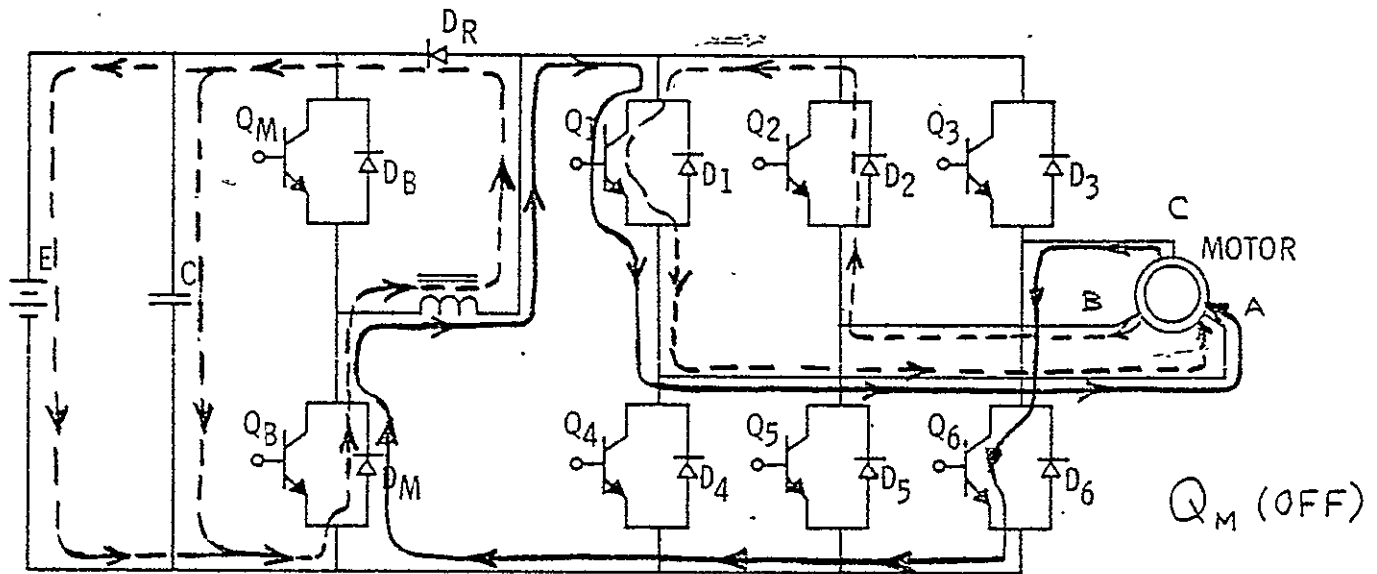
3

* STATE 2-(a)

FIG.(2-3) Mode(1)-St2-a

c.v.s. demanded
July 1, 1976

(4)



Power Electronics Schematic

ELECTRICAL ANGLE

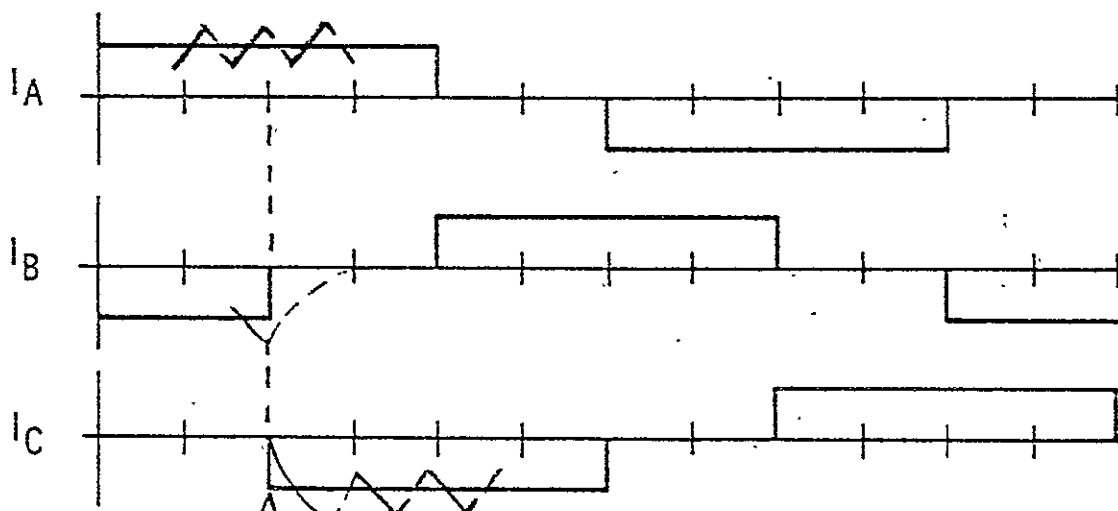
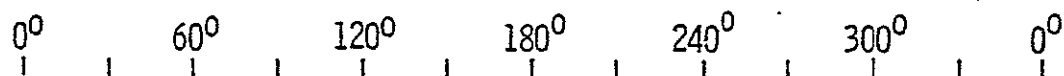


Figure 1-5. Idealized Motor Phase Currents

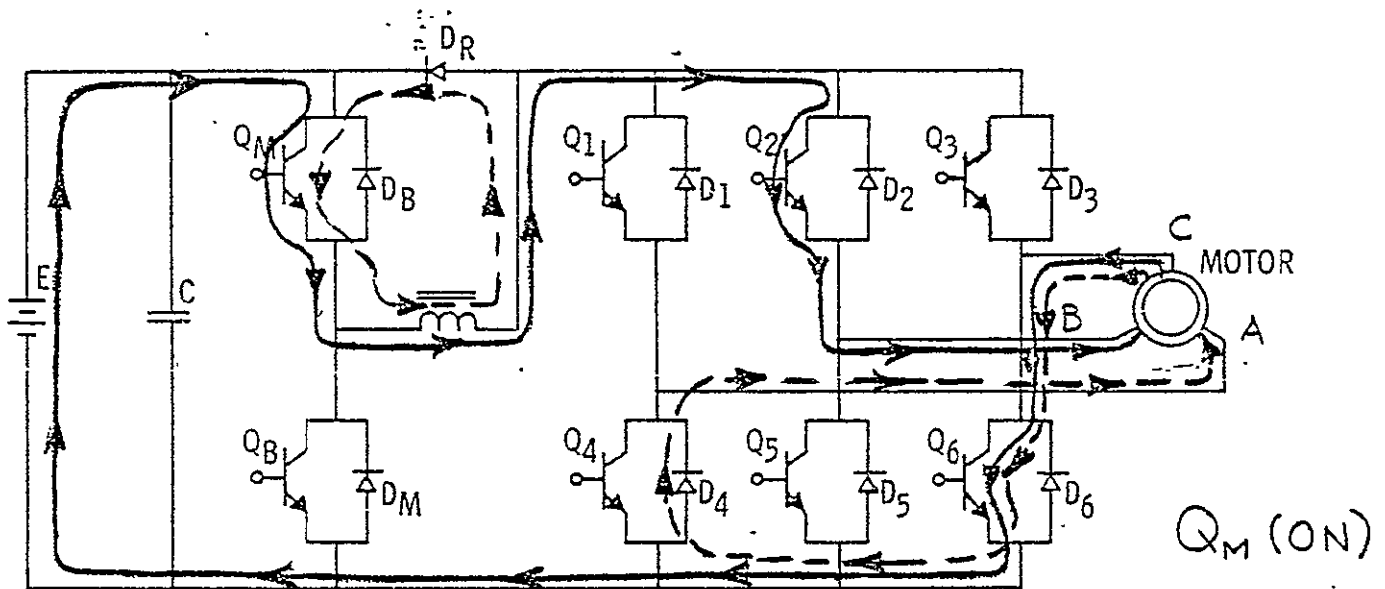
4

* STATE 2-(b)

FIG.(2-4) Mode(1)-St[#]_{2-b}

w. A. Demerdash
July 1, 1976

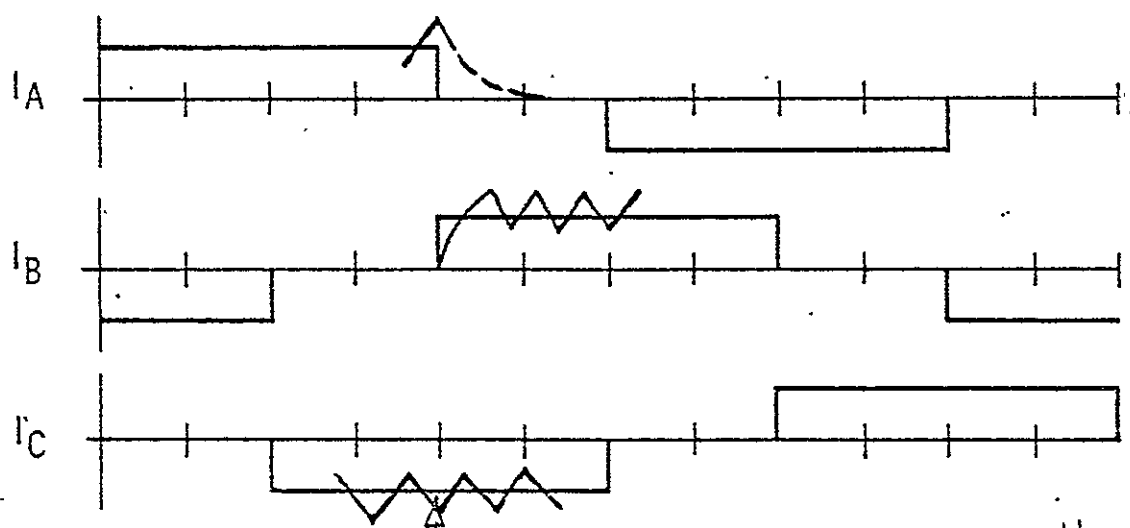
(5)



Power Electronics Schematic

ELECTRICAL ANGLE

0° 60° 120° 180° 240° 300° 0°

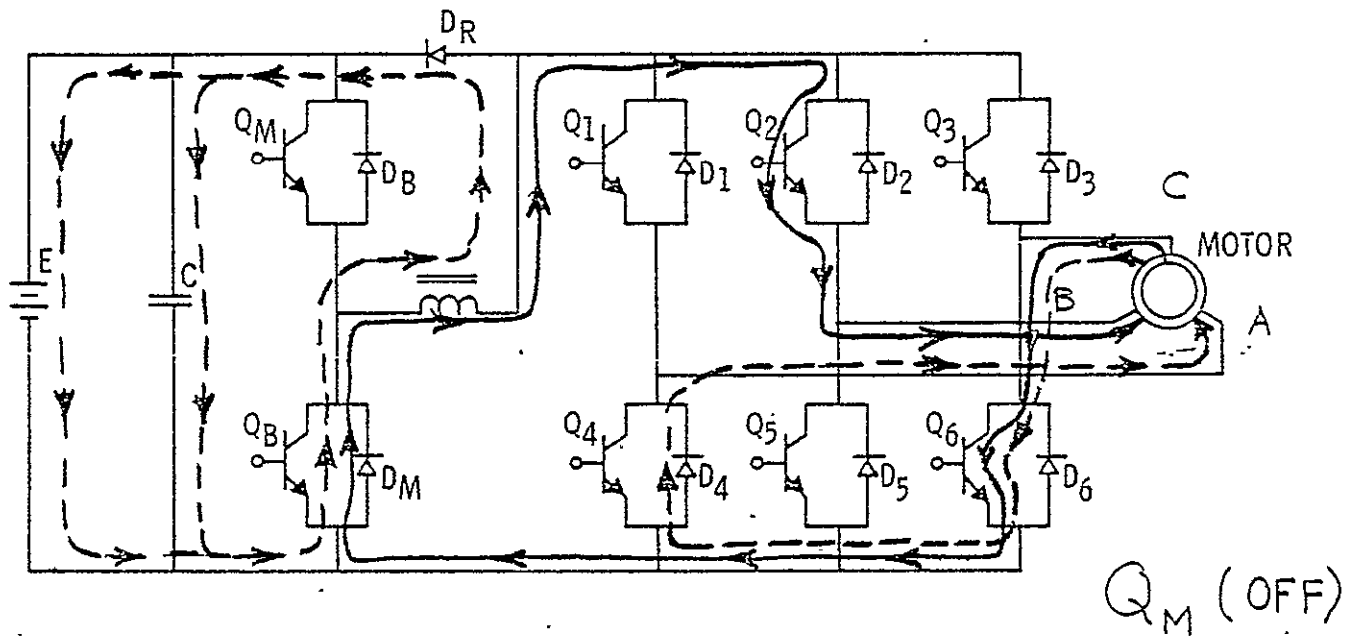


* STATE 3 - (a)

5

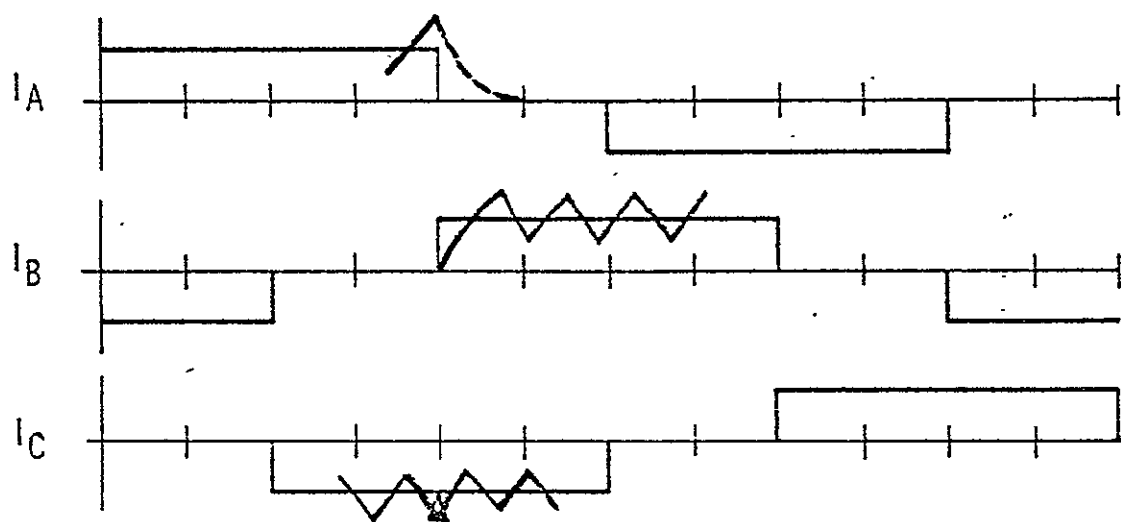
FIG.(2-5) Mode (1)-St[#]_{3-a} *c.v. A. Demerdash*
July 1, 1976

(6)



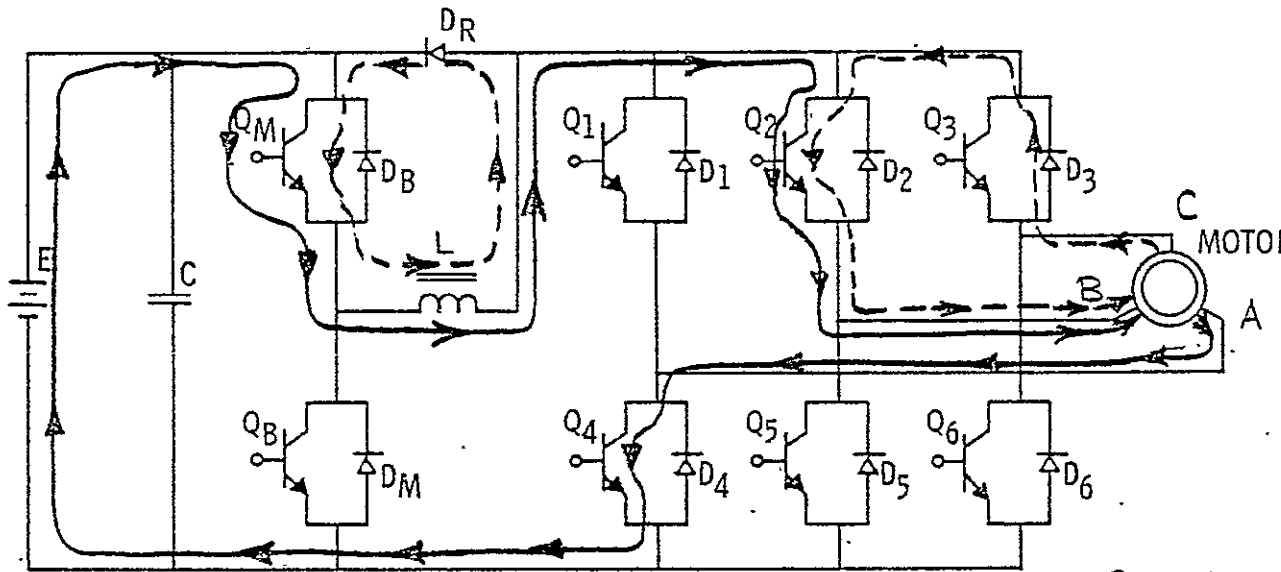
ELECTRICAL ANGLE

0° 60° 120° 180° 240° 300° 0°



* STATE 3 - (b) #6
 FIG.(2-6) Mode(1)-st[#]3-b w. A. Demendash
 July 1, 1976

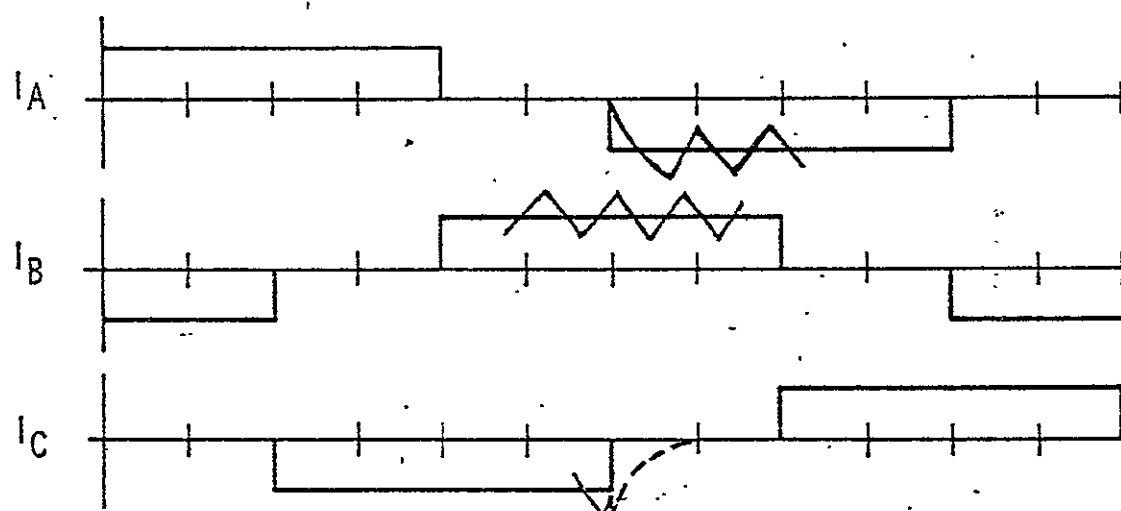
(7)

 Q_M (ON)

Power Electronics Schematic

ELECTRICAL ANGLE

0° 60° 120° 180° 240° 300° 0°



Idealized Motor Phase Currents

7

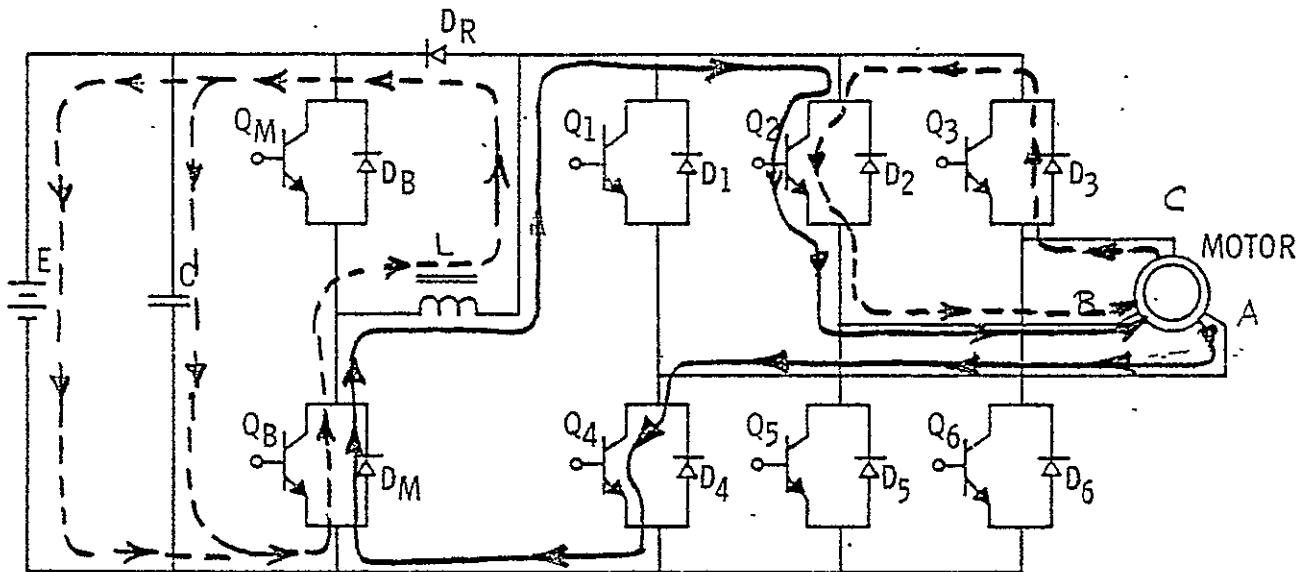
* STATE 4-(a)

FIG.(2-7) Mode(1)-St#4-a

29

W. A. Demendach
July 1, 1976

(8)

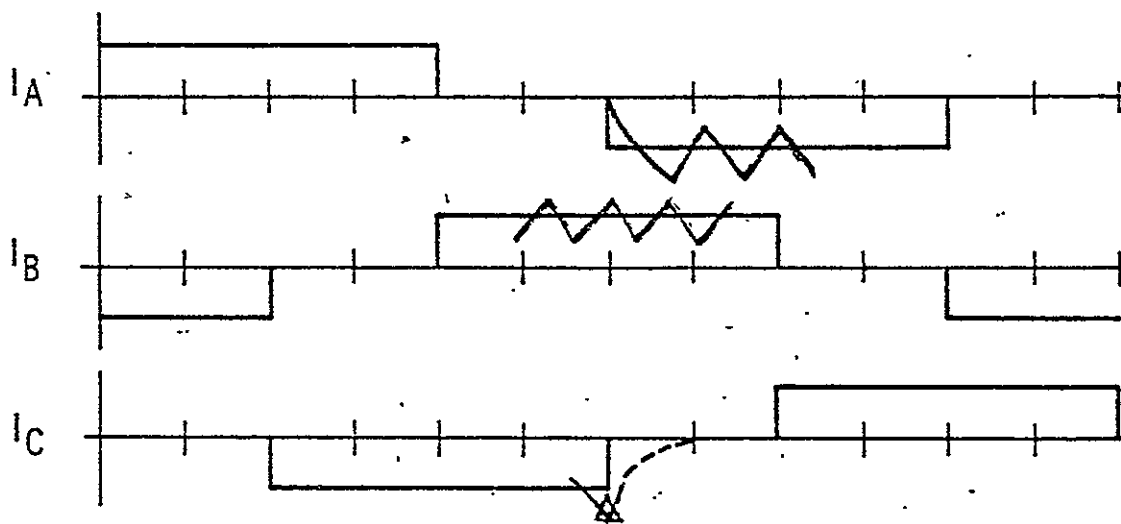


Q_M (OFF)

Power Electronics Schematic

ELECTRICAL ANGLE

0° 60° 120° 180° 240° 300° 0°



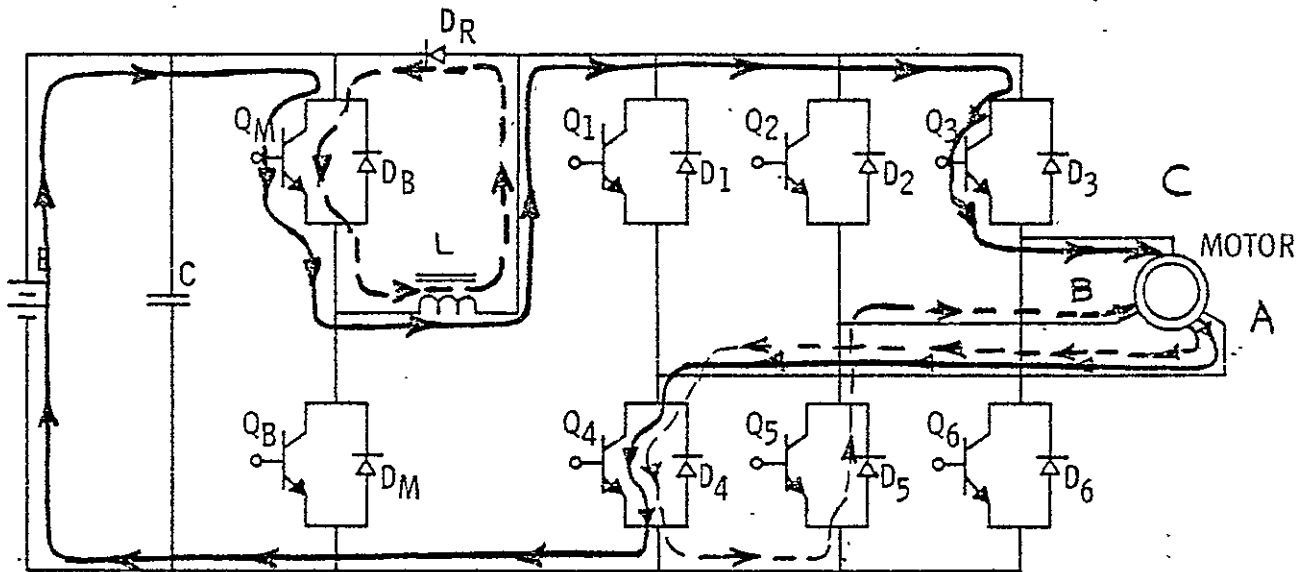
Idealized Motor Phase Currents

8

* STATE 4 - (b)
FIG.(z-8) Mode (1)-St#4-b
30

W. A. Demirchian
July 1, 1976

(9)

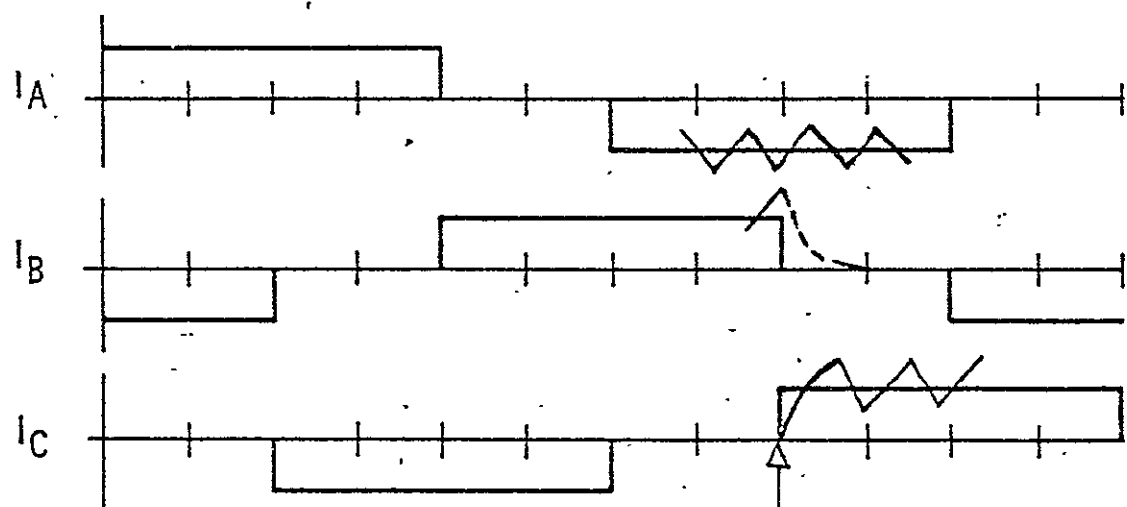


Q_M (ON)

Power Electronics Schematic

ELECTRICAL ANGLE

0° 60° 120° 180° 240° 300° 0°



Idealized Motor Phase Currents

9

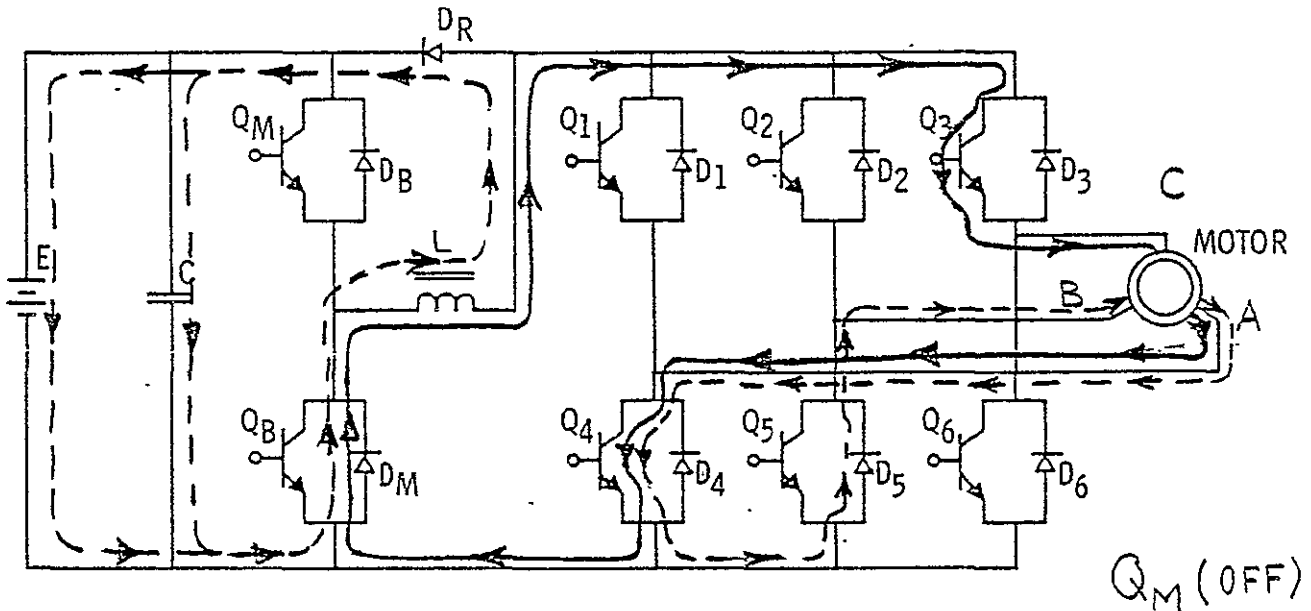
FIG.(2-9) Mode(1)-St[#]_{5-a}

31

* STATE 5-(a)

w. A. Demender
July 1, 1976

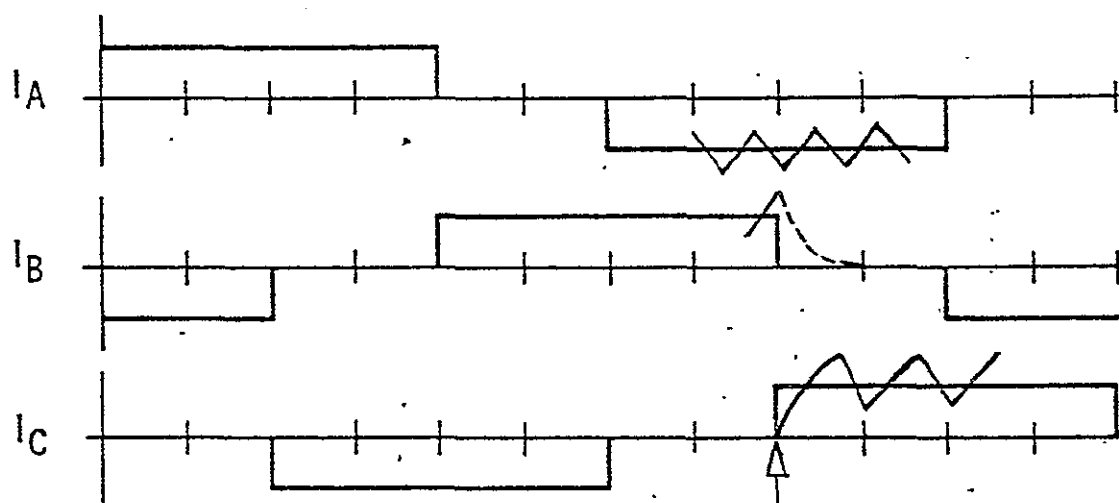
10



Power Electronics Schematic

ELECTRICAL ANGLE.

0° 60° 120° 180° 240° 300° 0°

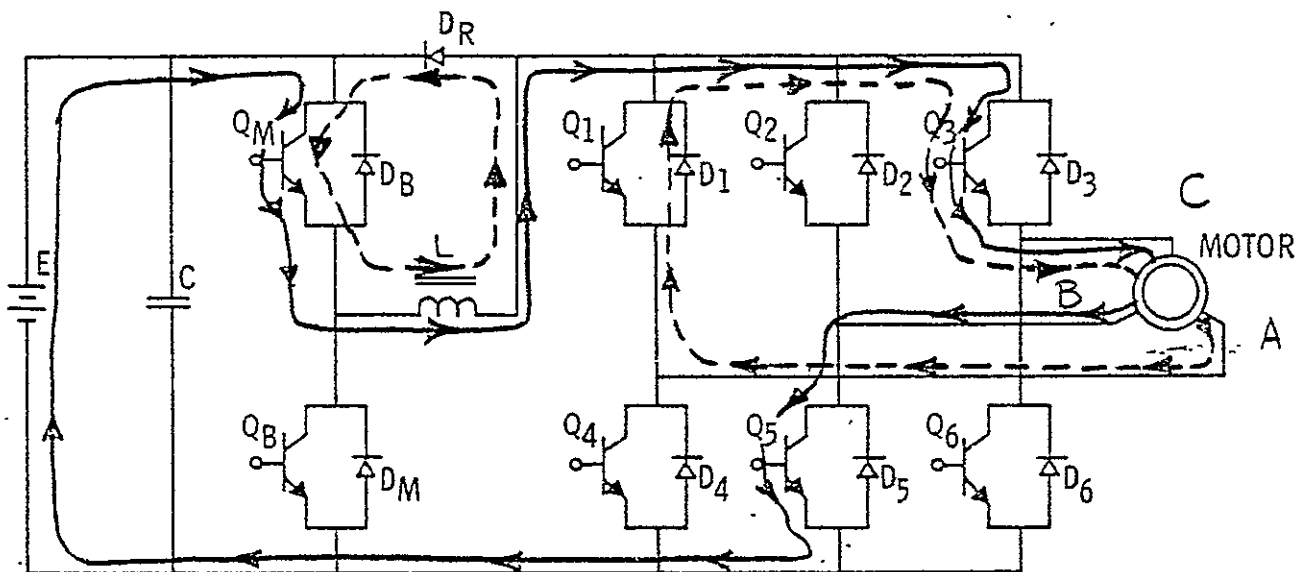


Idealized Motor Phase Currents

10

FIG.(z-10) Mode(1)-St[#]_{5-b} STATE 5 - (b)

(11)

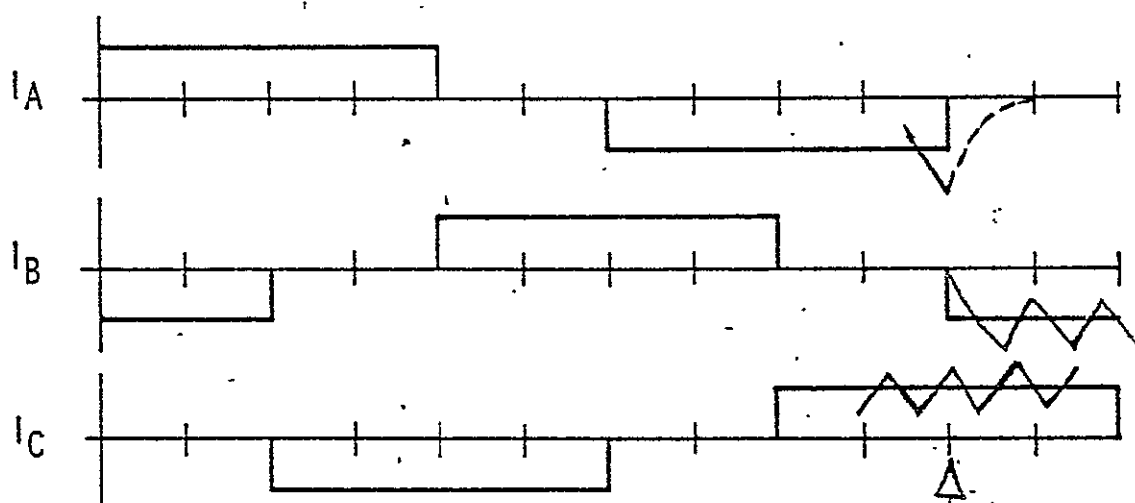


Q_M (ON)

Power Electronics Schematic

ELECTRICAL ANGLE

0° 60° 120° 180° 240° 300° 0°

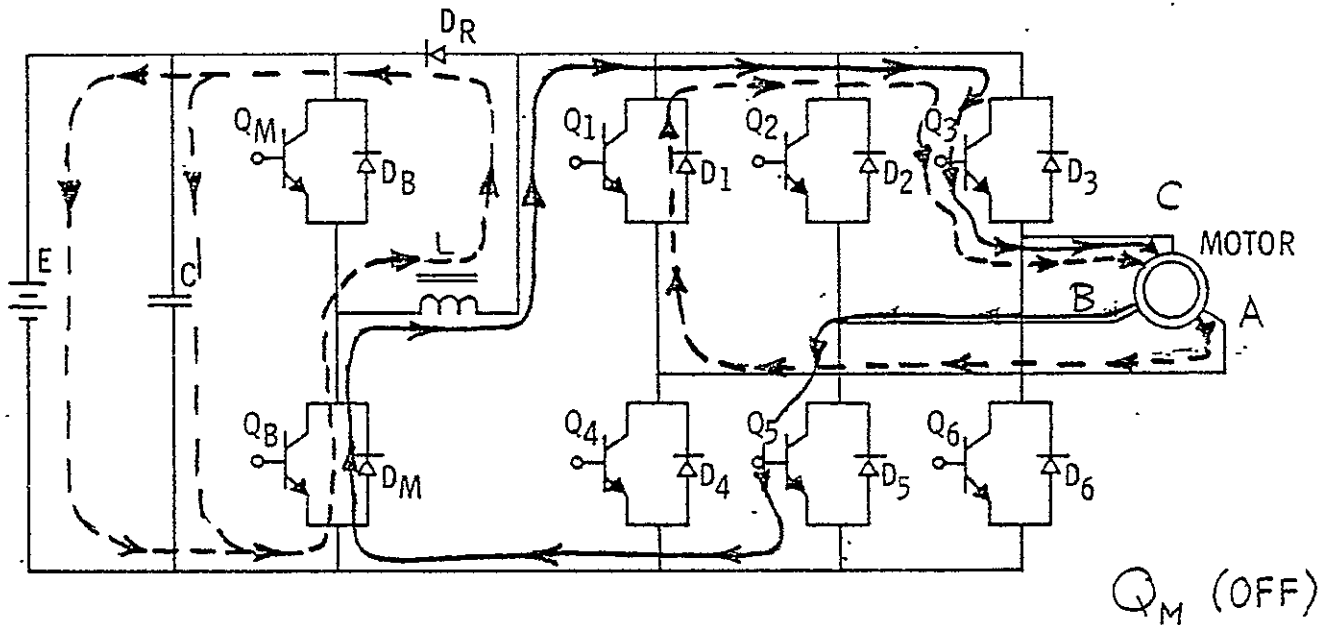


Idealized Motor Phase Currents

FIG.(z-11) Mode(1)-St[#]6-a STATE 6-(a)

Dr. A. Demircioglu
July 1, 1976

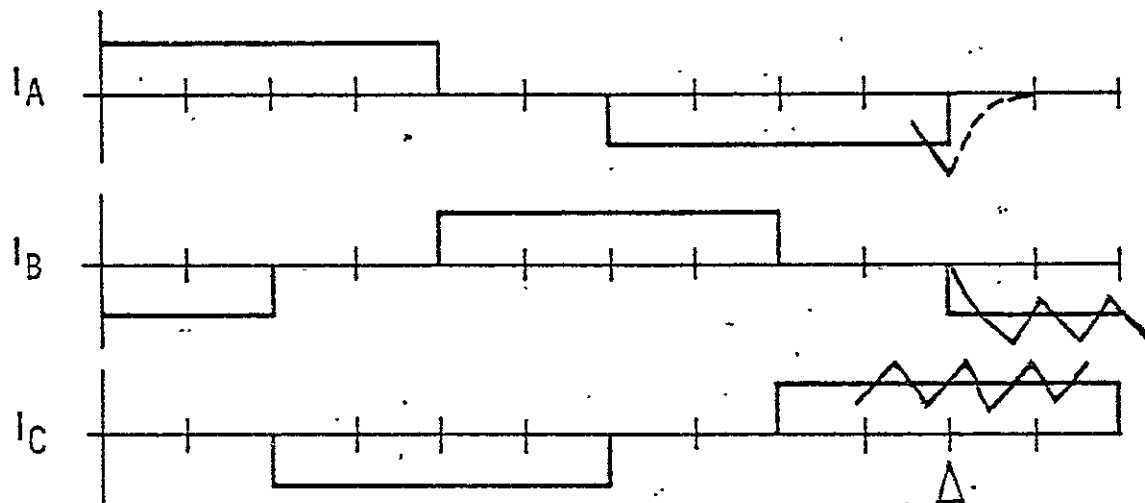
12



Power Electronics Schematic

ELECTRICAL ANGLE

0° 60° 120° 180° 240° 300° 0°

FIG.(2-12) Mode(1)-St[#] 6-b

TRANSISTOR SWITCHING SEQUENCE

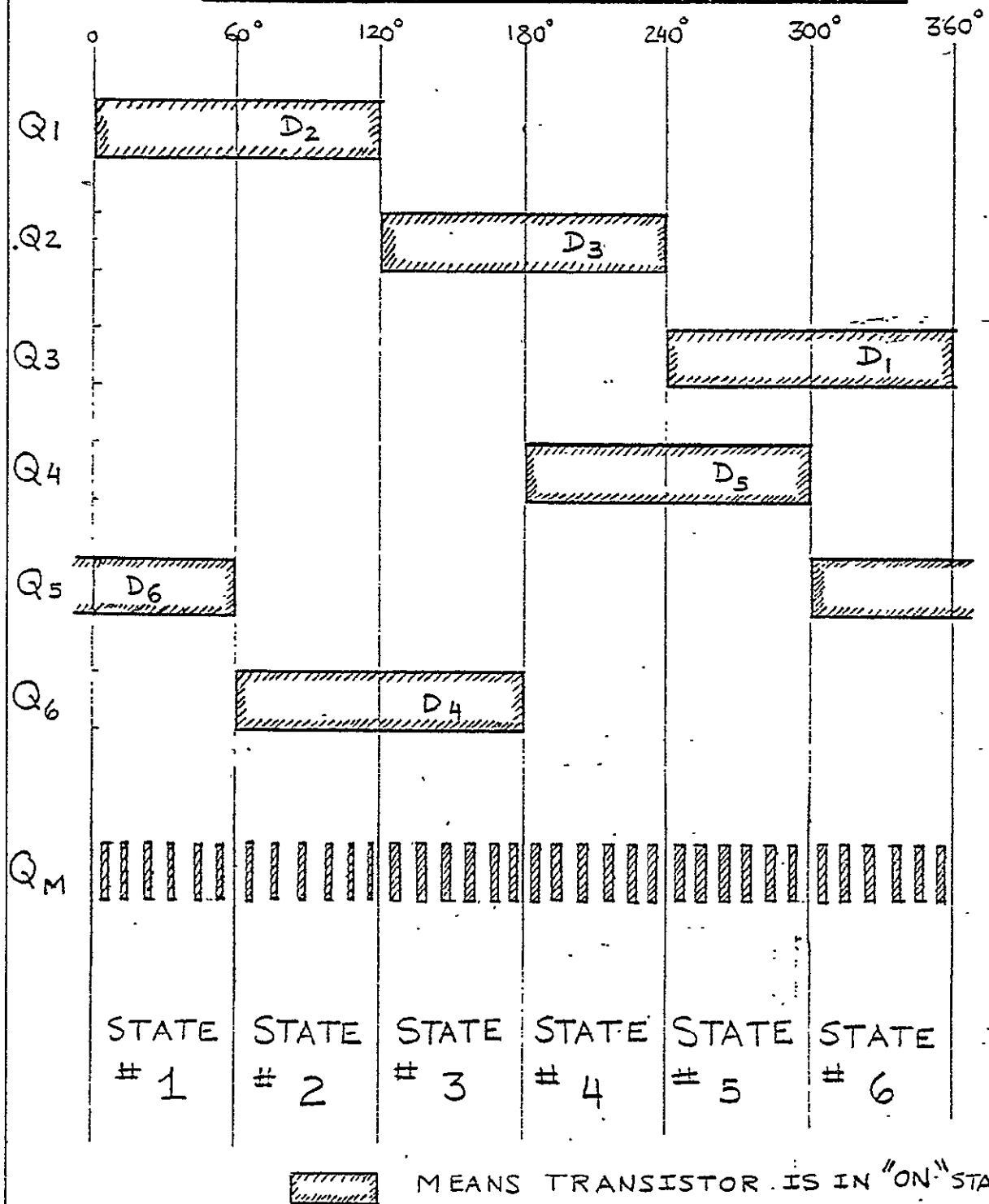
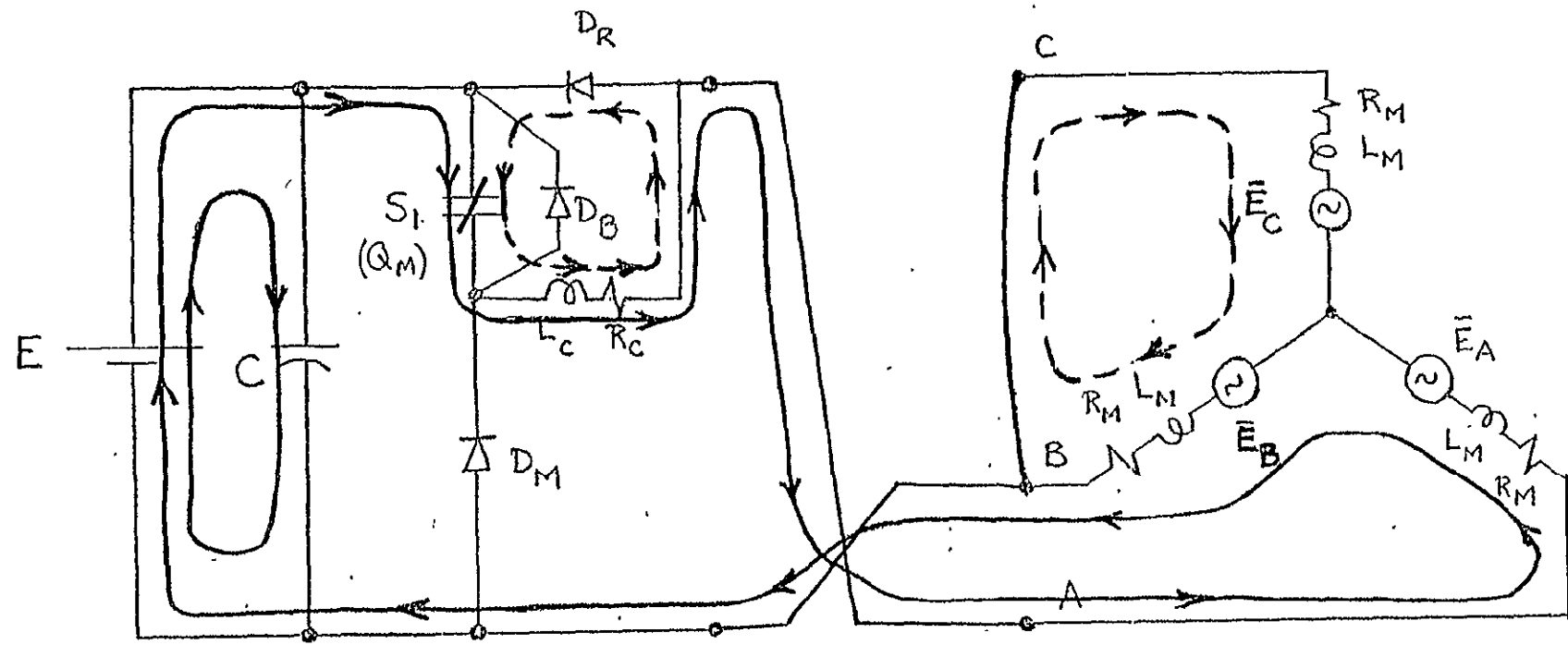


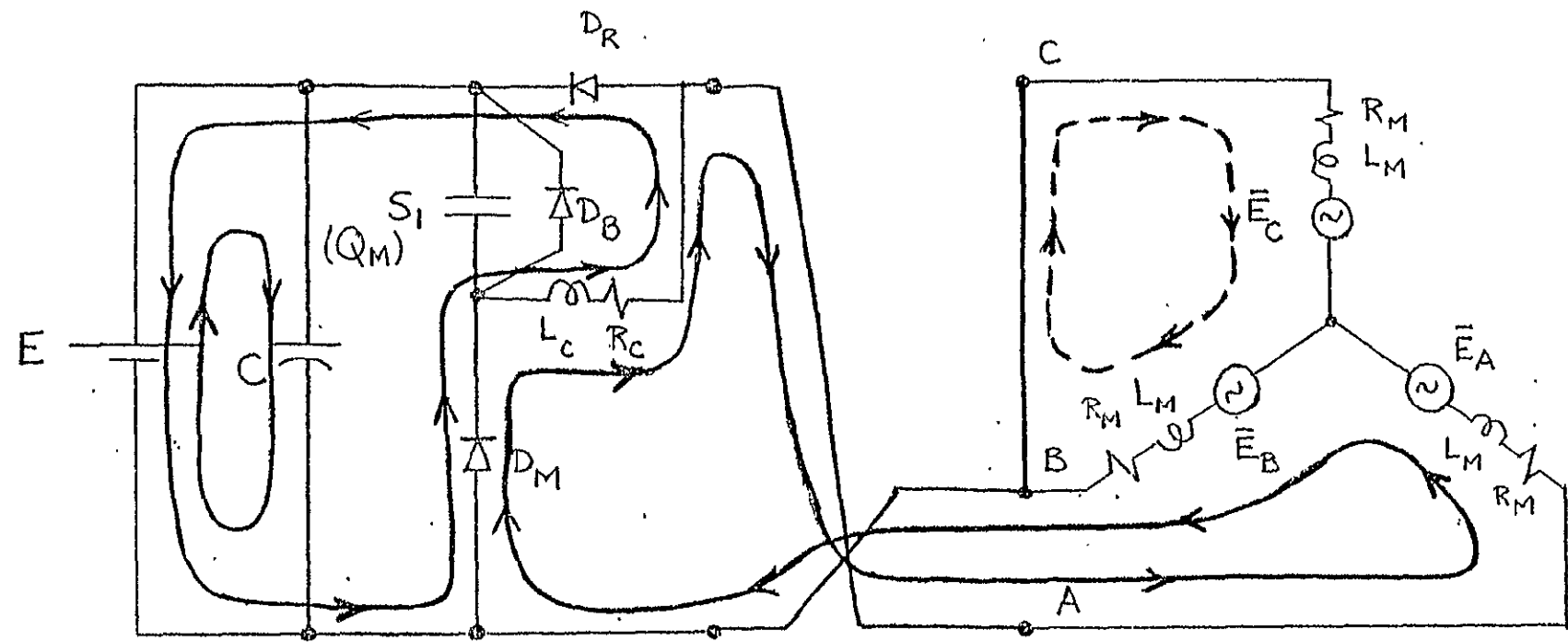
FIG.(2-13) TRANSISTOR SWITCHING SEQUENCE
MODE (1) - MOTOR



STATE # 1 - (a) : Q_M (ON)

FIG. (2-14) Loops - Mode(1) - St[#] 1-a!

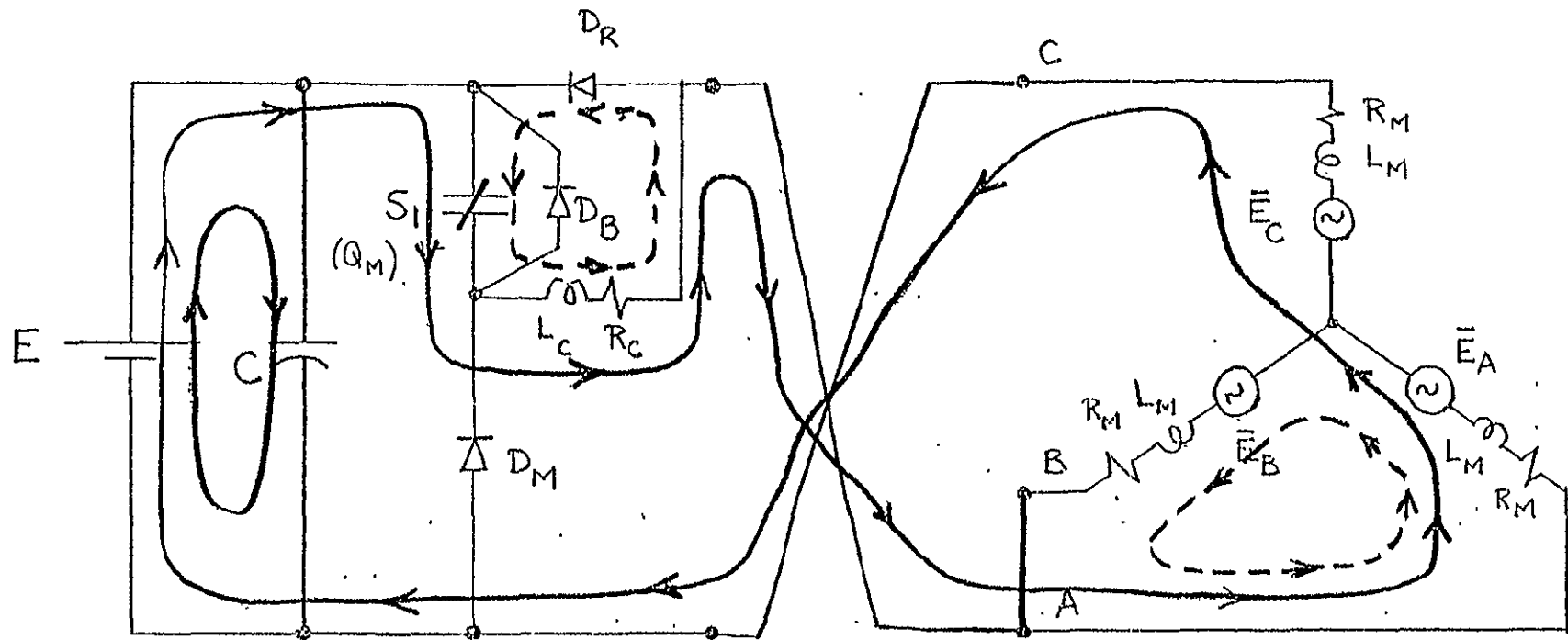
C.V. St. Demetrich
July 1, 1976



STATE $\#$ 1 - (b) Q_M (OFF)

FIG.(2-15) Loops - Mode(1) - St $\#$ 1-b

W. H. DeMondash
July 7, 1976

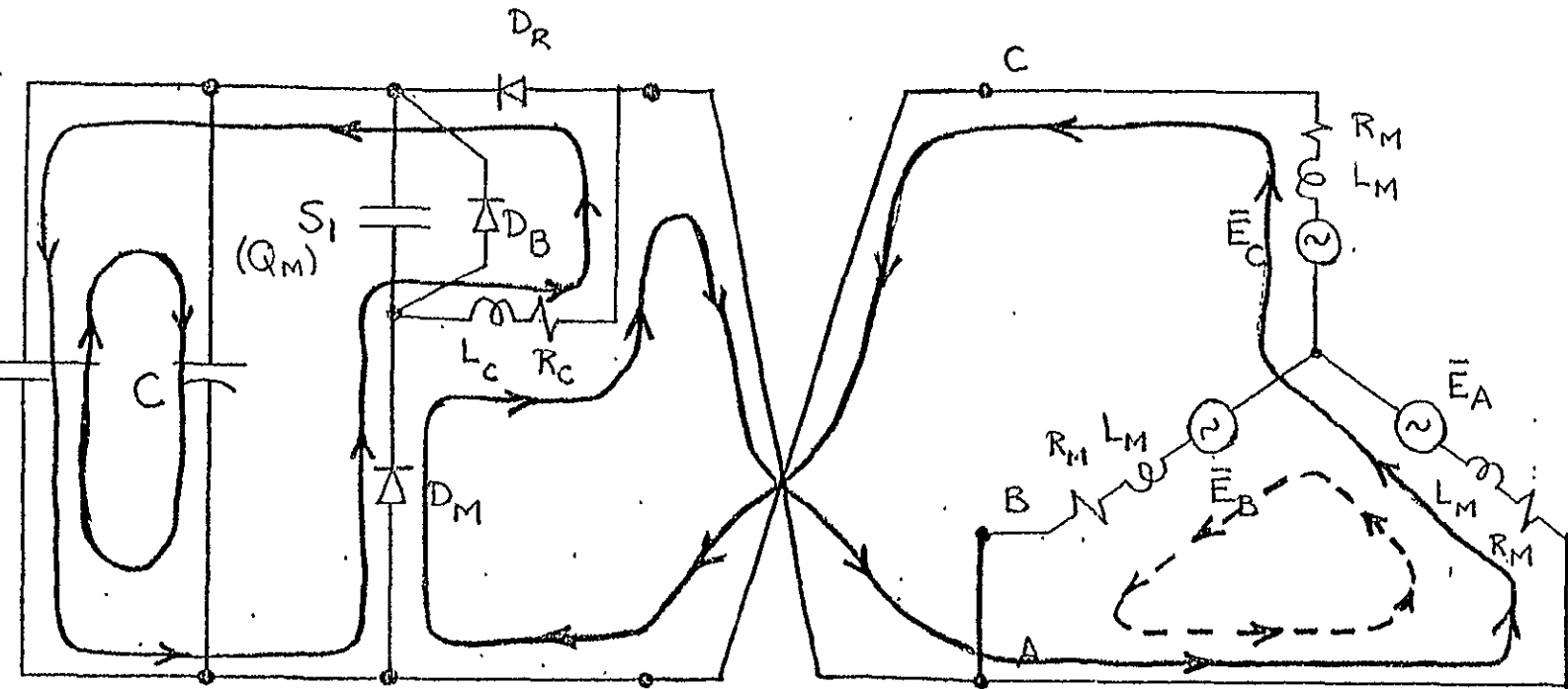


STATE # 2 - (a) , Q_M (ON)

FIG.(z-16) Loops - Mode(1) - St[#] 2-a

G.V.R. Venkatesh
July 7, 1976

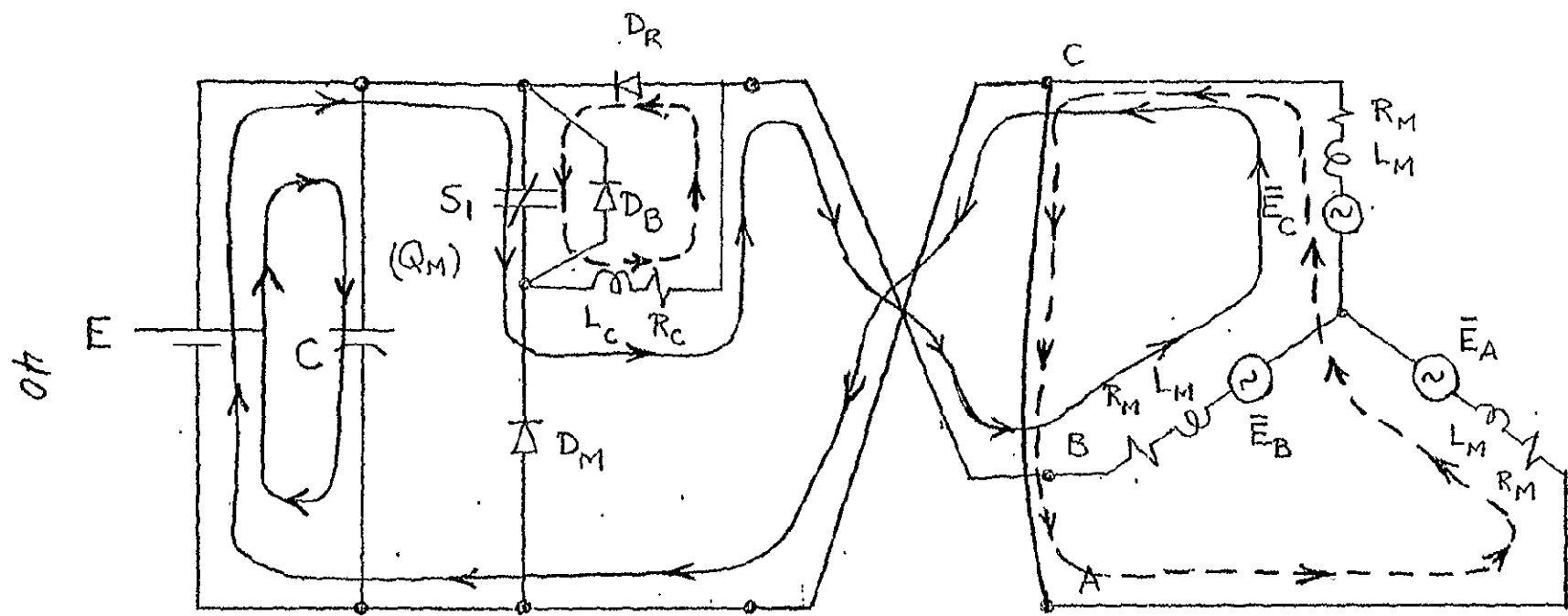
65



STATE $\#$ 2 - (b) Q_M (OFF)

FIG.(2-17) Loops - Mode(1) - St $\#$ 2-b

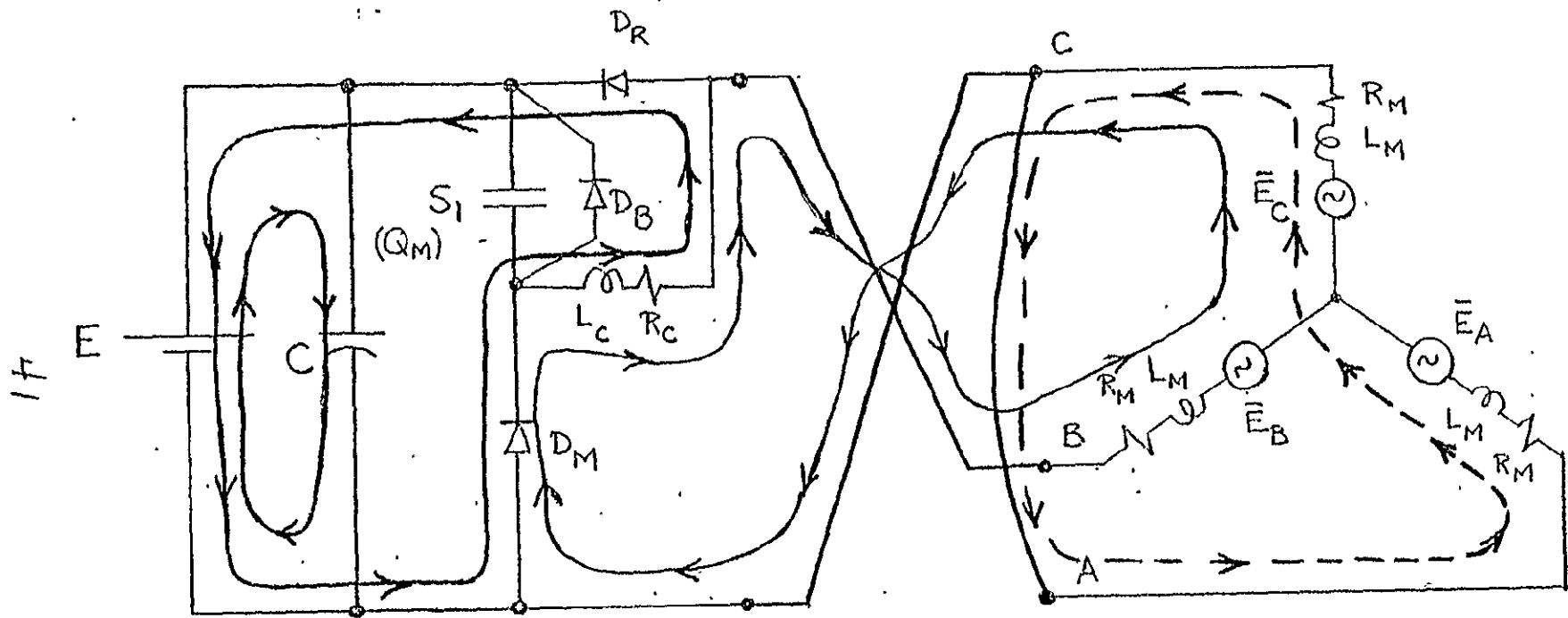
W. H. Demendash
July 7, 1976



STATE [#] 3 - (a) , Q_M (ON)

FIG.(2-18) Loops - Mode(1) - St[#] 3-a

C. A. Dimiceli
July 7, 1976

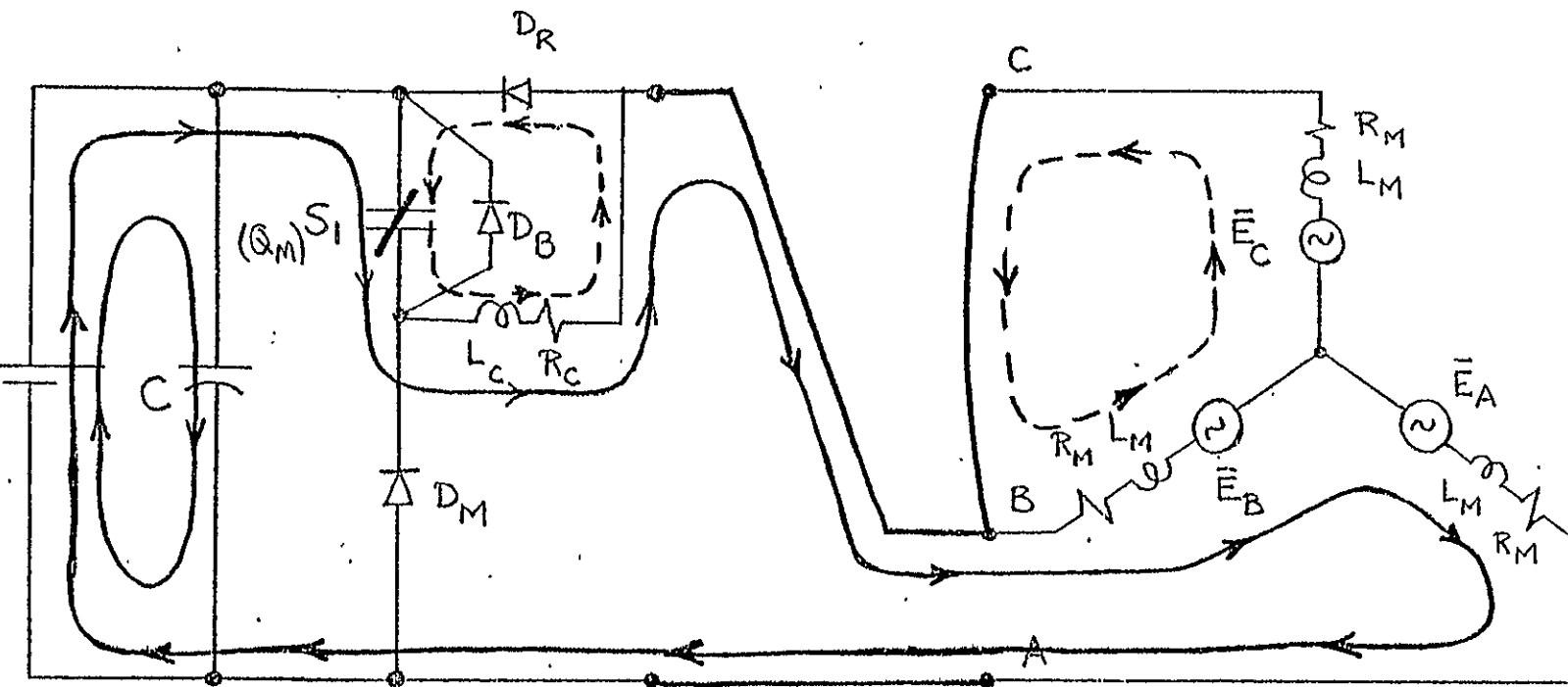


STATE # 3 - (b) Q_M (OFF)

FIG.(2-19) Loops - Mode (1)- St[#] 3-b

W. C. Demedas
July 7, 1976

42

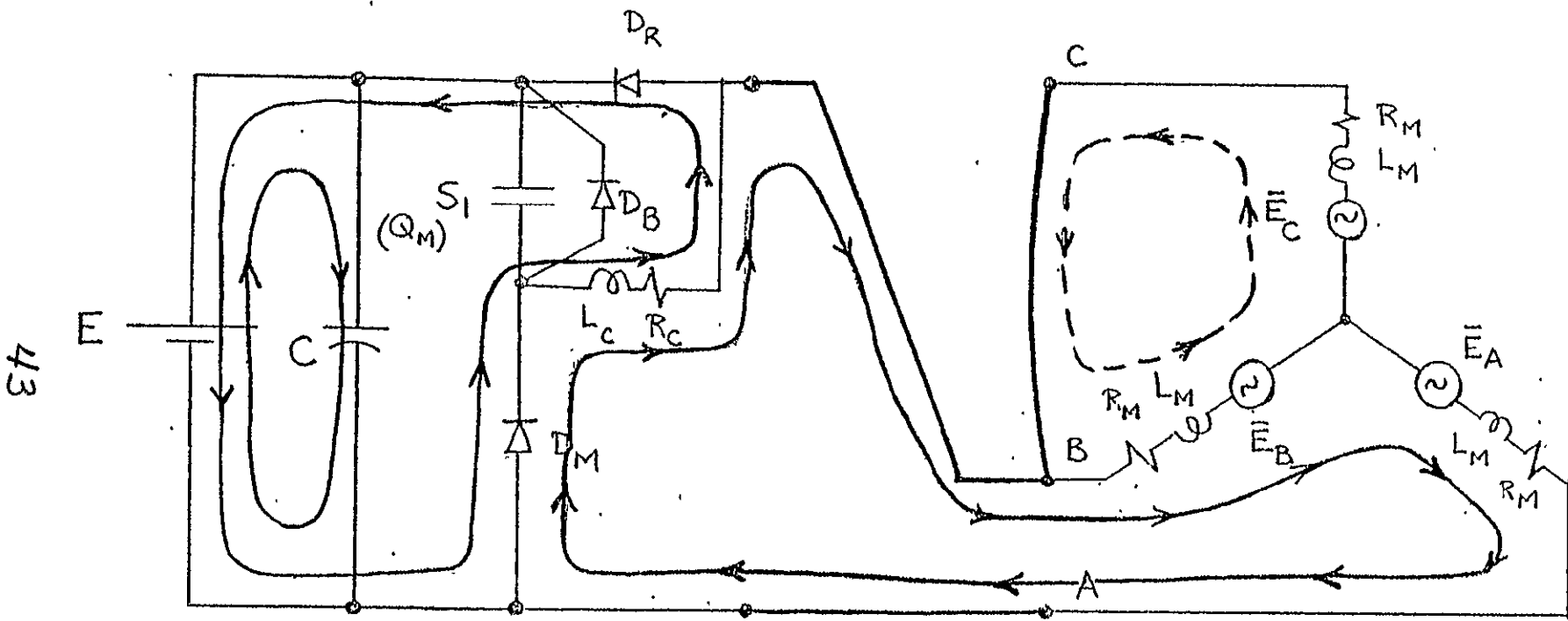


STATE $\#$ 4 - (a)

Q_M (ON)

FIG.(2-20) Loops - Mode (1) - St. $\#$ 4-a

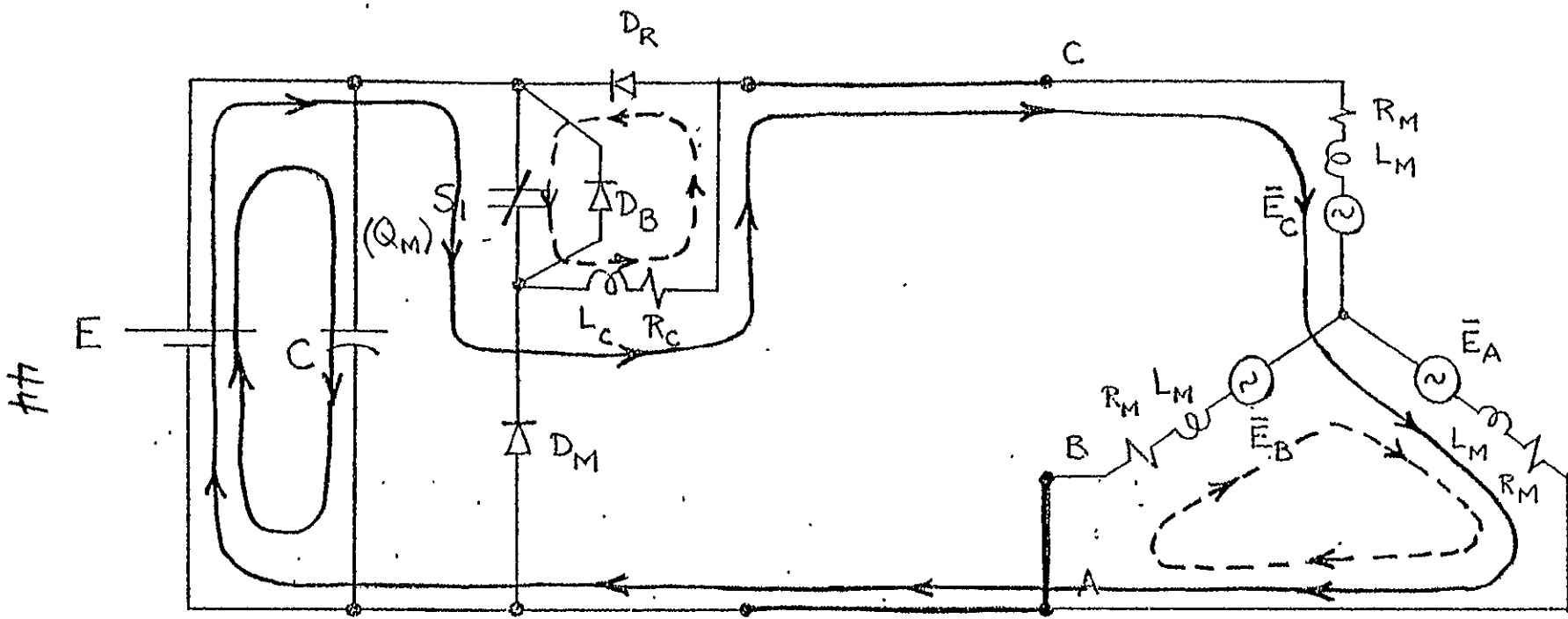
W. H. Demarest
July 7, 1976



STATE # 4 - (b) Q_M (OFF)

FIG.(2-21) Loops- Mode(1) - St. 4-b

W.A. Demarsash
July 7, 1976

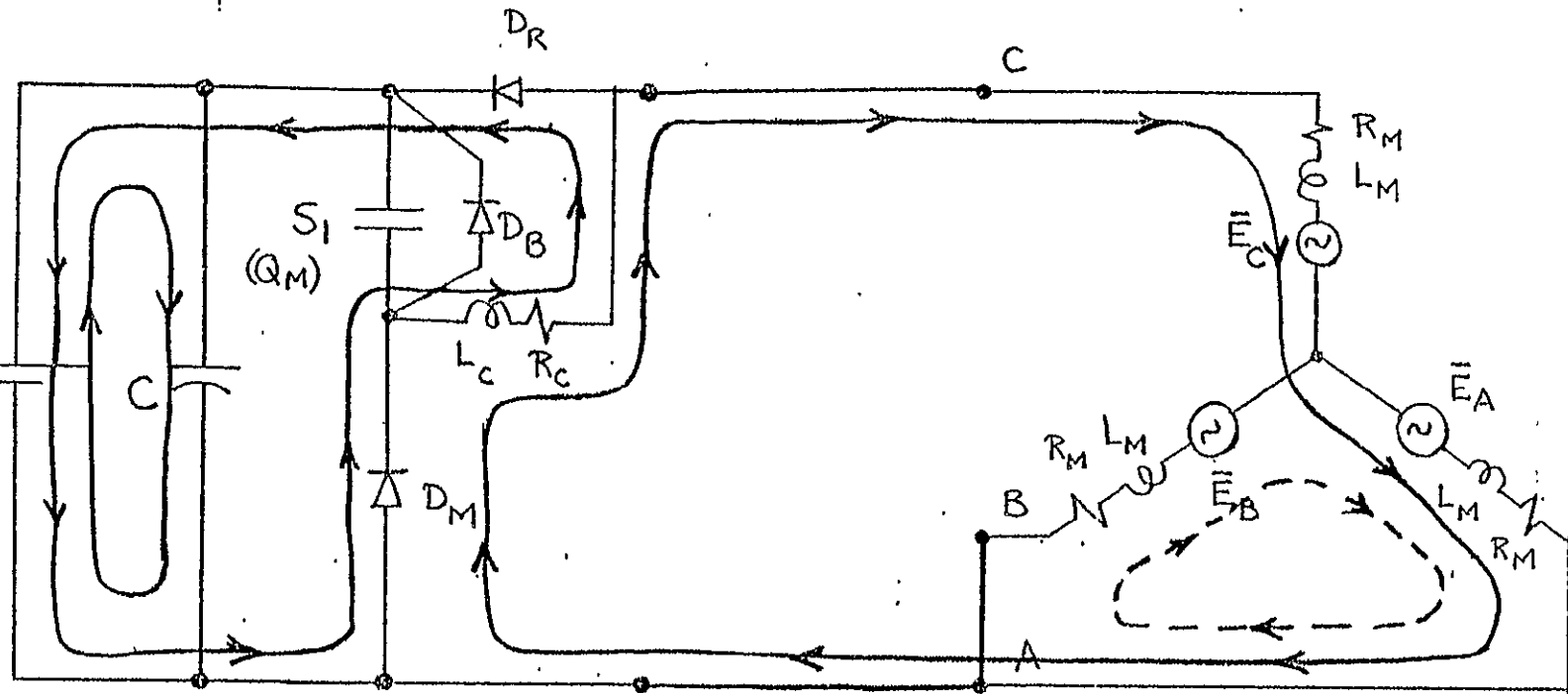


STATE # 5 - (a) Q_M (ON)

FIG.(2-22) Loops - Mode(1) - St # 5-a

W. A. Demarest
July 7, 1976

St

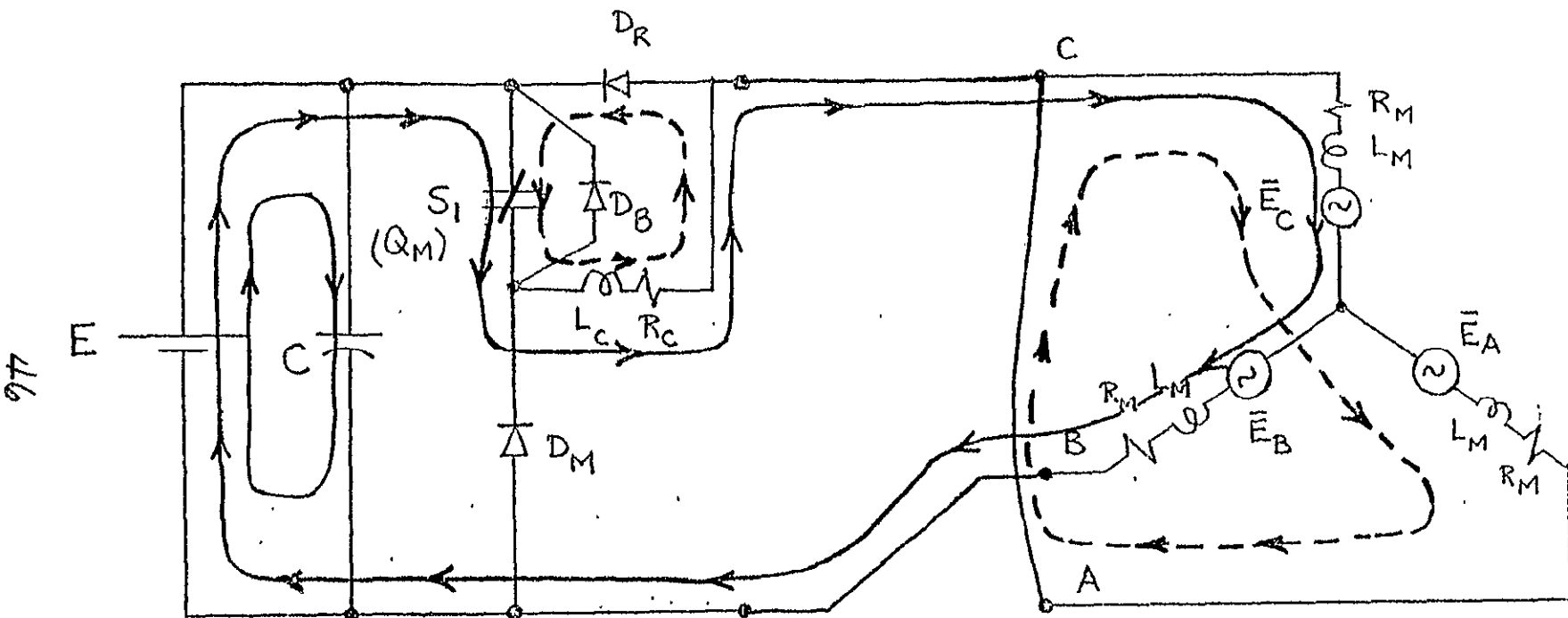


STATE [#] 5 - (b)

Q_M (OFF)

FIG.(2-23) Loops - Mode(1) - St[#] 5-b

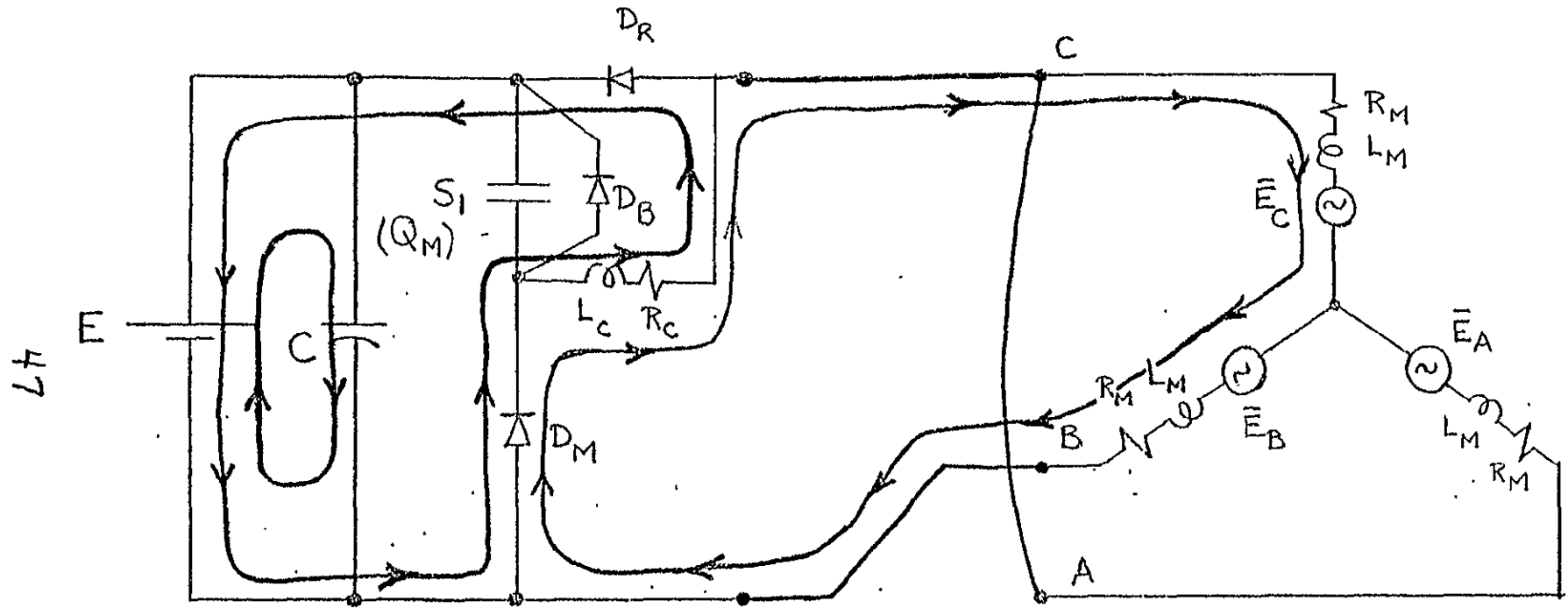
W.A. Dennerback
July 7, 1976



STATE $\#6 - (a)$ Q_M (ON)

FIG.(z-24) Loops - Mode(1) - St $\#6-a$

C. H. Demarest
July 7, 1976



STATE [#] 6 - (b) Q_M (OFF)

FIG.(2-25) Loops - Mode (1) - St[#] 6-b

W. X. Demerdash
July 7, 1976

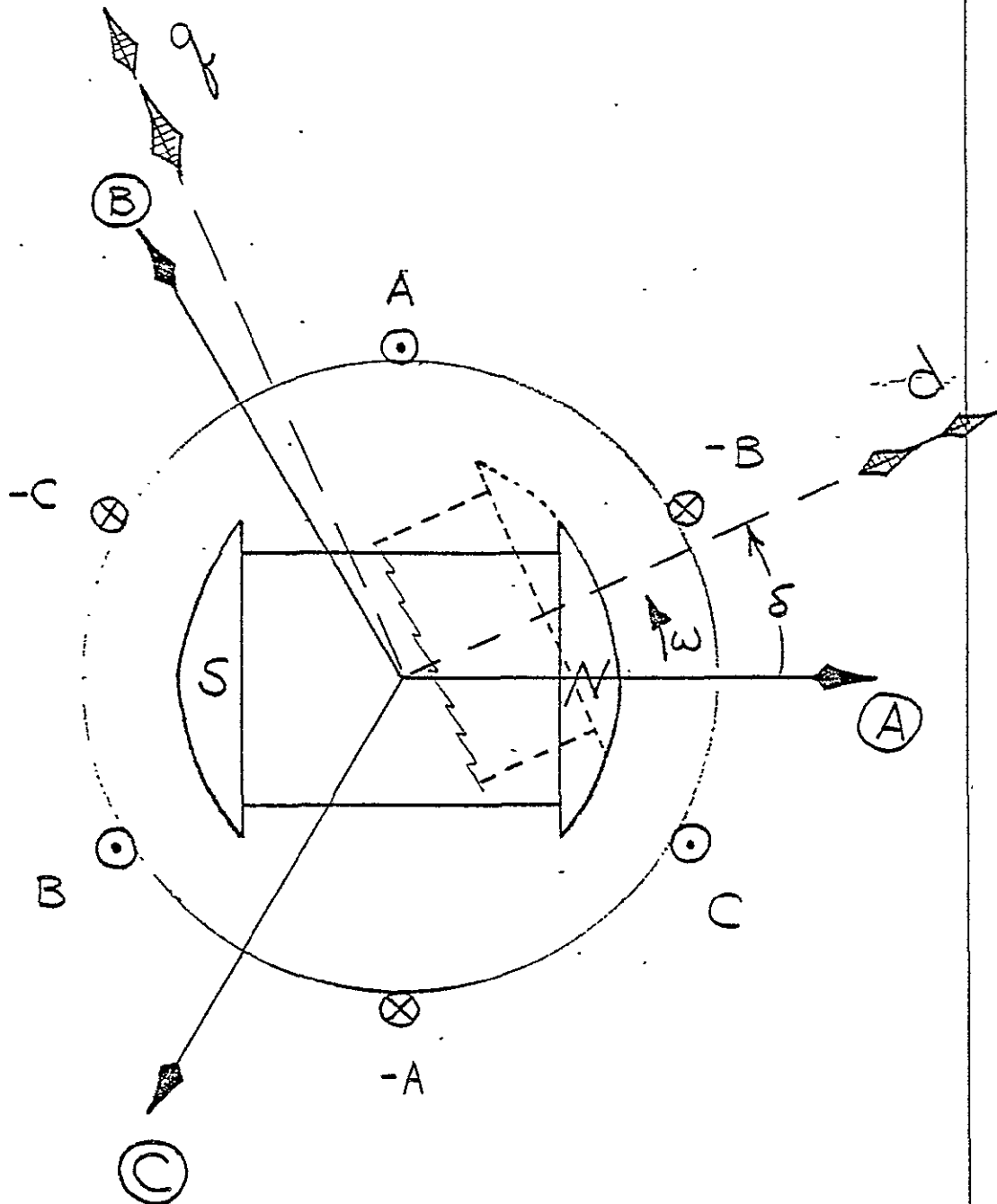
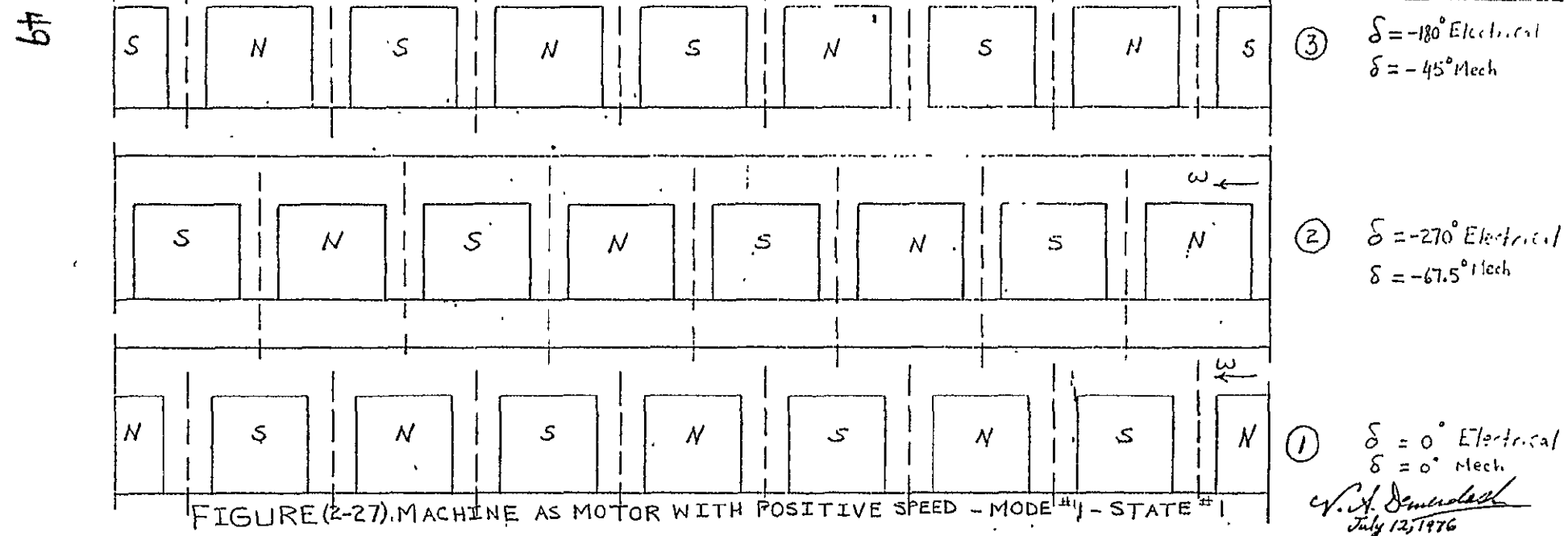
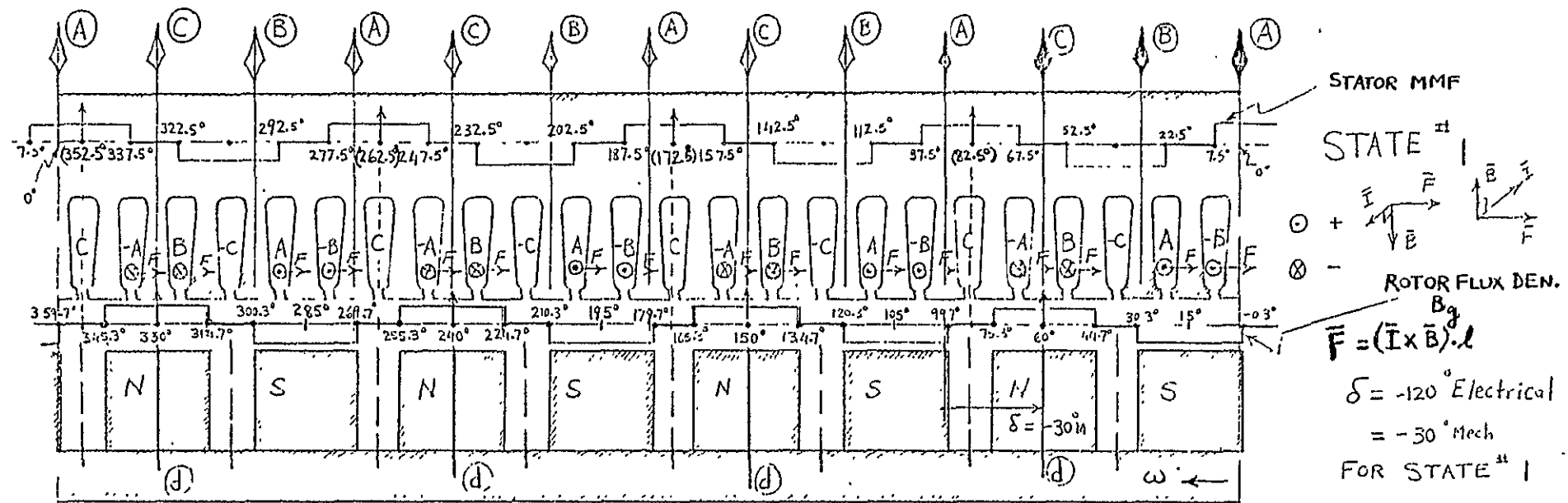
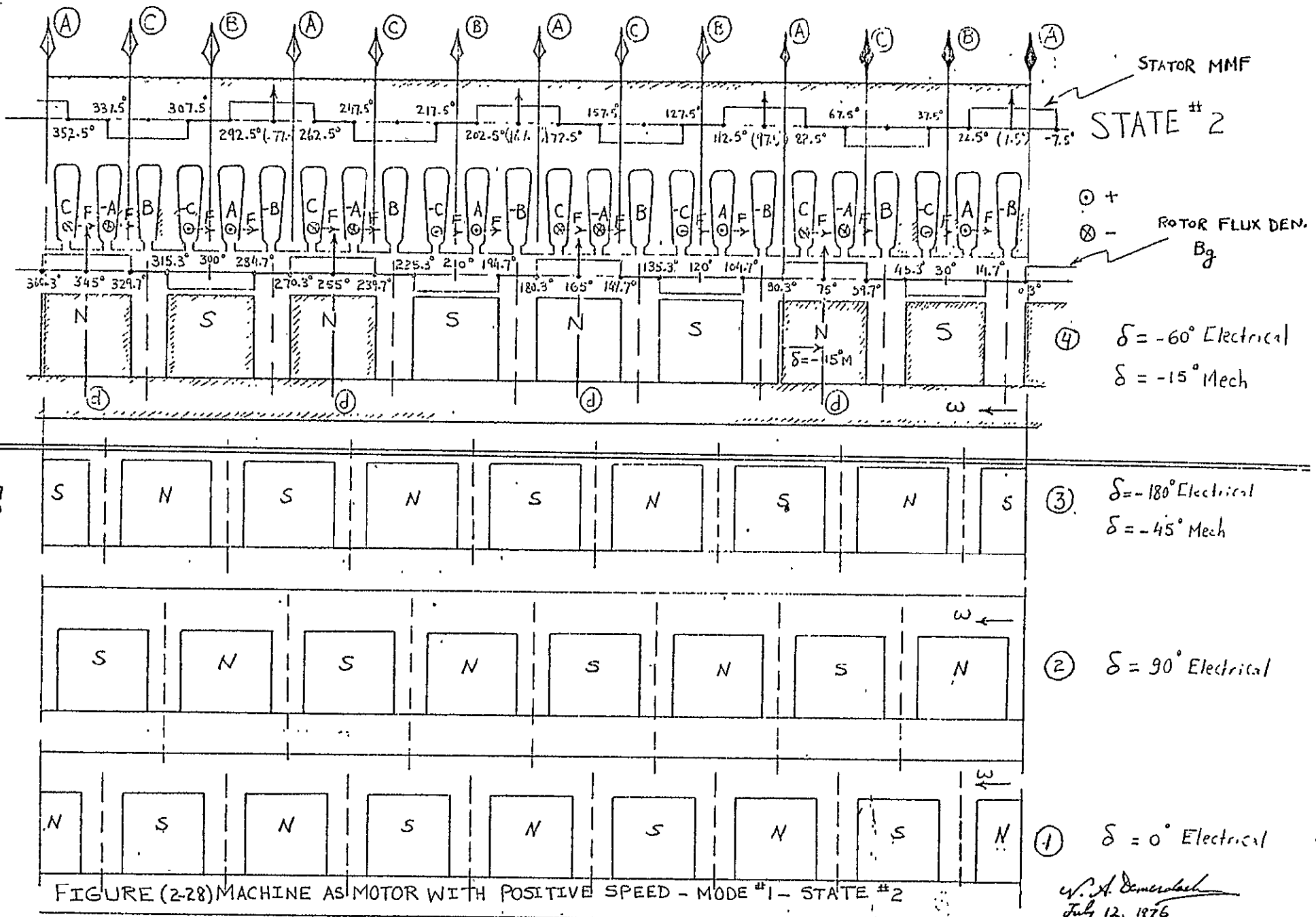
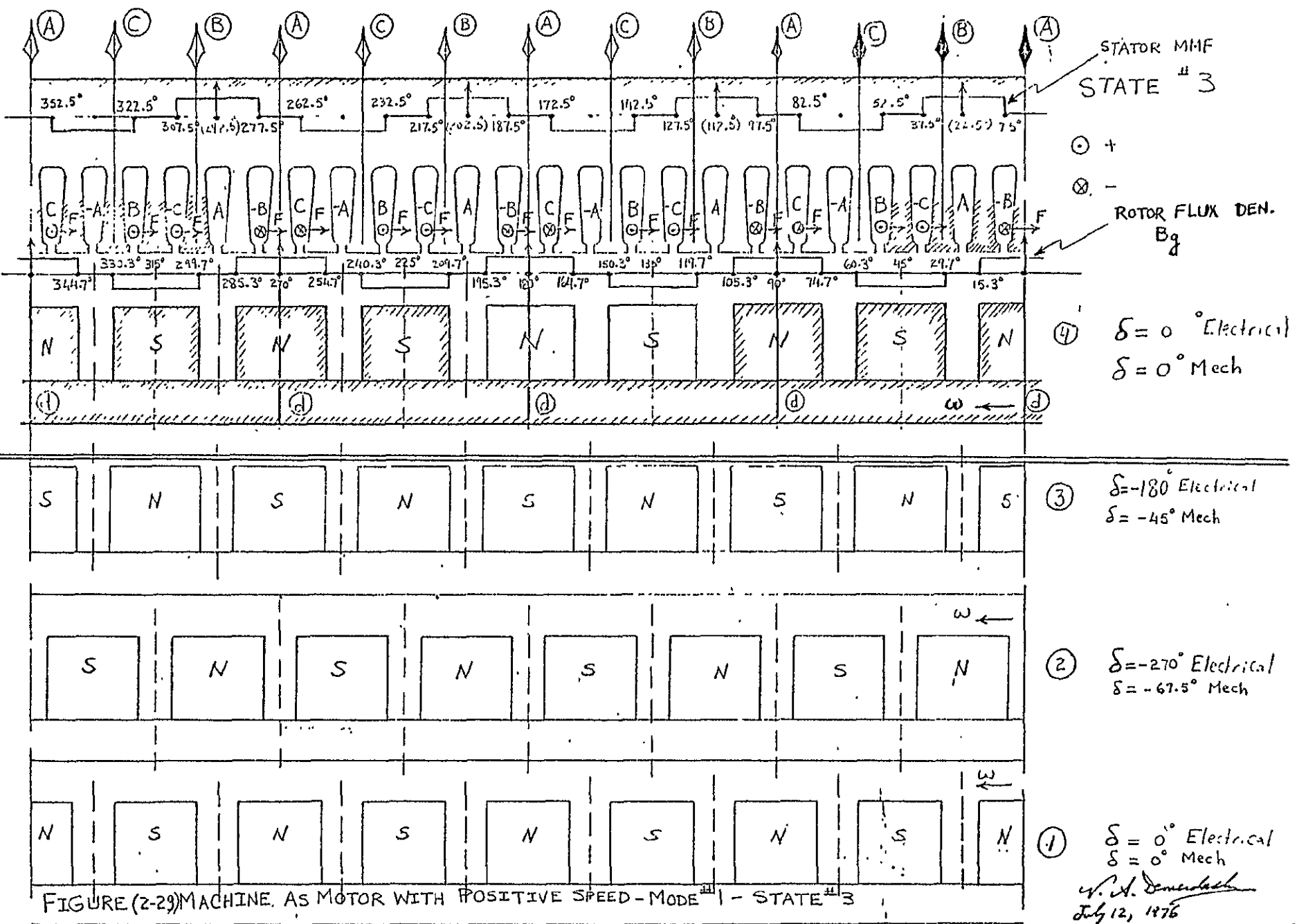


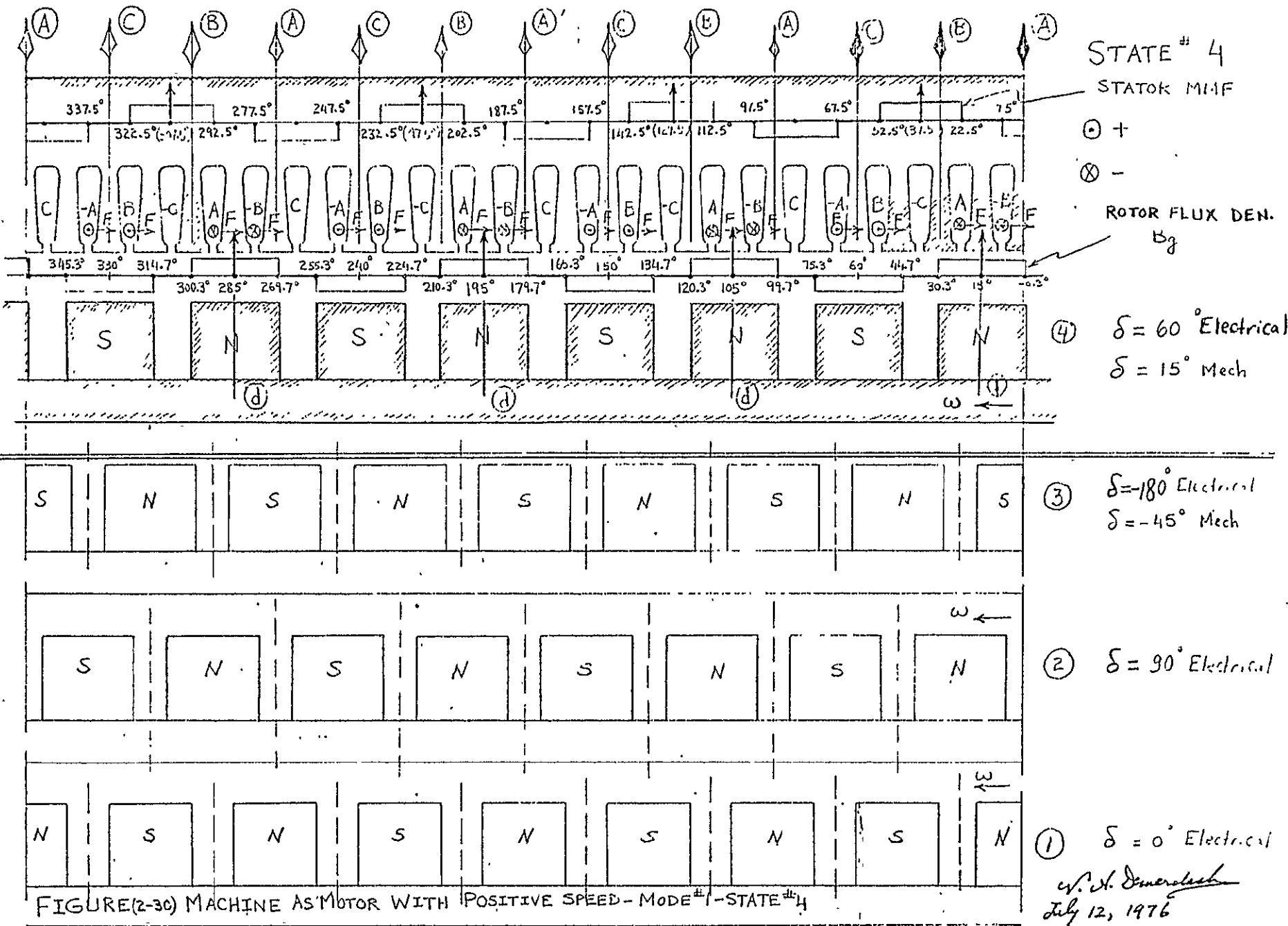
Fig.(2-26) Rotor Position and Windings

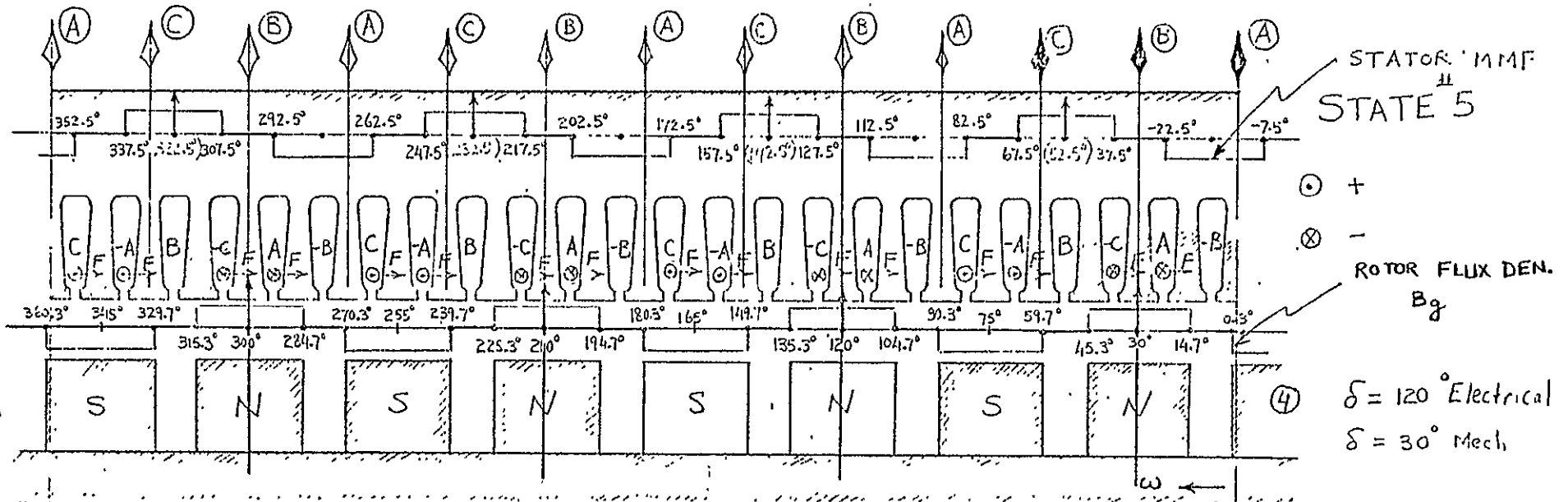
Schematic Diagram



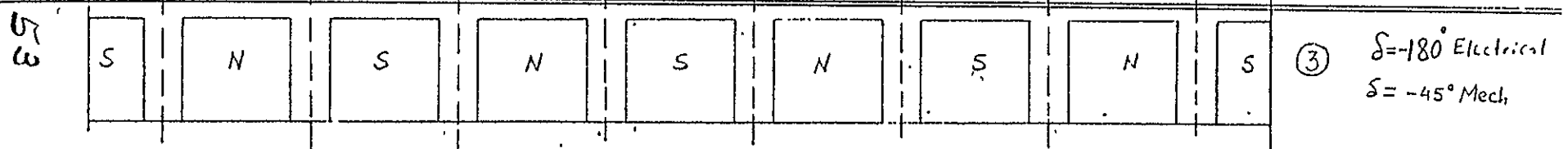




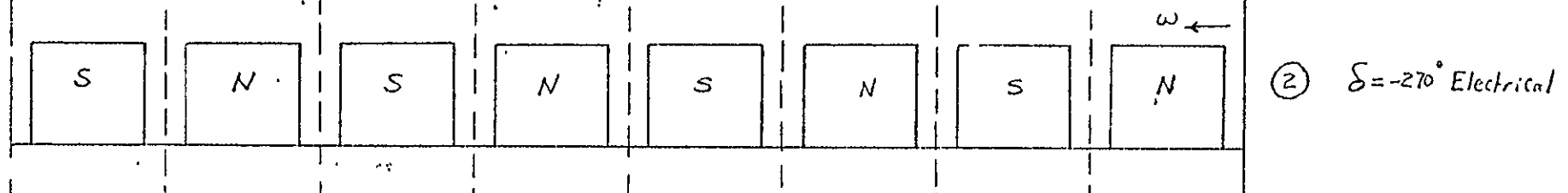




$$\begin{aligned} \delta &= 120^\circ \text{ Electrical} \\ \delta &= 30^\circ \text{ Mech} \end{aligned}$$

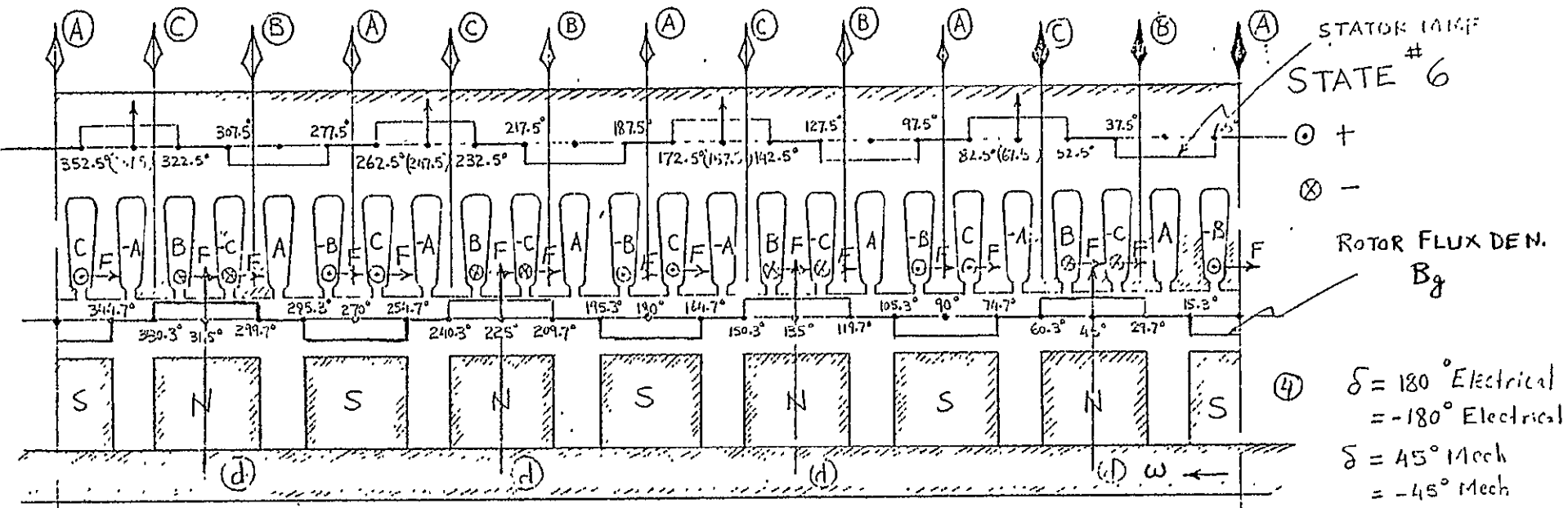


$$\begin{aligned} \delta &= 180^\circ \text{ Electrical} \\ \delta &= -45^\circ \text{ Mech} \end{aligned}$$

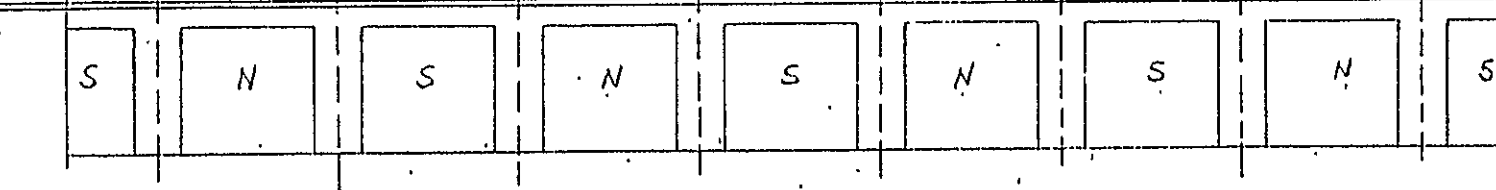


$$\begin{aligned} \delta &= 0^\circ \text{ Electrical} \\ \text{w.t. demand} \\ \text{July 12, 1976} \end{aligned}$$

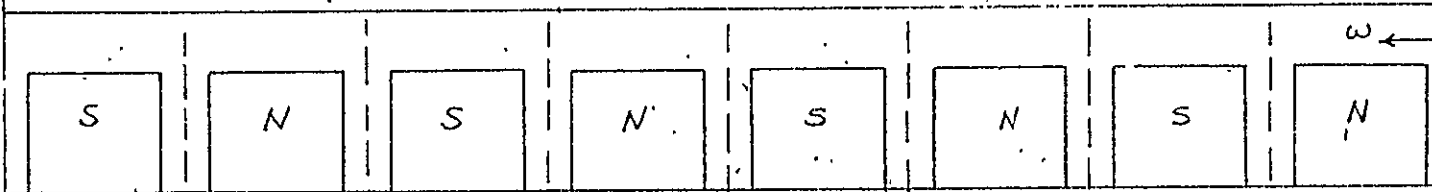
FIGURE(2-3) MACHINE AS MOTOR WITH POSITIVE SPEED - MODE #1 - STATE #5



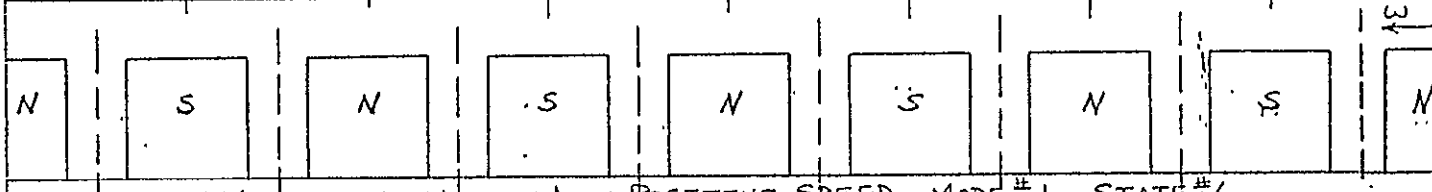
$$\begin{aligned} \textcircled{4} \quad \delta &= 180^\circ \text{ Electrical} \\ &= -180^\circ \text{ Electrical} \\ \delta &= 45^\circ \text{ Mech} \\ &= -45^\circ \text{ Mech} \end{aligned}$$



$$\begin{aligned} \textcircled{3} \quad \delta &= 180^\circ \text{ Electrical} \\ &= -180^\circ \text{ Electrical} \\ \delta &= 45^\circ \text{ Mech} \\ &= -45^\circ \text{ Mech} \end{aligned}$$



$$\begin{aligned} \textcircled{2} \quad \delta &= 90^\circ \text{ Electrical} \\ &= -270^\circ \text{ Electrical} \end{aligned}$$



$$\begin{aligned} \textcircled{1} \quad \delta &= 0^\circ \text{ Electrical} \\ &\text{W. A. Damodar} \\ &\text{July 12, 1926} \end{aligned}$$

FIGURE(2-32) MACHINE AS MOTOR WITH POSITIVE SPEED - MODE #1 - STATE #6

TORQUE (NEWTON METER)
5.8375 I.R
10.66325 I.R

EFFECT OF ACCOUNTING
FOR DISTRIBUTED
CURRENT IN THE SLOTS

N.C. Donahue
July 16, 1976

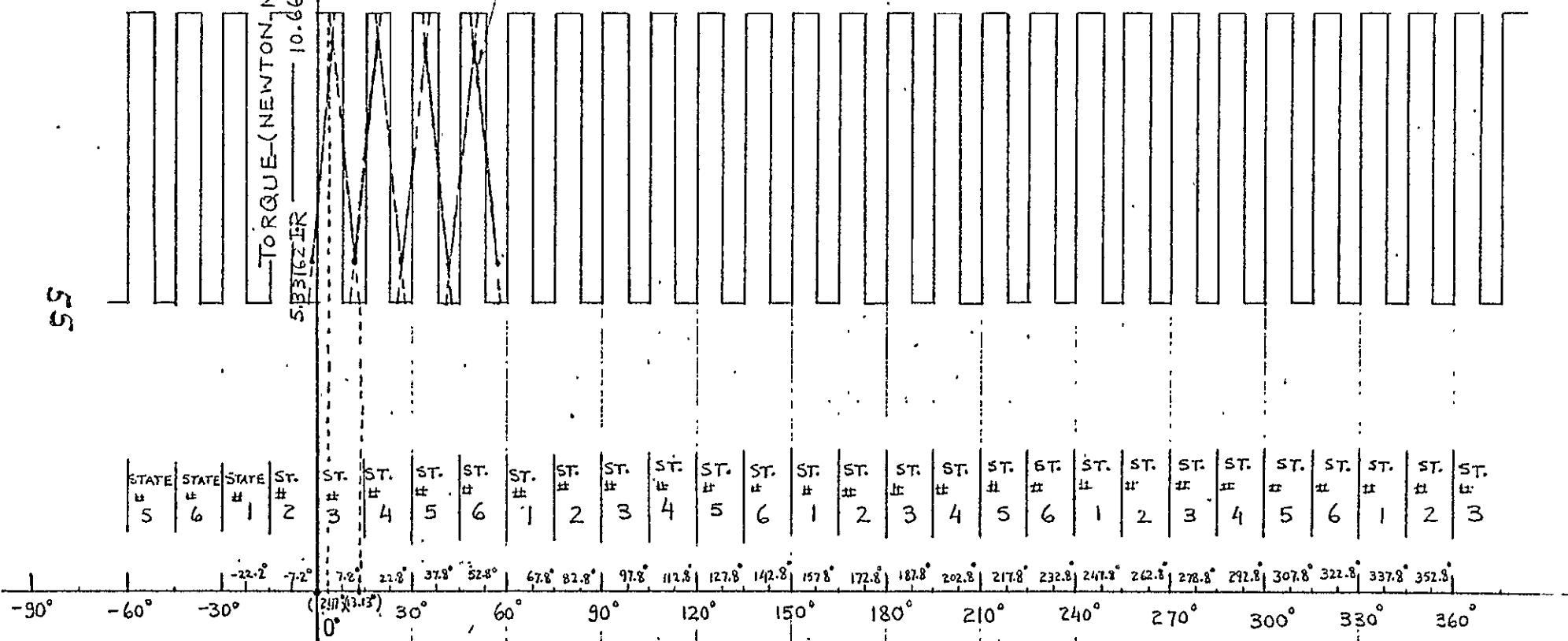
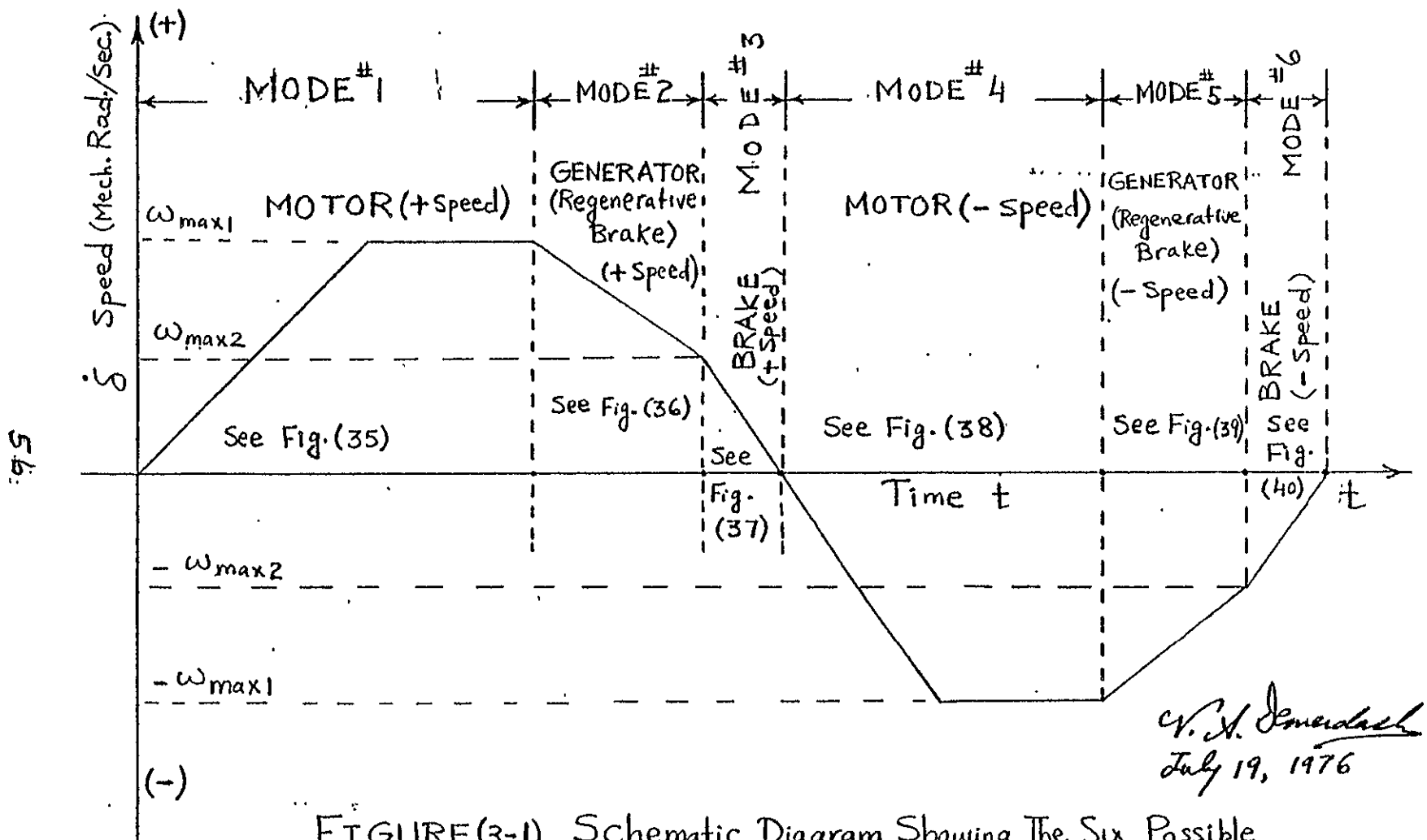


FIG.(2-33) TORQUE- ROTOR POSITION CHARACTERISTIC
OF BRUSHLESS D-C MOTOR- MODE [#]1

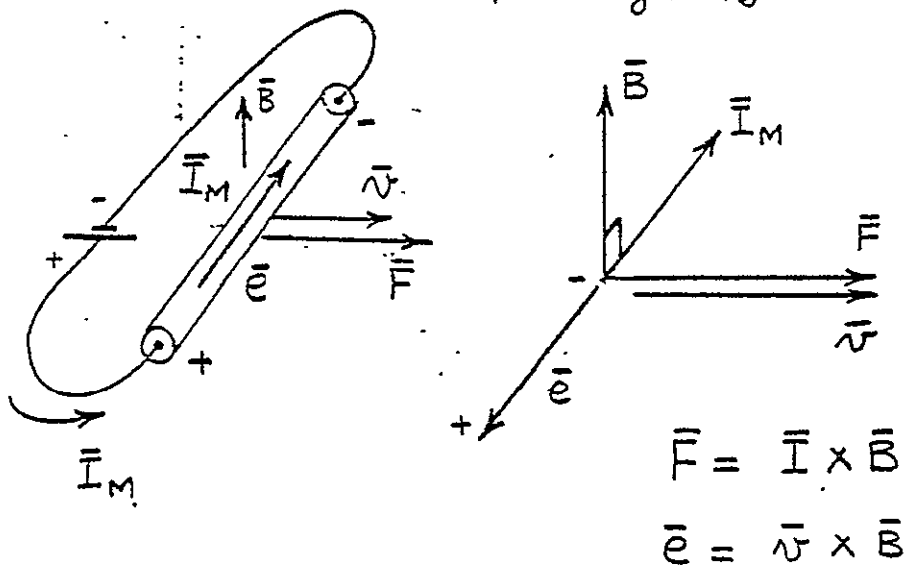


FIGURE(3-1) Schematic Diagram Showing The Six Possible Modes of Operation Modes^{#1} Through^{#6}

MOTOR (Positive Speed)

Controlled Firing Sequence(ABC)For The Six Transistors

Q_1 Through Q_6



\bar{I} is the Current Space Vector

\bar{B} is the Flux Density Space Vector

\bar{v} is the Velocity (Speed) Space Vector

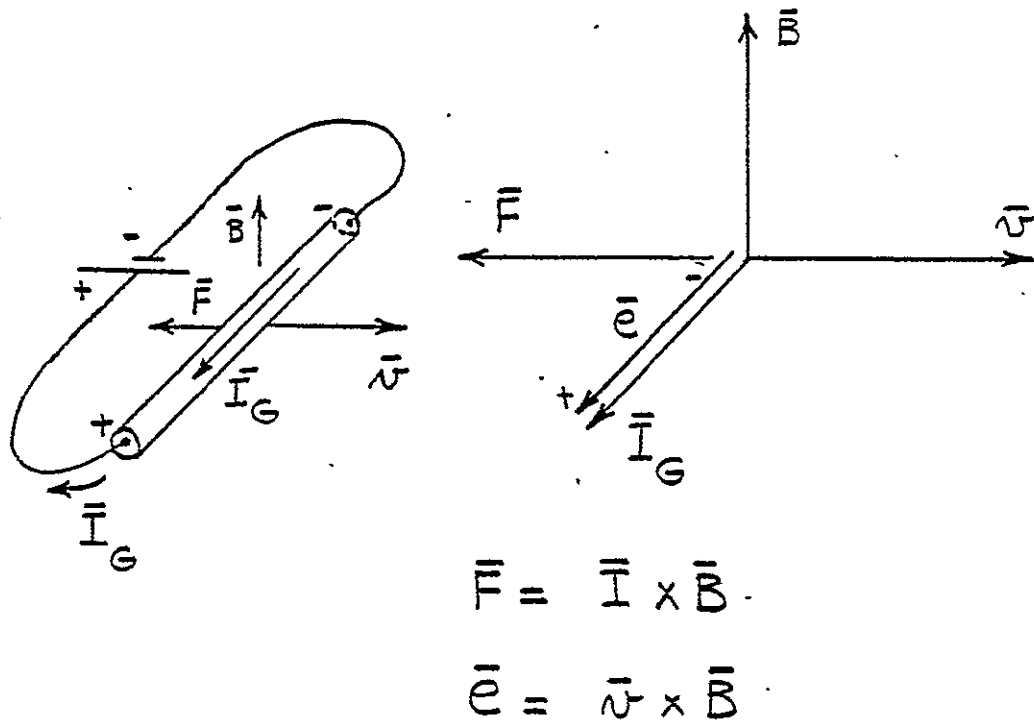
\bar{F} is the Force Space Vector Per Unit
Conductor Length

\bar{e} is the Induced (Back) EMF Per Unit
Conductor Length

FIGURE(3-2) MODE #1 - Motor With
Positive Speed

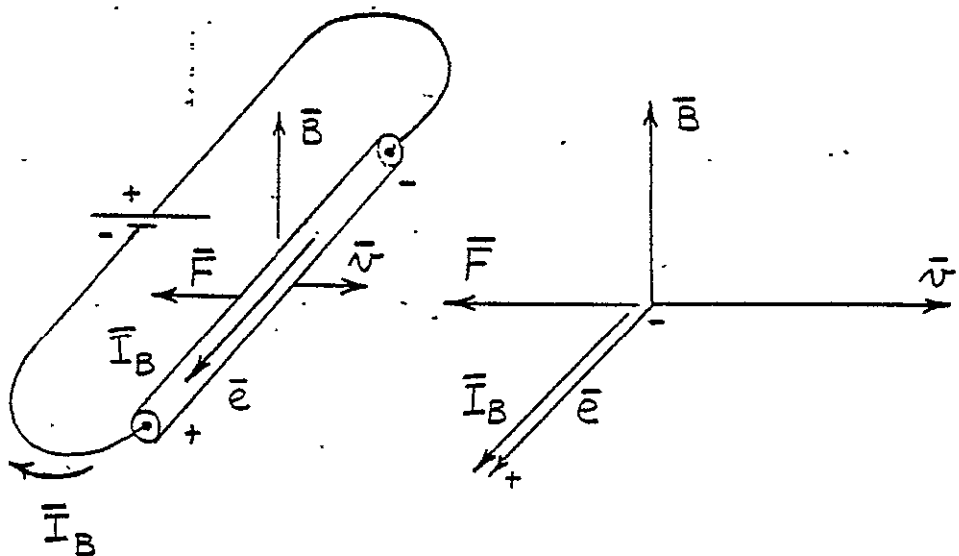
GENERATOR (Positive Speed) - REGENERATIVE BRAKE

No. Role For Transistors Q₁ Through Q₆ - Conduction
 Via Diodes D₁ Through D₆



FIGURE(3-3) MODE #2 - Generator
 (Regenerative Brake) With Positive Speed

BRAKE (Positive Speed)
 Controlled Firing Sequence (ABC) For The Six
 Transistors Q_1 Through Q_6 (Reverse Battery)



$$\bar{F} = \bar{I} \times \bar{B}$$

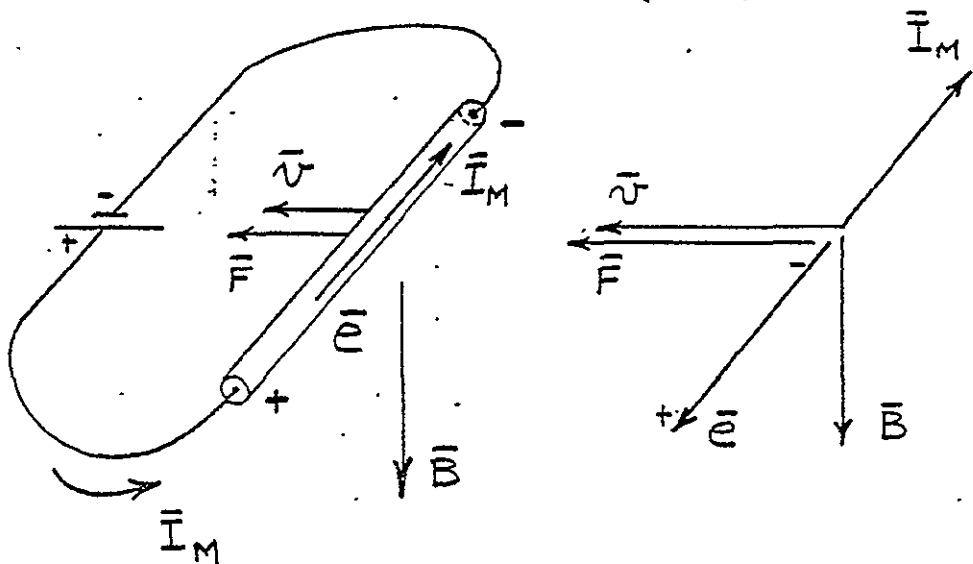
$$\bar{e} = \bar{v} \times \bar{B}$$

FIGURE (3-4) MODE #3 - Brake With
 Positive Speed.

G. H. Dimondback
 July 20, 1976

MOTOR (Negative Speed)

Controlled Firing Reverse Sequence (ACB) For The Six Transistors Q_1 Through Q_6

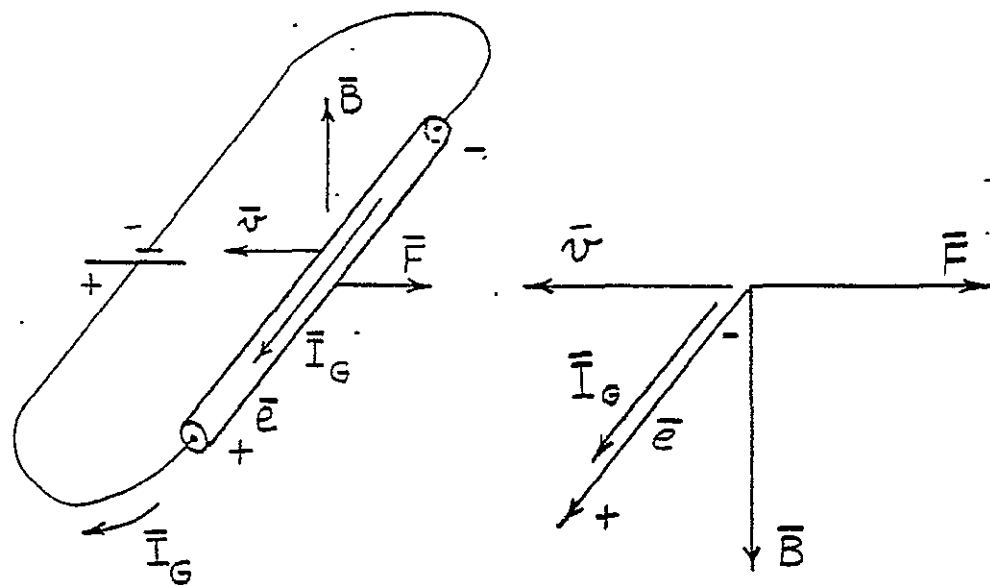


$$\bar{F} = \bar{I} \times \bar{B}$$

$$\bar{e} = \bar{v} \times \bar{B}$$

FIGURE (3-5) MODE #4 - Motor With Negative Speed

GENERATOR (Negative Speed) - REGERATIVE BRAKE
 No Role For Transistors Q₁ Through Q₆ - Conduction
 Via Diodes D₁ Through D₆



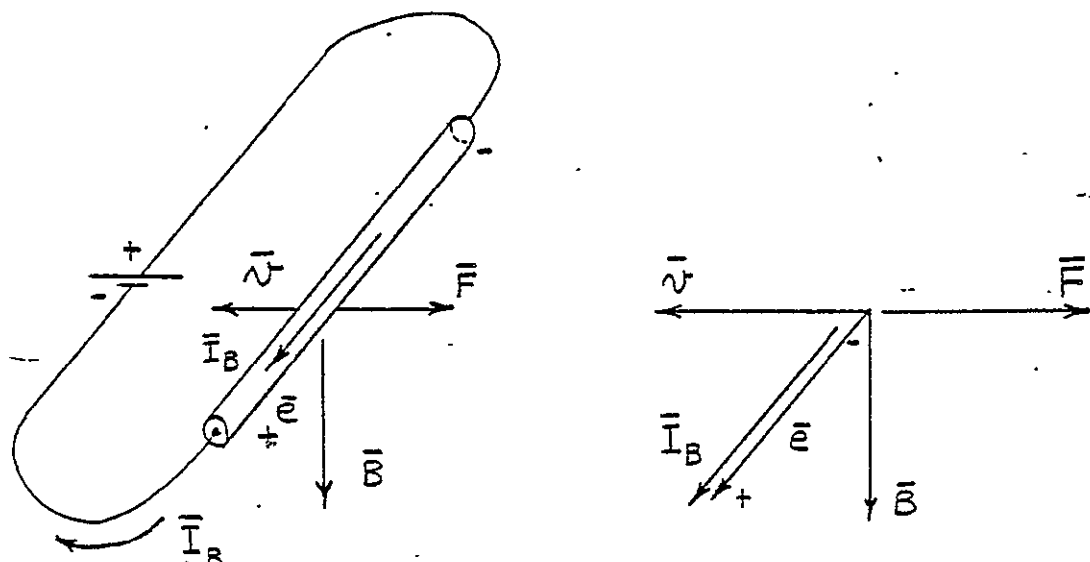
$$\bar{F} = \bar{I} \times \bar{B}$$

$$\bar{e} = \bar{v} \times \bar{B}$$

FIGURE (3-6) MODE #5 - Generator
 (Regenerative Brake) With Negative Speed

BRAKE (Negative Speed)

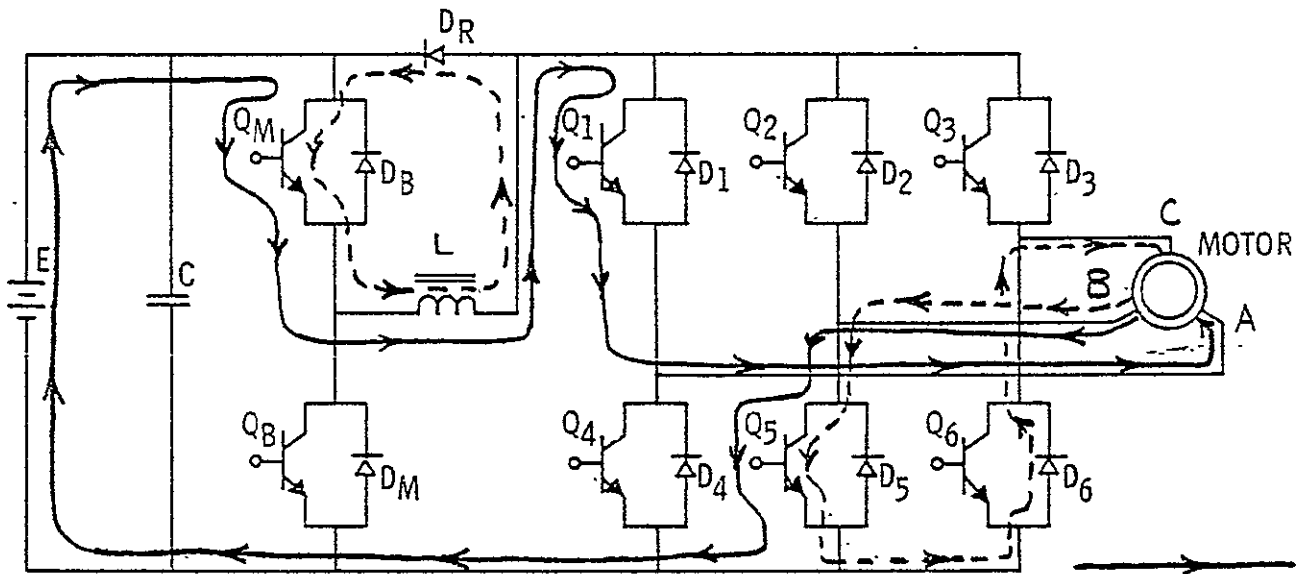
Controlled Firing Sequence (ACB) For The Six Transistors Q_1 Through Q_6



$$\bar{F} = \bar{I} \times \bar{B}$$

$$\bar{e} = \bar{v} \times \bar{B}$$

FIGURE(3-7) MODE #6 - Brake With Negative Speed



Firing Sequence ABC - Current Pattern With Q_M ON

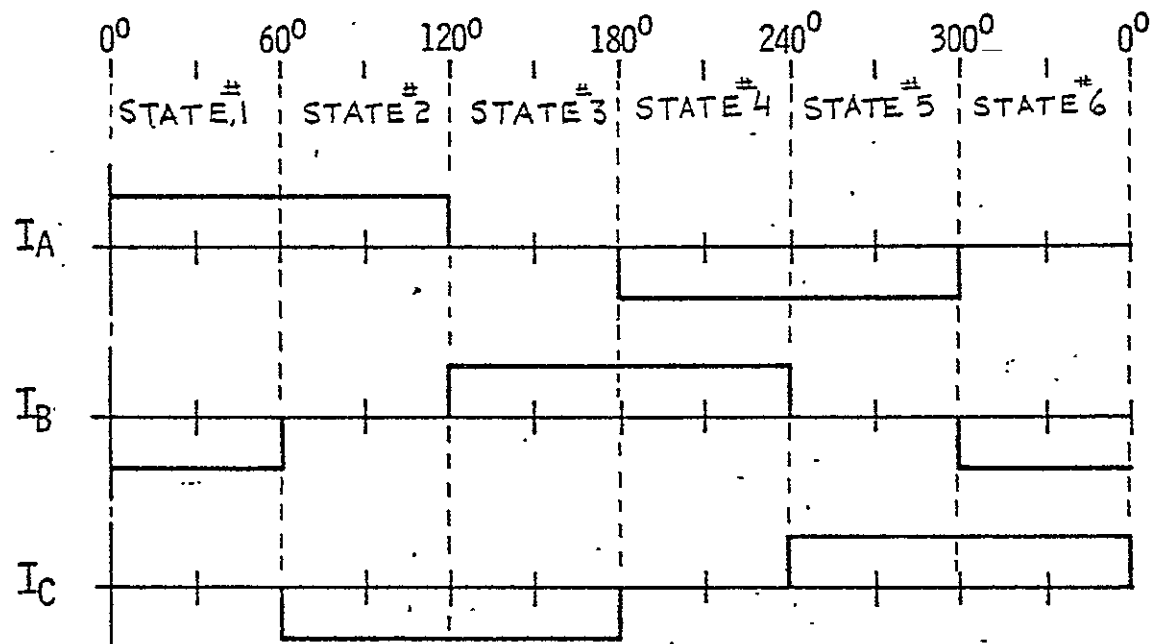
STATE $\#1$

Power Electronics Schematic

Main Currents

Decaying Currents

ELECTRICAL ANGLE

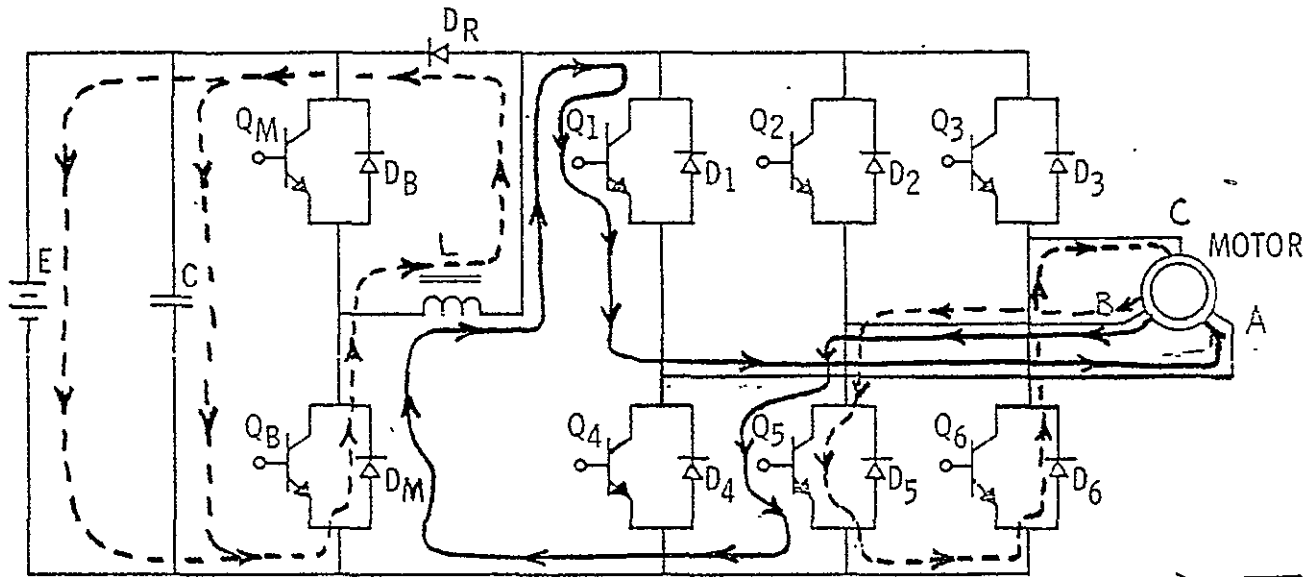


Idealized Motor Phase Currents

C. J. Dineen
July 21, 1976

FIGURE (3-8) Mode (1) Currents

Motor - Positive Speed - Q_M ON



Firing Sequence ABC - Current Pattern With Q_M OFF

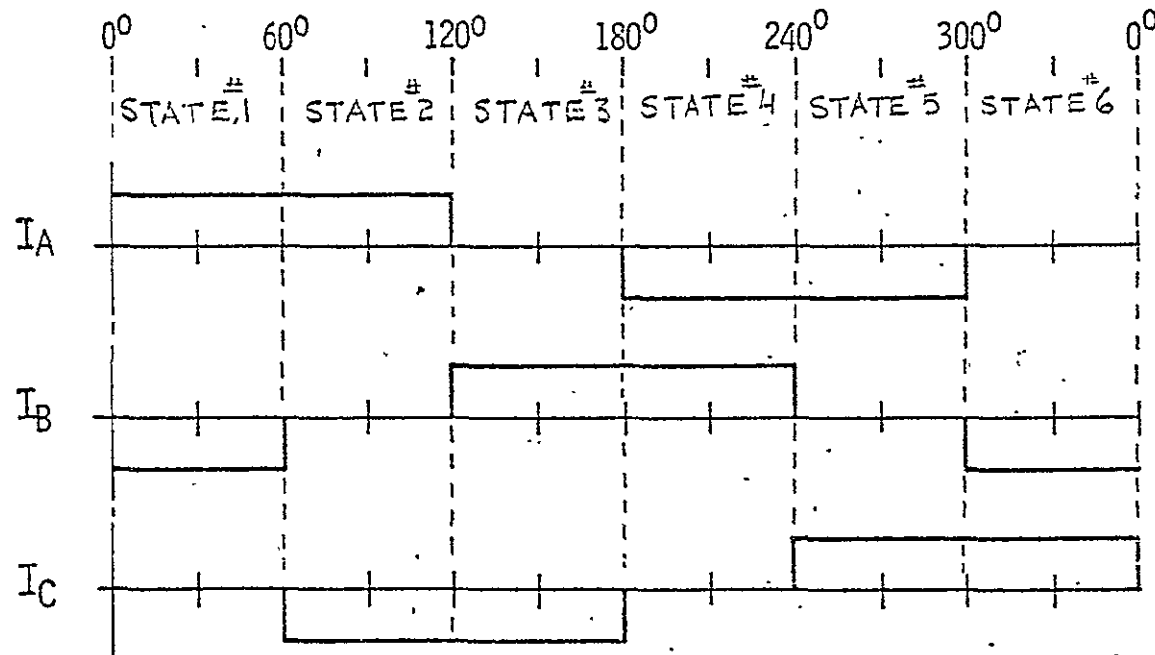
Main Currents

STATE #1

Power Electronics Schematic

ELECTRICAL ANGLE

Decaying Currents

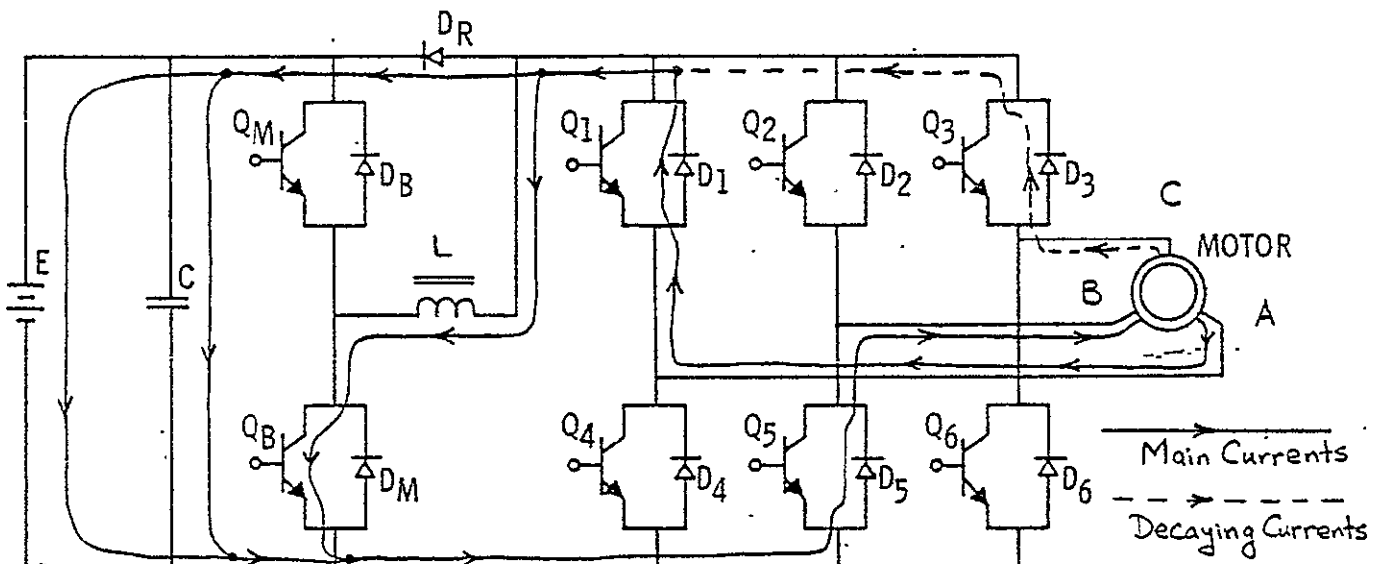


Idealized Motor Phase Currents

C. A. Dimendaal
July 21, 1976

FIGURE (3-9) Mode (1) Currents

Motor - Positive Speed - Q_M OFF

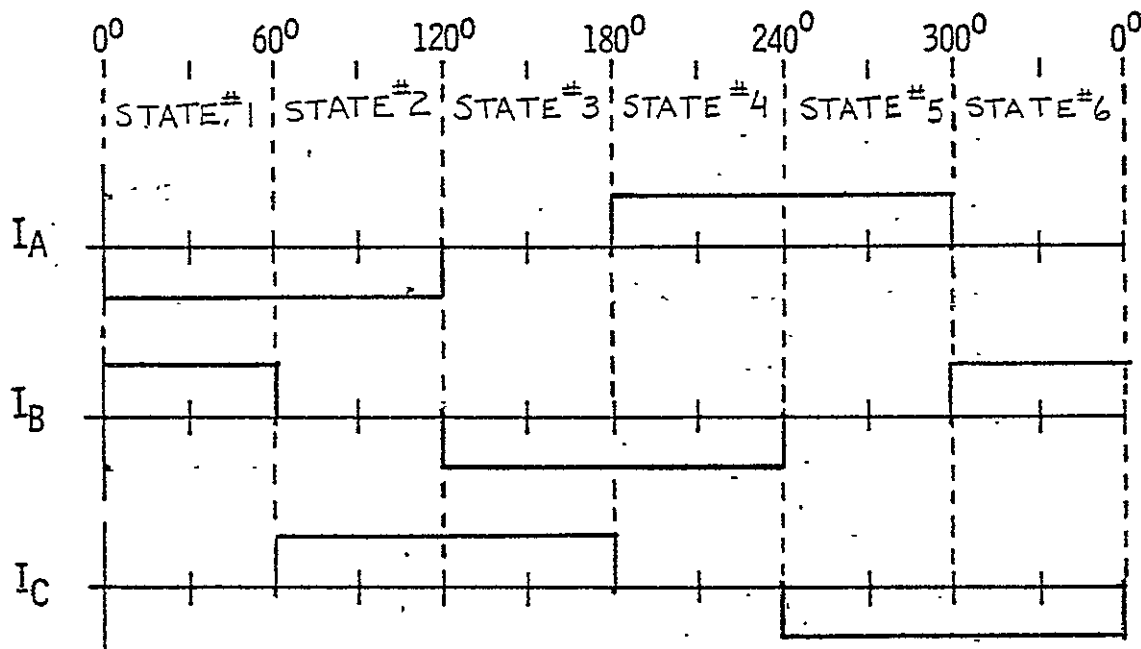


Diod Conduction Sequence ABC - Current Pattern With Q_B ON

STATE #1

Power Electronics Schematic

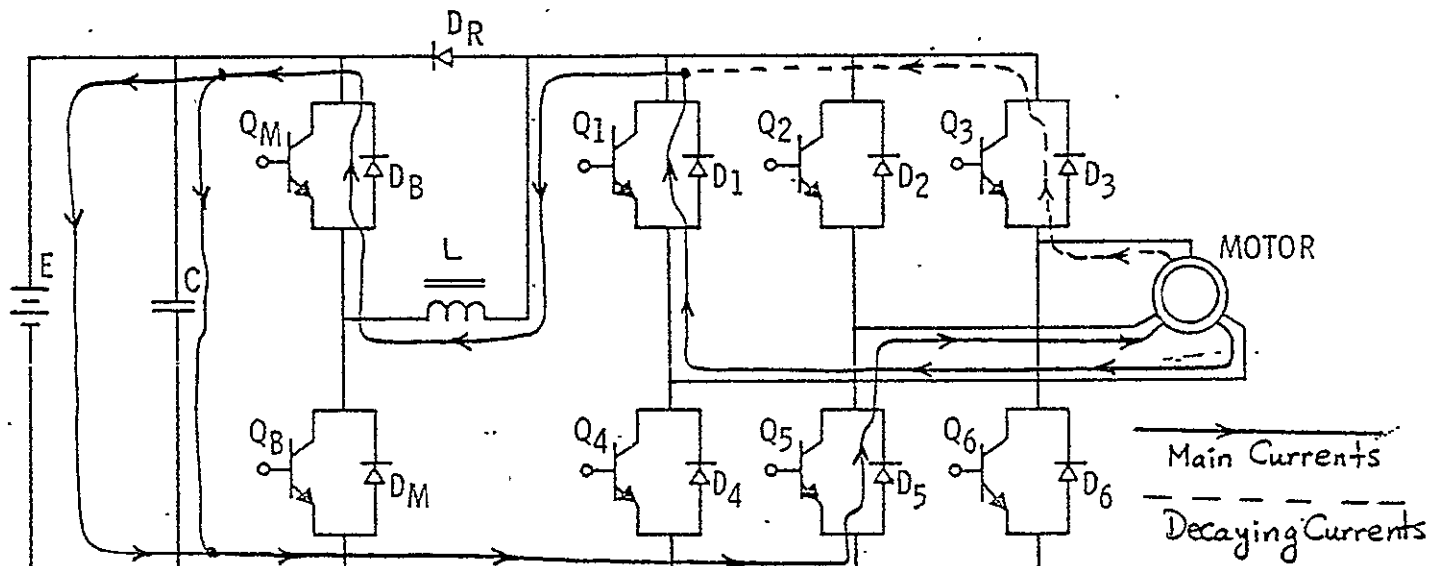
ELECTRICAL ANGLE



Schematic of Idealized Gen. Phase Currents

C. A. Demetsky
August 9, 1976

FIGURE (3-10) Mode (2) Currents - Generator
Positive Speed - Q_B ON

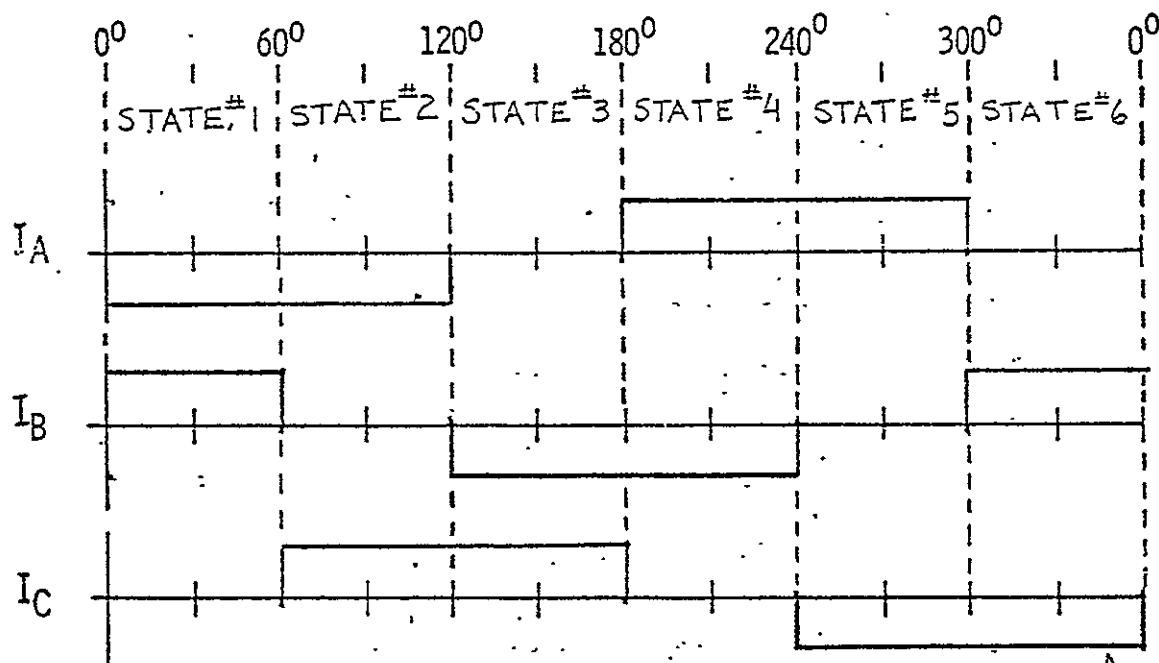


Diode Conduction Sequence ABC - Current Pattern With Q_B OFF

STATE #1

Power Electronics Schematic

ELECTRICAL ANGLE

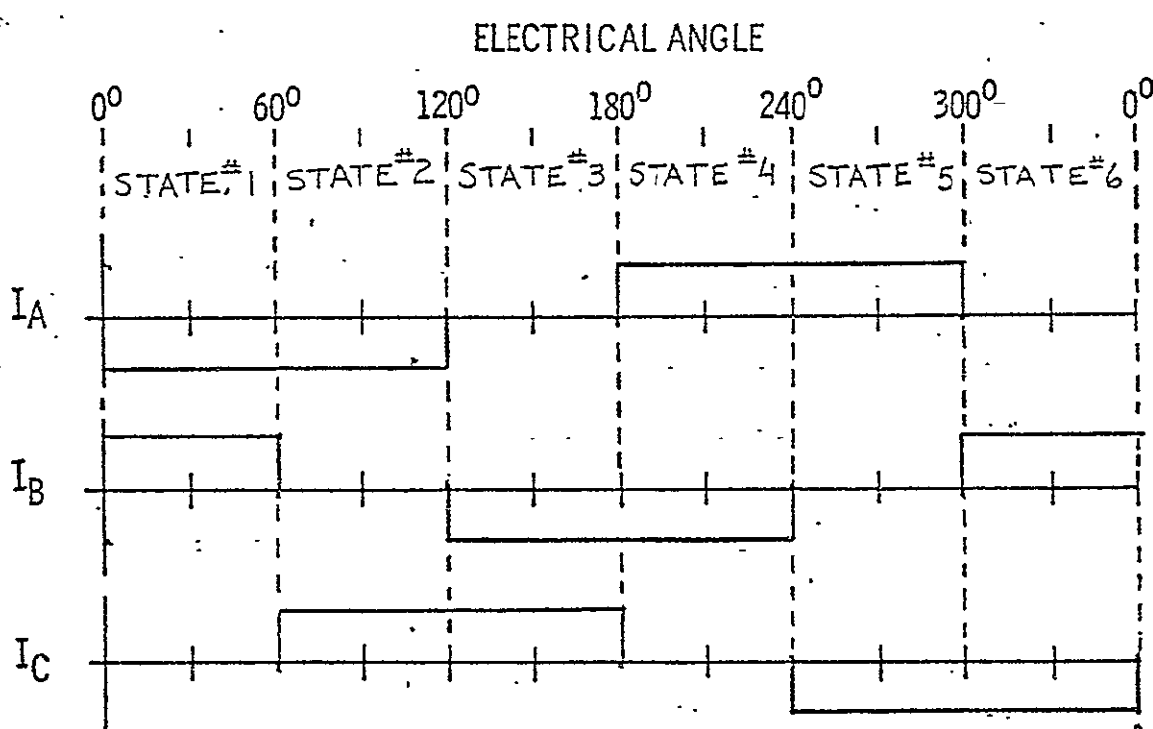
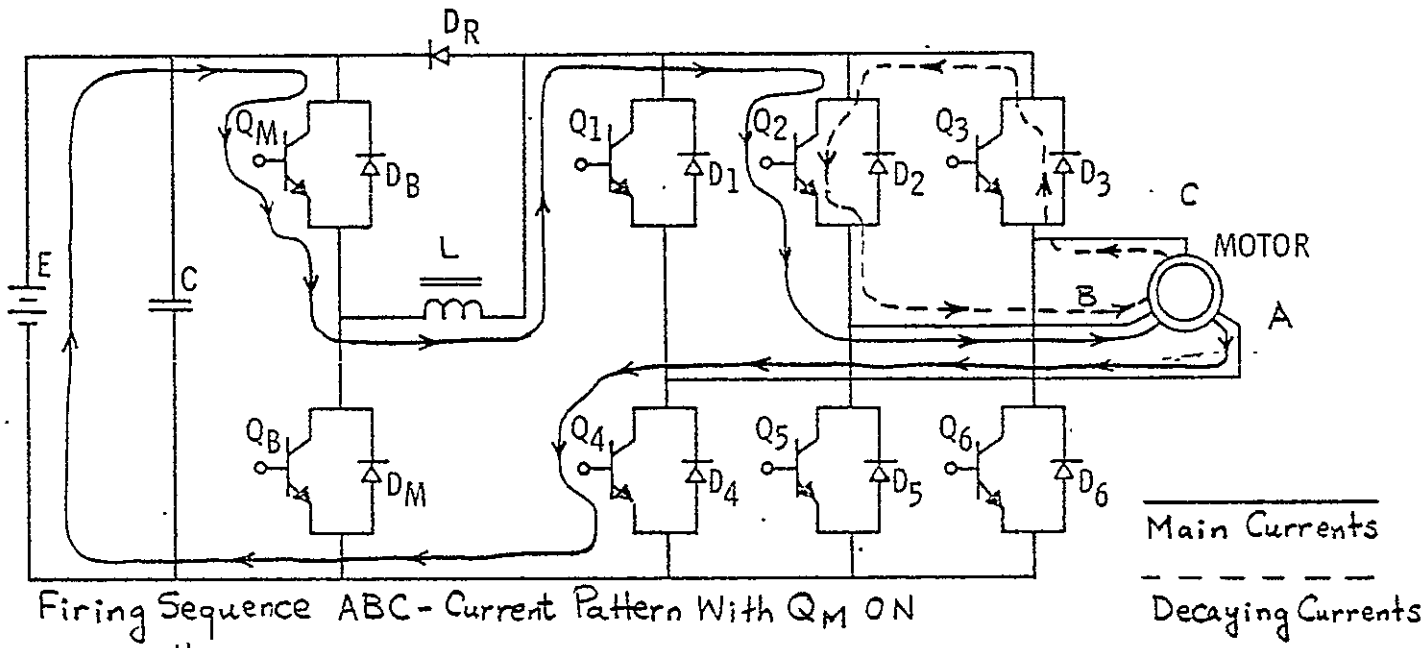


Schematic of Idealized Gen. Phase Currents

G. A. Demarest
August 9, 1976

FIGURE (3-11) Mode (z) Currents - Generator

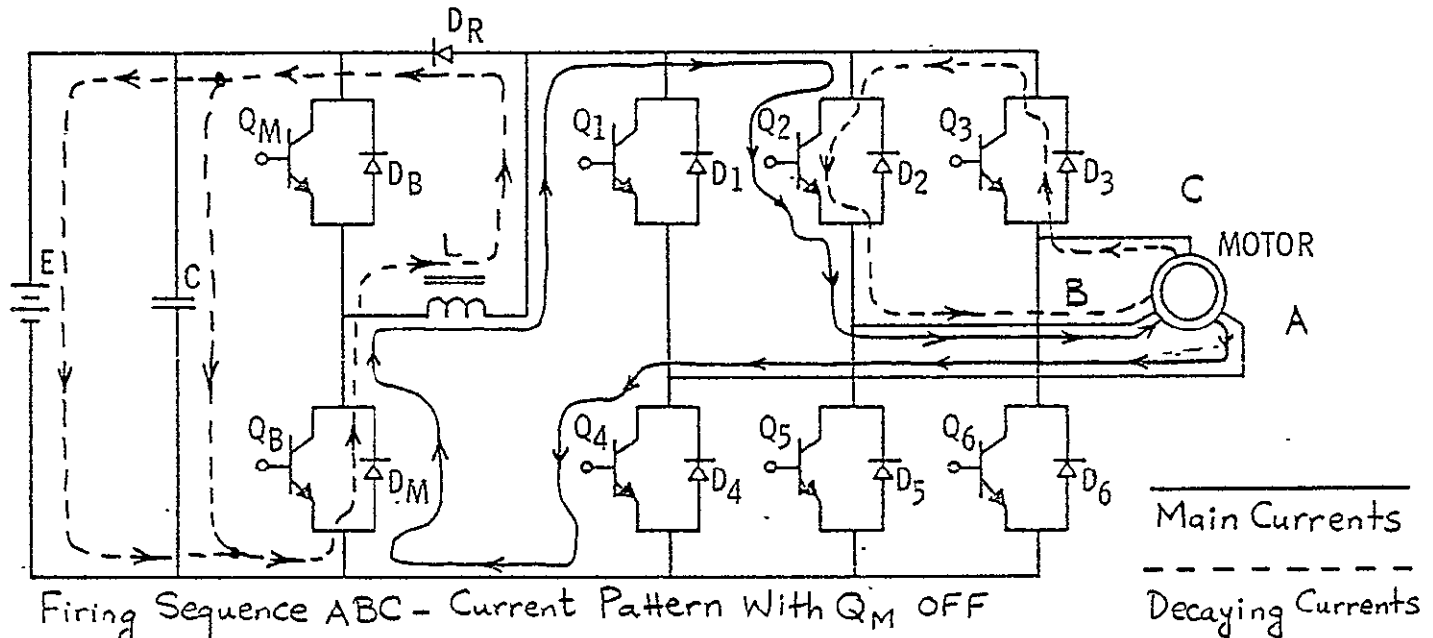
Positive Speed - Q_B OFF



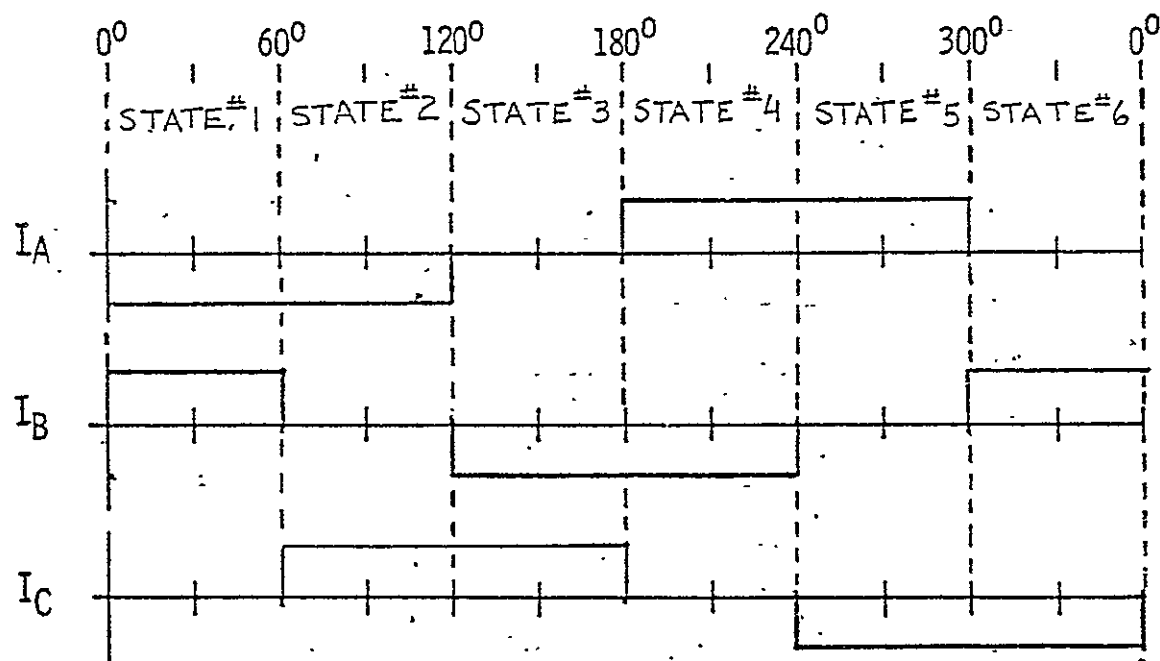
Schematic of Idealized Brake Phase Currents

W. A. Demerdash
August 5, 1976

FIGURE (3-12) Mode (3) Currents - Brake
Positive Speed - Q_M ON



ELECTRICAL ANGLE



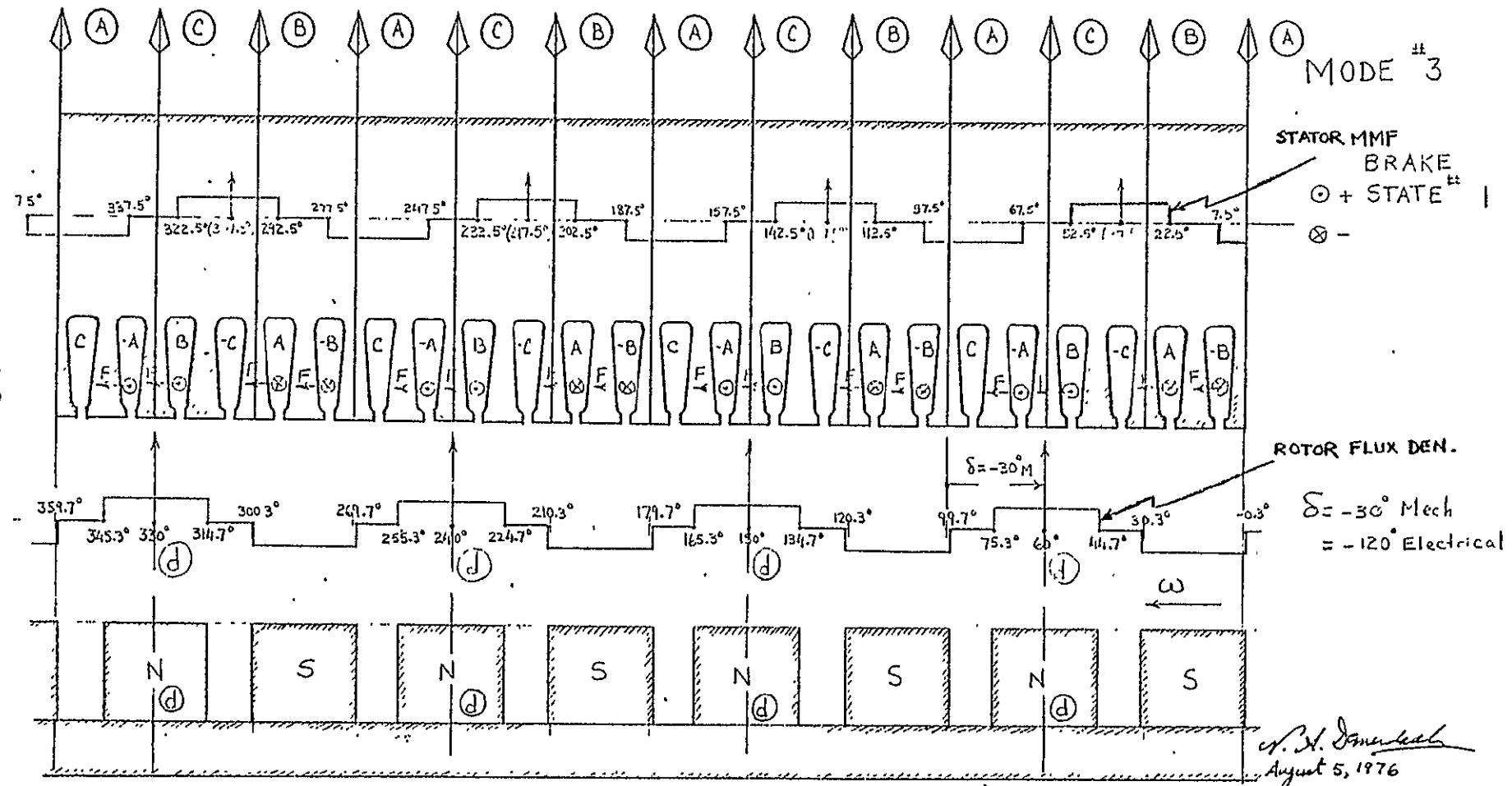
Schematic of Idealized Brake Phase Currents

W. A. Demerelesh
August 5, 1976

FIGURE (3-13) Mode (3) Currents - Brake

Positive Speed - Q_M OFF

69



FIGURE(4-1) MACHINE AS BRAKE WITH POSITIVE SPEED
MODE #3 - STATE #1

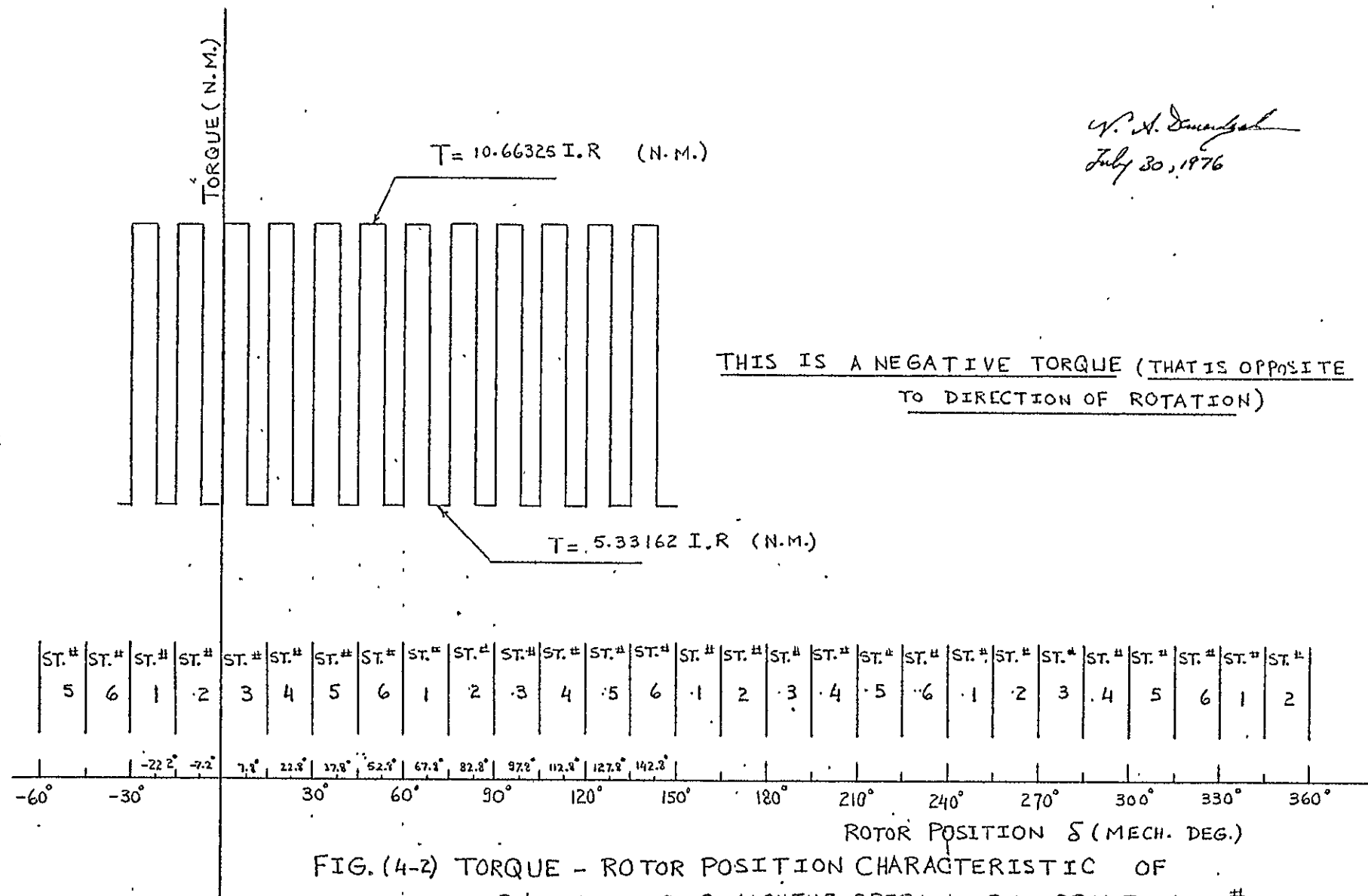


FIG. (4-2) TORQUE - ROTOR POSITION CHARACTERISTIC OF
BRUSHLESS D-C MACHINE OPERATING AS BRAKE MODE #3

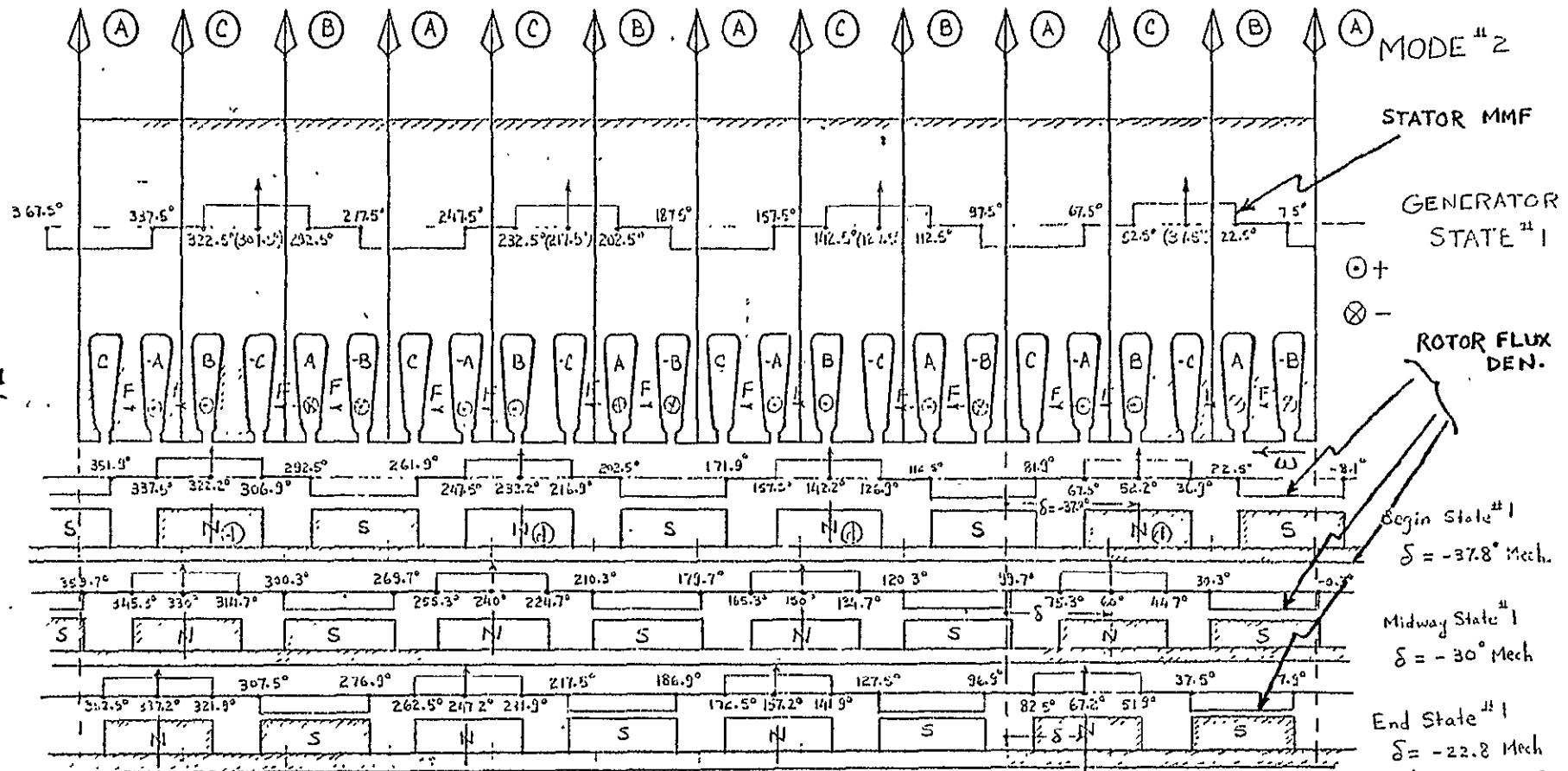
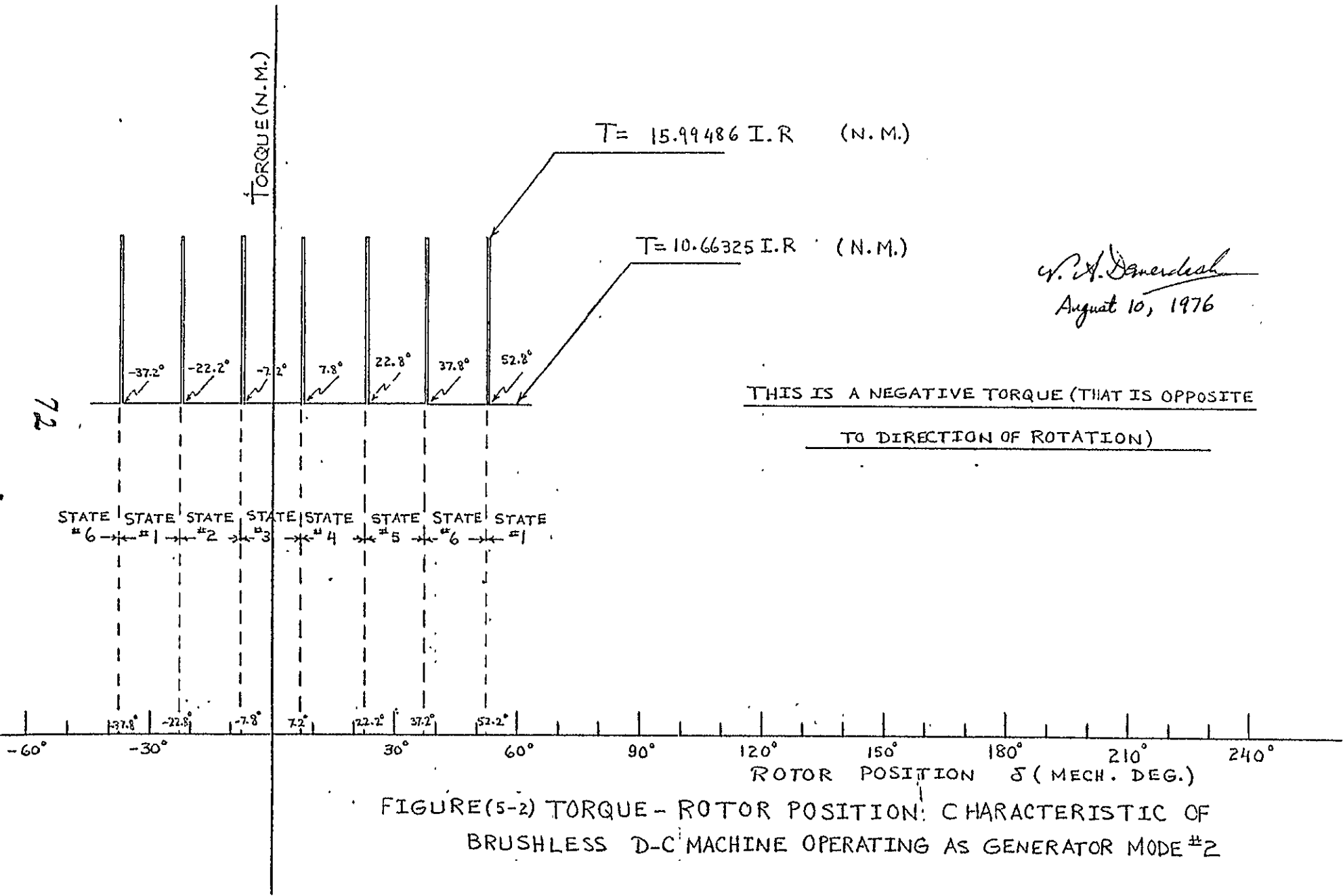


FIGURE (5-1) MACHINE AS GENERATOR WITH POSITIVE SPEED - MODE $\#2$ - STATE $\#1$

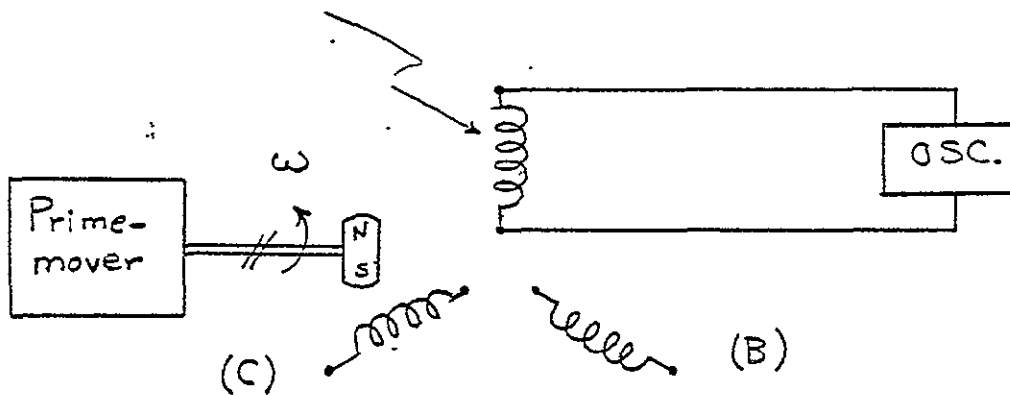
G.P. A. Demetsky
August 9, 1976



Test # 1

Open Ct. Voltage and Flux Density Wave Forms

Motor Winding (A)



Test at $\omega = 900$ rpm

= 4500 rpm

= 9000 rpm

Record Open Circuit Voltage Wave Form of Phase (A)
and /or (B) and /or (C).

Conditions No Armature Current.

C. A. Demesh
August 11, 1976

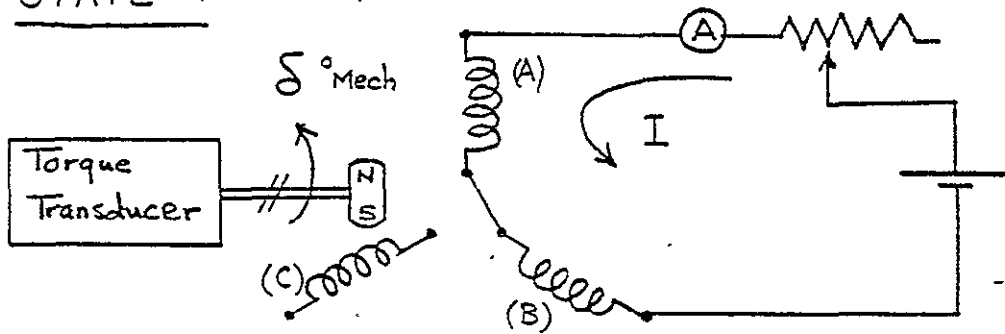
Open Circuit Voltage and Flux Density
Distribution Wave Forms at NO-LOAD

Figure (7-1) Test # 1

Test # 2

Motor Torque - Position Characteristics

STATE #1

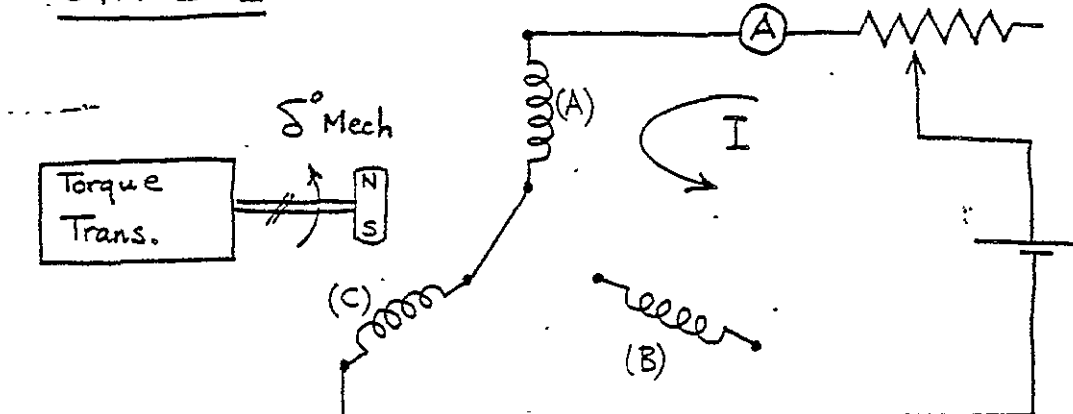


Test at $I = \text{Rated Current}$

Record Torque

Conditions $-30^\circ \leq \delta \leq -15^\circ$ OR $0^\circ \leq \delta \leq 360^\circ$

STATE #2



Test same as above

w. A. Dennerly
August 16, 1976

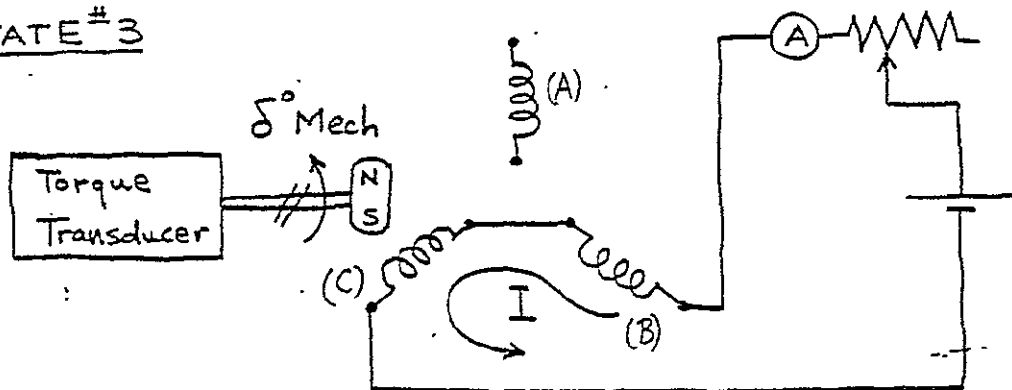
Record Same as above

Condition $-15^\circ \leq \delta \leq 0^\circ$ OR $0^\circ \leq \delta \leq 360^\circ$

Figure (7-2) Test #2

Cont. Test # 2

STATE # 3

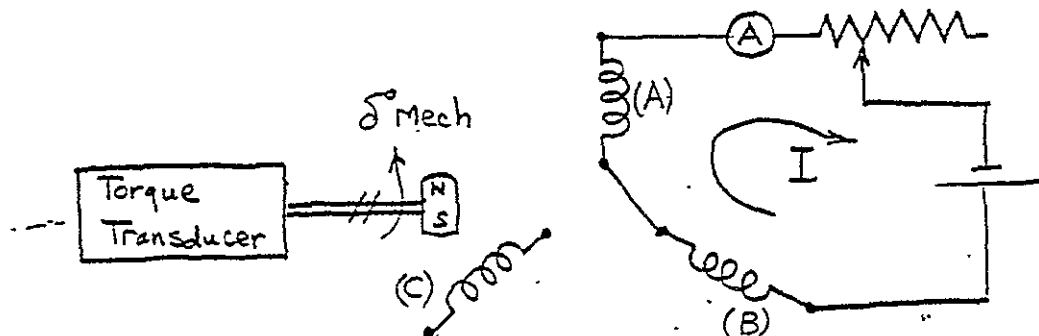


Test Same as state # 1

Record Same as state # 1

Condition $0^\circ \leq \delta \leq 15^\circ$ OR $0^\circ \leq \delta \leq 360^\circ$

STATE # 4



Test Same as state # 1.

W. W. Demuth
August 11, 1976

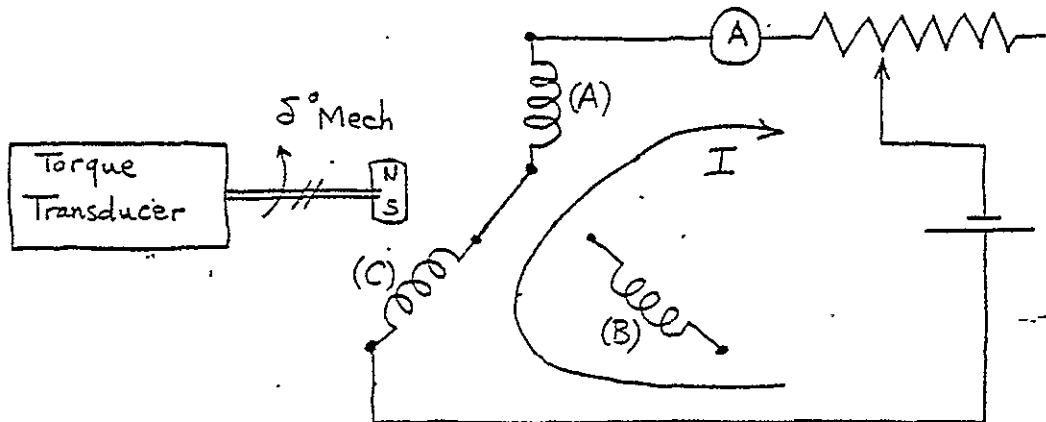
Record " " " "

Condition $15^\circ \leq \delta \leq 30^\circ$ OR $0^\circ \leq \delta \leq 360^\circ$

Figure (7-3) Cont. Test # 2

Cont. Test #2

STATE #5

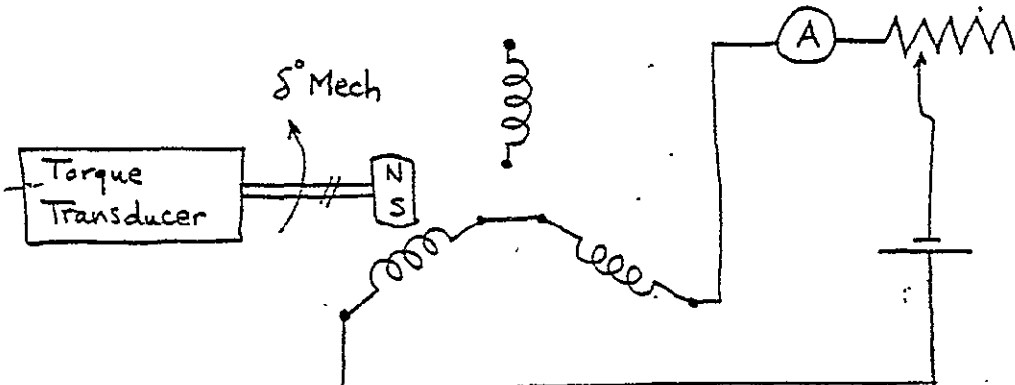


Test same as state #1

Record " " " "

Condition $30^\circ \leq \delta \leq 45^\circ$ OR $0 \leq \delta \leq 360^\circ$

STATE #6



Test same as state #1

W.C. Deneke

August 11, 1976

Record " " " "

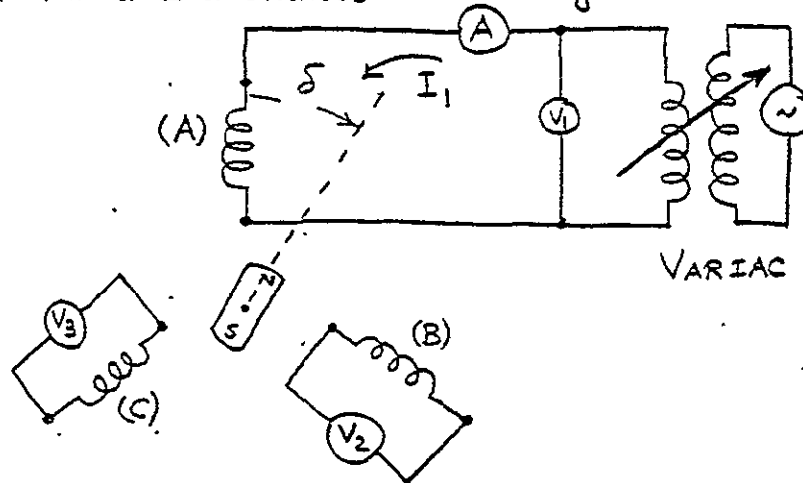
Condition $45^\circ \leq \delta \leq 60^\circ$ OR $0 \leq \delta \leq 360^\circ$

Figure(7-4) Cont. Test #2

76

Test # 3

Self and Mutual Inductances of Windings



Test at $I_1 = 5\%$ rated, 10% rated & 15% rated

And $I_1 = 50\%$ rated, 75% , 100% , 125% & 150% rated

At Freq = 60 Hz , 300 Hz and 600 Hz

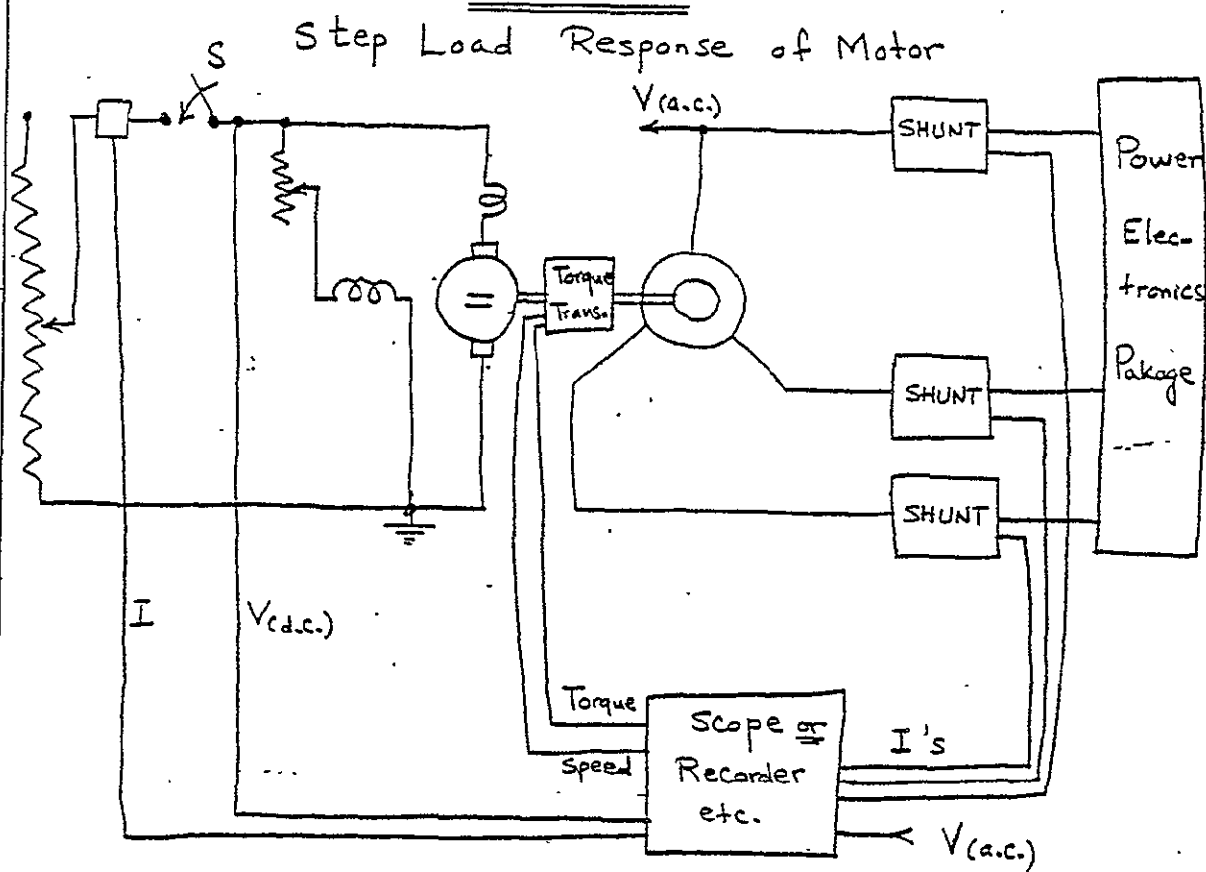
Record I_1 , V_1 , V_2 & V_3

Condition $-22.5^\circ \leq \delta \leq 22.5^\circ$ OR $0^\circ \leq \delta \leq 360^\circ$

Figure (7-5) Test # 3

W. A. Demarest
August 11, 1976

Test # 4



Test at 2.5, 5.0, 7.5, --: HP etc.

Record All Variables Fed Into Scope Above

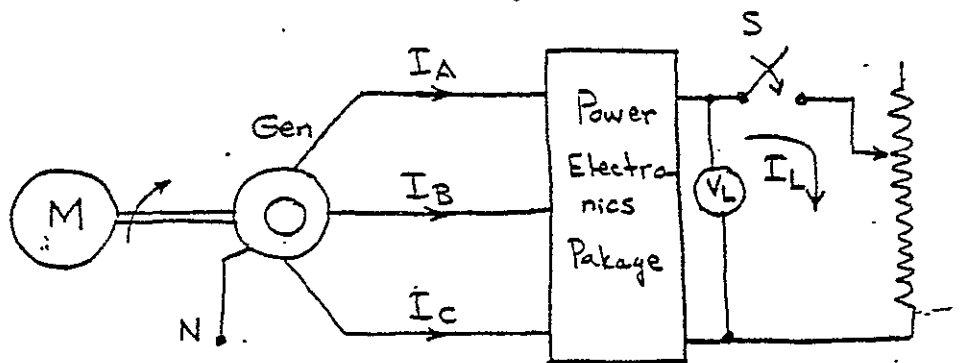
Condition Sudden Load - Permit Steady State to Develop

Figure (7-6) Test # 4

C. H. Denenbach
August 11, 1976

Test # 5

Generator Loading



Test at 50% Rated & 100% Rated
(Steady State Rated)

Record I_A , I_B & I_C

V_{AN} , V_{BN} & V_{CN}

I_L & V_L

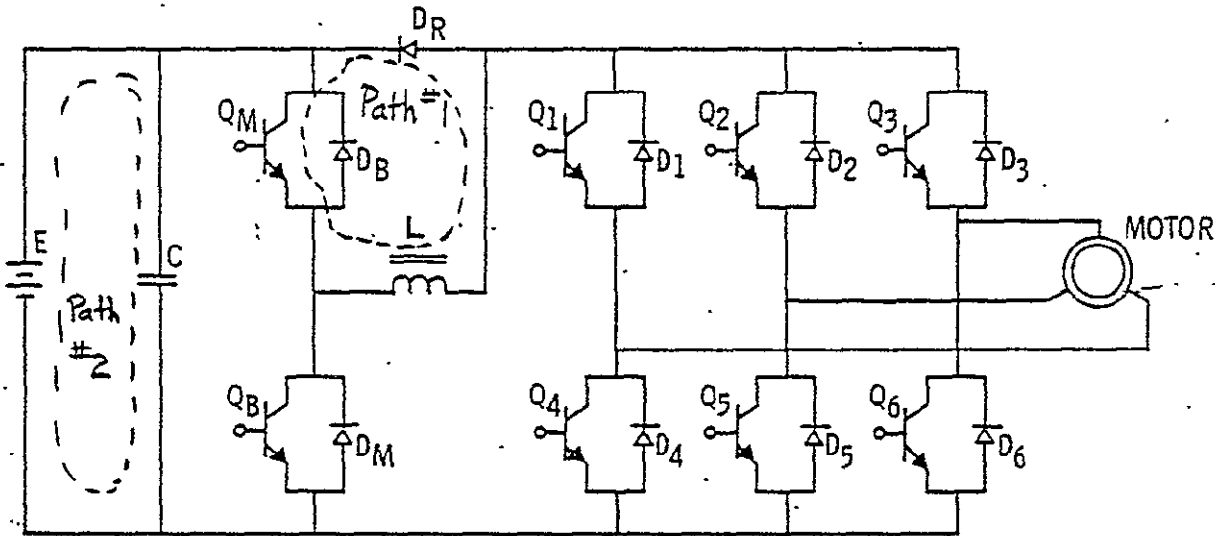
Condition Sudden Load - Permit Steady State to Develop.

Figure (7-7) Test # 5

G. H. Demarest
August 11, 1976

Test # 6

Current Path Determination



Test at Motoring .
 Generating
 Breaking .

Record Currents in Paths # 1, 2, --, etc.

Condition Normal Operating Conditions

Figure (7-8) Test # 6

W. J. Demarest
August 11, 1976

APPENDIX A
ELECTROMECHANICAL ACTUATOR SYSTEM

Figure A-1 shows the various flight control places in the Space Shuttle Orbiter where the electromechanical actuator system could replace the present hydraulic system. Figure A-2 shows schematic block diagram type of representation of the electromechanical actuator as conceived by Delco. Figure A-3 shows a schematic representation of one control channel with one actuator motor. Figure A-4 shows a simplified system transfer functional diagram of a single channel (one motor).

ELECTRIC MECHANICAL CONTROLS

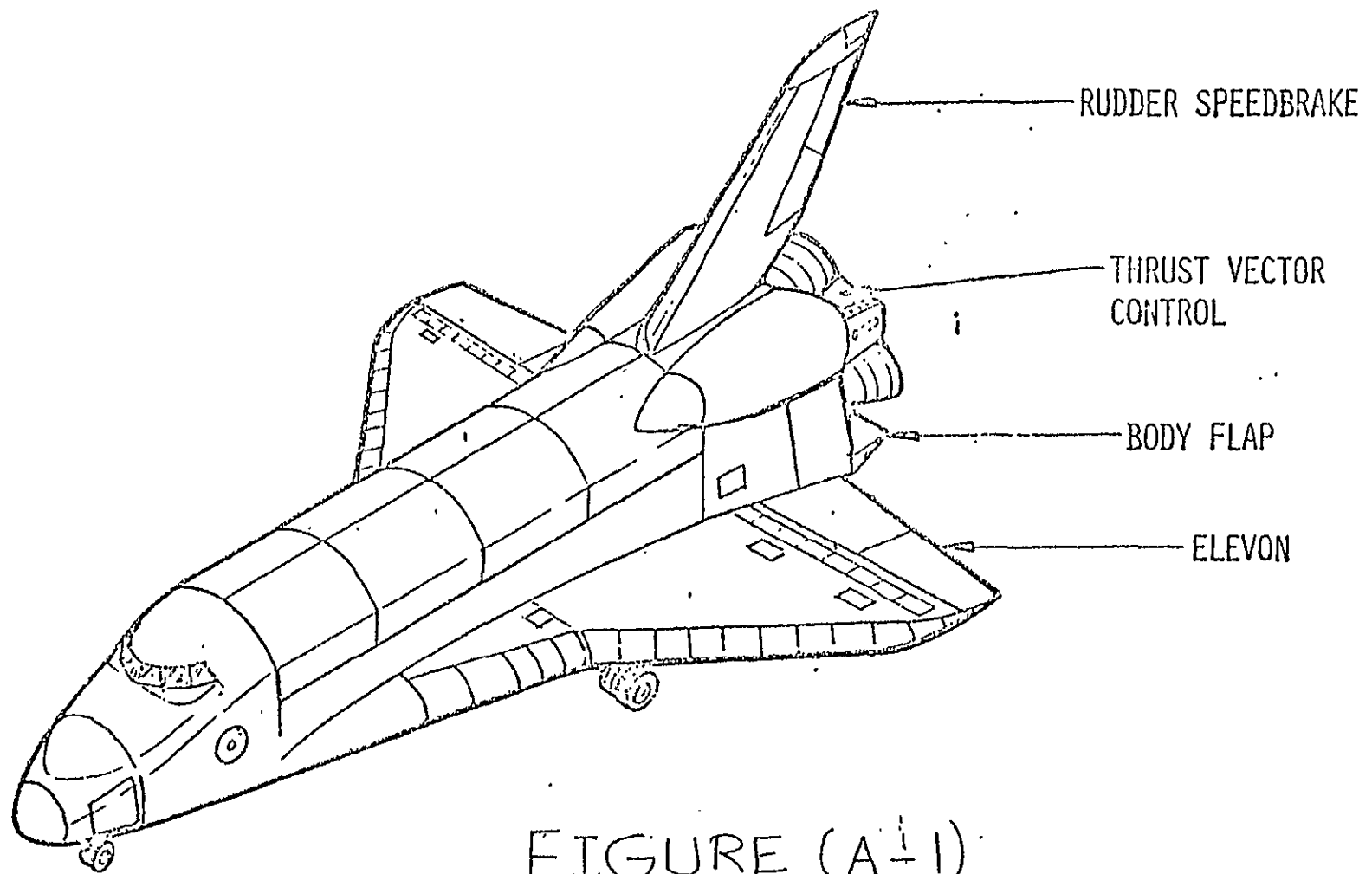
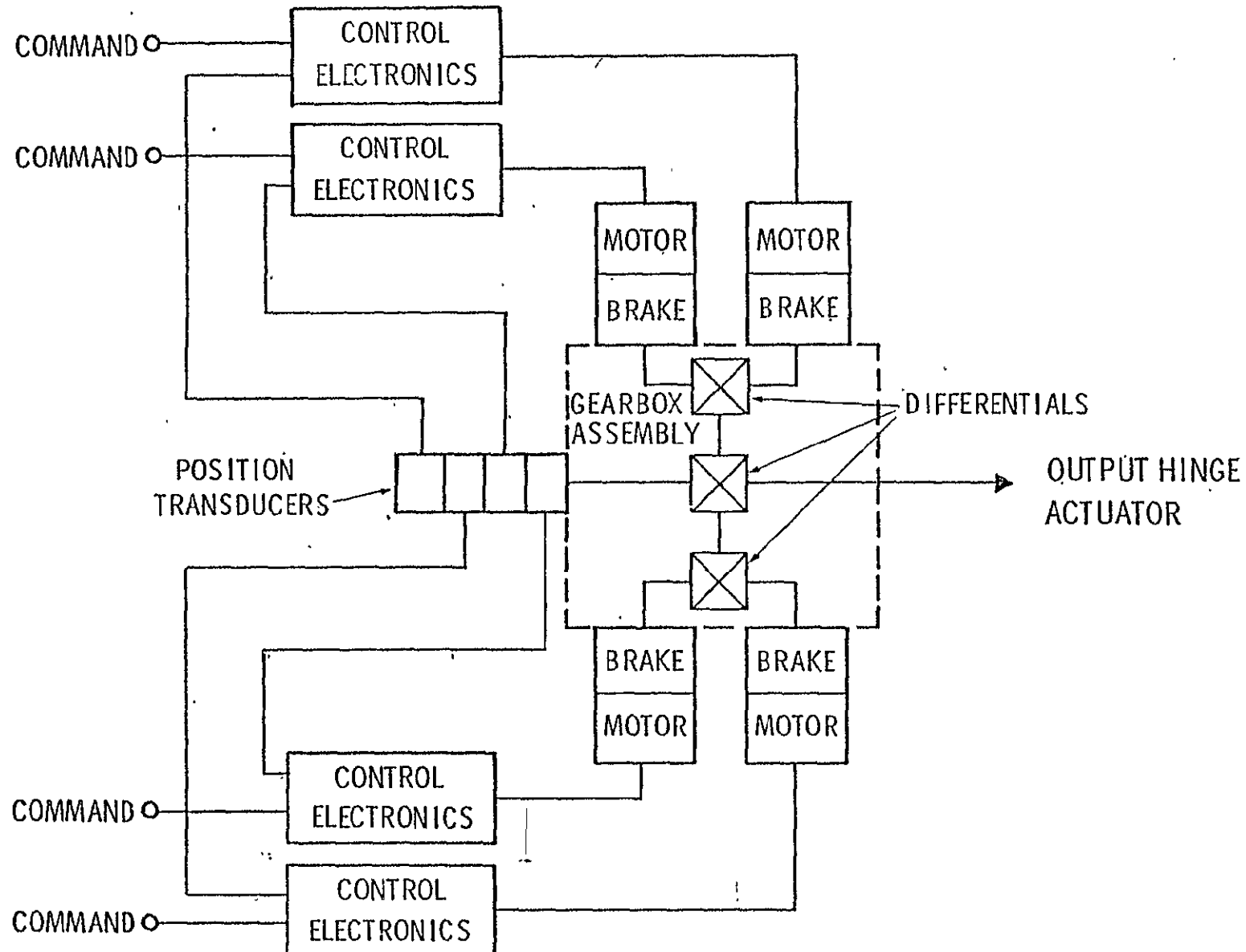
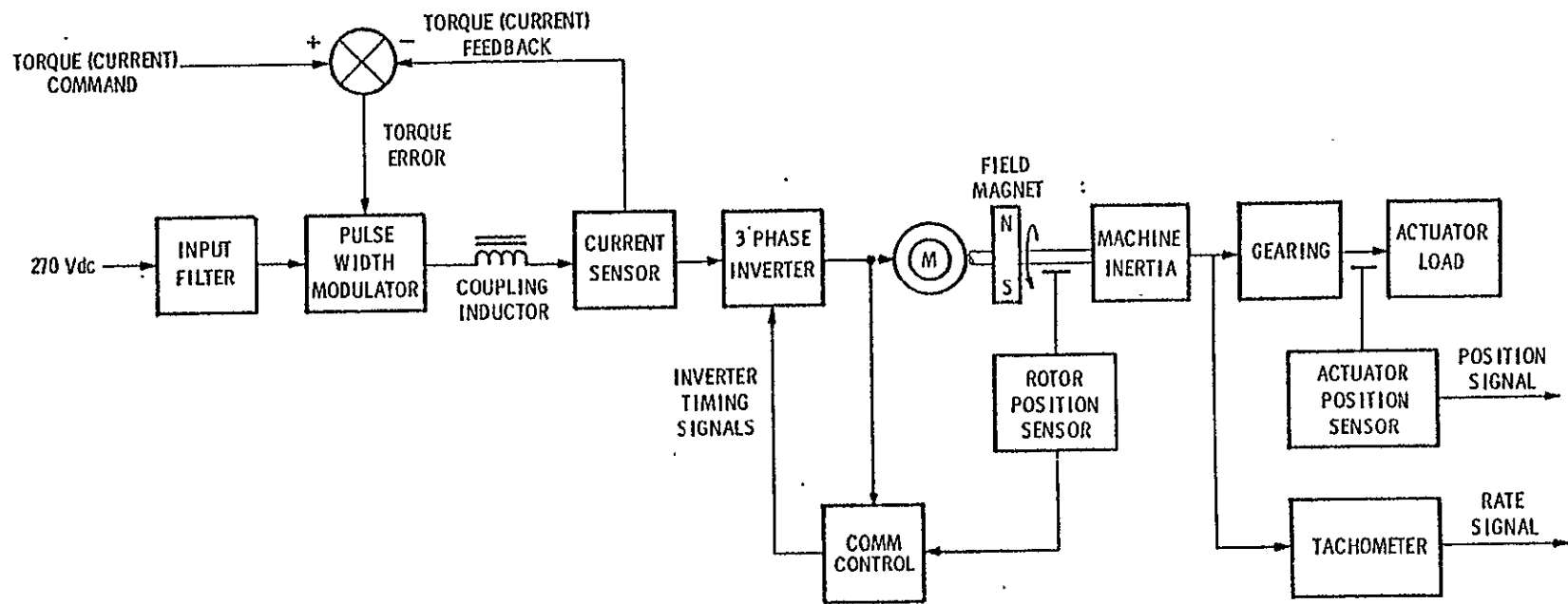


FIGURE (A-1)



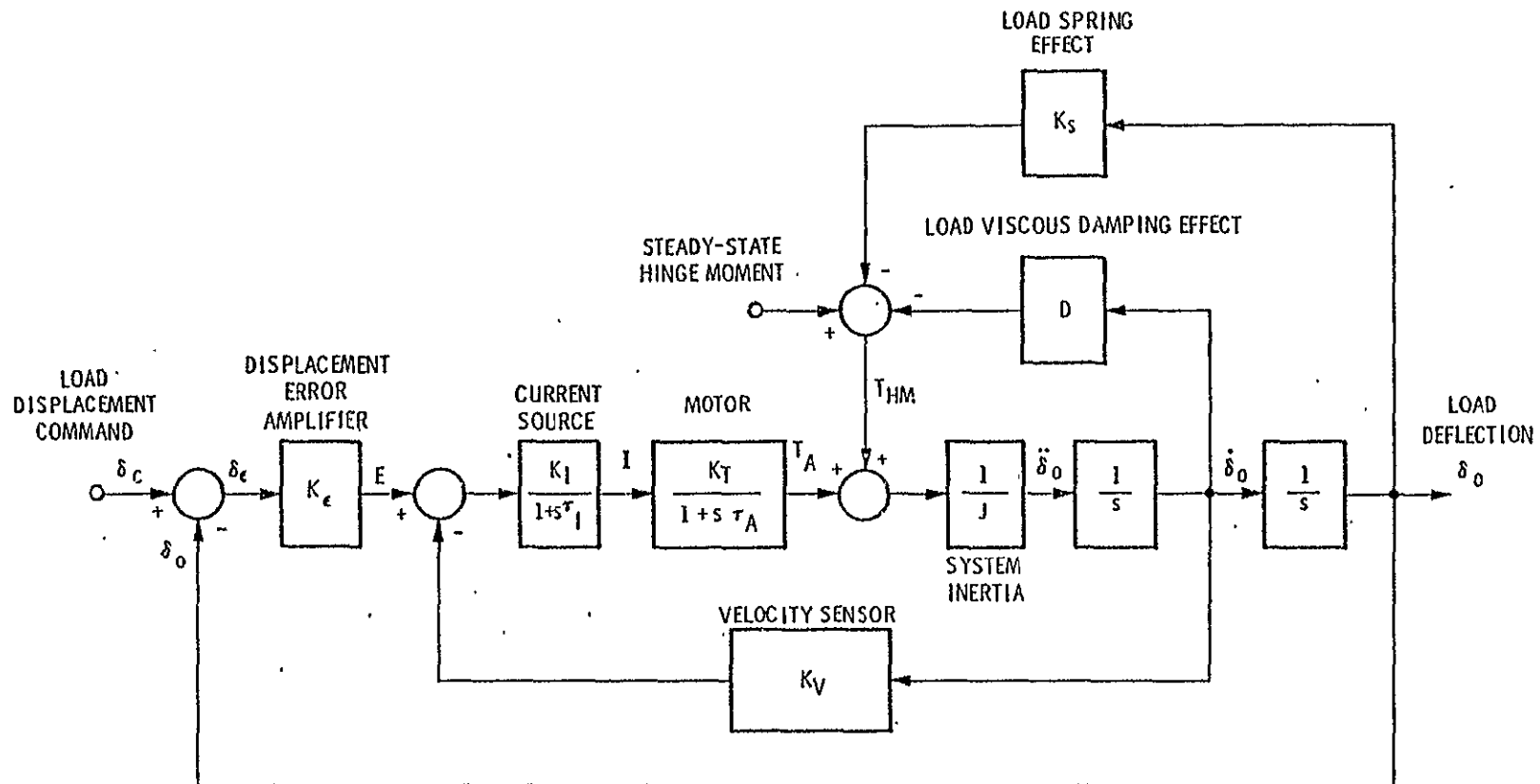
EM Actuator Block Diagram

FIGURE (A-2)



Controller Block Diagram

FIGURE (A-3)



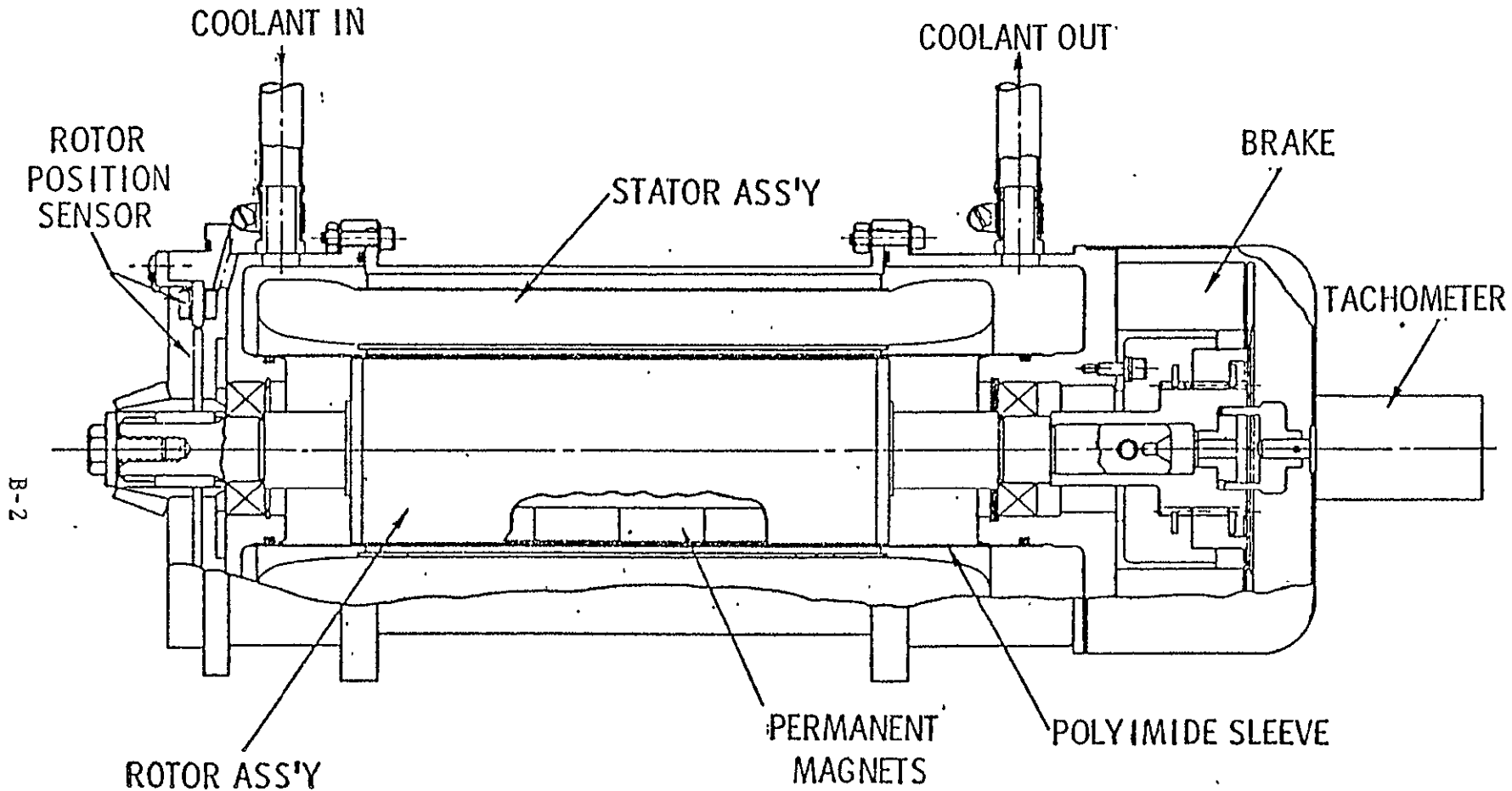
Simplified System Functional Diagram, Single Channel

FIGURE (A-4)

APPENDIX B

EXAMPLE MOTOR - SOME DESIGN FEATURES

Figures B-1 through B-3 give some design features of the
Delco motor used as an example in this investigation.



EM Actuator Motor Design

FIGURE (B - 1)

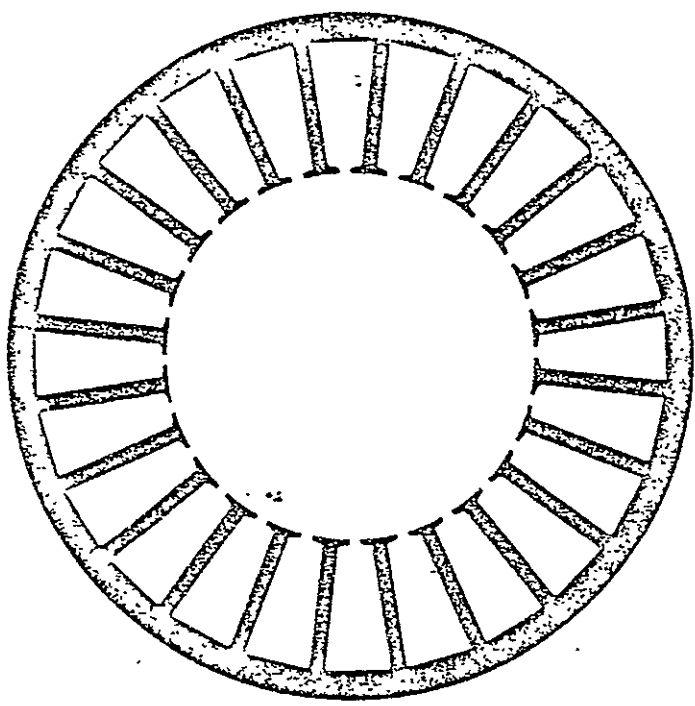


FIGURE (B - 2)
STATOR LAMINATIONS

B-4

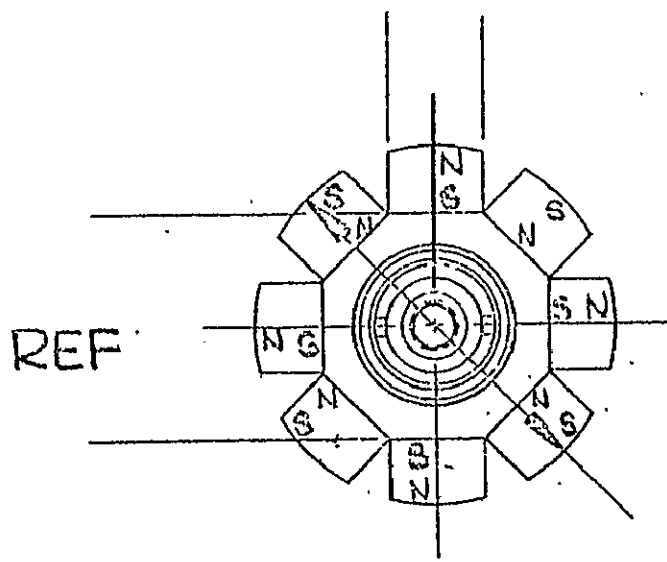


FIGURE (B-3)
ROTOR CONSTRUCTION

APPENDIX C
MOTOR TORQUE - POSITION CALCULATION

The following represents the arithmetical steps of calculating the torque-position characteristic for the motor given by Delco, the design particulars of which are given in Appendix B.

MOTOR
ROTOR TORQUE-POSITION
CHARACTERISTIC

STATE # 1 - Figure (2-27)

From Figure (26) for state # 1 ;

(a) For $-30^\circ \leq \delta \leq -22.2^\circ$ Mechanical , the torque, T , -
is equal to :

$$T = 16 F \cdot R \quad (1)$$

where F is the force per stator slot (i.e.
in this case the force per two coil sides, in a
given stator slot) .

R is the arm of that force (radial
distance from the middle of the conductor carrying area
to the center of the shaft)

In this Case

$$F = (\text{Number of Conductors / slot}) \cdot B_g \cdot I \cdot l_{\text{mach}}$$

where

B_g is the average air gap flux density

I is the current per conductor in Ampers

l_{mach} is the effective (conductor) machine axial length

In the case of the motor given by Delco we have:

$$B_g = 35803 \text{ lines/in}^2 = \underline{0.5551 \text{ Wb/m}^2}$$

$$l_{\text{mach}} = 5.25 \text{ in} = \underline{0.1334 \text{ m}}$$

$$\text{Number of Conductors/Slot} = \underline{9 \text{ Cond.}}$$

$$R \left[\text{estimated as } \frac{1}{2}(3.65 + 1.949) \text{ in} \right] / 2$$

$$R = 2.7995 / 2 \text{ in} = \underline{\underline{0.0711 / 2 \text{ m}}} \\ = \underline{0.0355 \text{ m}}$$

$$\therefore F = 9 \times 0.5551 \times 0.1334 I \text{ Newtons}$$

$$F = \underline{0.66645 I} \text{ Newtons}$$

$$\therefore T = 1.6 \times 0.66645 I \cdot R \text{ Newton.Meter}$$

$$T = \boxed{10.66325 I R} \text{ NM} \quad (2)$$

(b) For $-22.2^\circ < \delta < -15^\circ$ Mechanical, the torque, T , is equal to (See Figures (27) and (28)) :

$$T = 8 F \cdot R \quad \text{NM}$$

$$T = 5.33162 I \cdot R \quad \text{NM} \quad (3)$$

STATE # 2 - Figure (2-28)

(a) For $-15^\circ \leq \delta \leq -7.2^\circ$ Mech

$$T = 16 F \cdot R \quad \text{NM}$$

$$T = 10.66325 I \cdot R \quad \text{NM} \quad (4)$$

(b) For $-7.2^\circ < \delta < 0^\circ$ Mech

$$T = 8 F \cdot R \quad \text{NM}$$

$$T = 5.33162 I \cdot R \quad (5)$$

Thus the average torque, T_{av} , is

$$T_{av} = \frac{1}{2} \cdot (5.33162 + 10.66325) \cdot I \cdot R$$

$$T_{av} = 7.997 I \cdot R$$

Newton Meter (NM)

Example: For a typical motor (see design data submitted by Delco - Appendix (B))

for $I = 60$ Amps & $R = \frac{1}{2}(0.0711)$ Meter

$$T_{av} = 7.997 \times 60 \times 0.0356 = \underline{\underline{17.058 \text{ NM}}}$$

$$\therefore T_{av} = 17.058 \times 0.738 = \underline{\underline{12.588 \text{ Lb.ft.}}}$$

While the Delco design data given for the same example

$$T_{net} = 140 \text{ Lb.in} = \underline{\underline{11.667 \text{ Lb.ft.}}}$$

and

$$T_{developed} = \underline{\underline{11.920 \text{ Lb.ft.}}}$$

Also, for 9000 r.p.m.

$$P_{av} = 17.058 \times \frac{9000 \times 2\pi}{60} = \underline{\underline{16069 \text{ Watts}}}$$

Compared to $P_{in} = \underline{\underline{16243 \text{ Watts}}}$ and

$$P_{out} = \underline{\underline{14915 \text{ Watts}}}$$

NASA-JSC